

**Multi-Fidelity Structural Modeling for Set Based Design (SBD) of
Advanced Marine Vehicles**

Oliver Neal Raj

Thesis submitted to the faculty of
Virginia Polytechnic Institute and State University
in partial fulfillment of the requirements for the degree of

MASTER OF SCIENCE
in
Ocean Engineering

Stefano Brizzolara, Chair

Alan J. Brown

Seongim S. Choi

27 April 2018

Blacksburg, Virginia

Keywords: Structural Analysis, Set Based Design, HY2-SWATH, Hydrofoil, Multi-Fidelity,
Advanced Marine Vehicle

Copyright © 2018 Oliver Neal Raj

Multi-Fidelity Structural Modeling for Set Based Design (SBD) of Advanced Marine Vehicles

Oliver Neal Raj

Abstract

This thesis demonstrates that a parametrically-modifiable Advanced Marine Vehicle Structural (AMVS) module (that can be integrated into a larger framework of marine vehicle analysis modules) enables stakeholders, as a group, to complete structurally feasible ship designs using the Set-Based Design (SBD) method. The SBD method allows stakeholders to identify and explore multiple solutions to stakeholder requirements and only eliminating the infeasible poorer solutions after all solutions are completely explored. SBD offers the advantage over traditional design methods such as Waterfall and Spiral because traditional methods do not adequately explore the design space to determine if they are eliminating more optimal solutions in terms of cost, risk and performance.

The fundamental focus for this thesis was on the development of a parametrically modifiable AMVS module using a low-fidelity structural analysis method implemented using a numerical 2D Finite Element Analysis (FEA) applied to the HY2-SWATH. To verify the AMVS module accuracy, a high-fidelity structural analysis was implemented in MAESTRO to analyze the reference marine vehicle model and provide a comparison baseline. To explore the design space, the AMVS module is written to be parametrically modified through input variables, effectively generating a new vessel structure when an input is changed. AMVS module is used to analyze an advanced marine vessel in its two operating modes: displacement and foil-borne. AMVS demonstrates the capability to explore the design space and evaluate the structural feasibility of the advanced marine vehicle designs through consideration of the material, stiffener/girder dimensions, stiffener/girder arrangement, and machinery/equipment weights onboard.

Keywords: Structural Analysis, Set Based Design, HY2-SWATH, Hydrofoil, Multi-Fidelity,
Advanced Marine Vehicle

General Audience Abstract

In designing large marine products, it is necessary to follow a structured process to ensure the final product adequately meets the needs of a stakeholder's requirements through engineering verification and validation analyses steps. This thesis demonstrates that the Advanced Marine Vehicle Structure (AMVS) module can be used by marine engineering professionals, in a group, to quickly analyze many structural variations of an advanced marine vehicle without freezing or locking in on an early and potentially suboptimal design. AMVS is intended to be integrated and to work in conjunction with other marine vehicle modules that, together, shipbuilder engineers can use to analyze all major design aspects of the marine vehicle in the total ship design process. Together the modules are implemented as a Set-Based Design (SBD) process to explore multiple total advanced marine vehicle solutions to the stakeholder's requirements and to eliminate the infeasible and worse solutions later during analysis.

Keywords: Structural Analysis, Set Based Design, HY2-SWATH, Hydrofoil, Multi-Fidelity,
Advanced Marine Vehicle

Acknowledgements

First, I would like to convey my appreciation to my advisor, Dr. Stefano Brizzolara for his time, enthusiasm, inspiration and patience with this research project. The door to Dr. Brizzolara's office was always open whenever I had a question. Our meetings were always valuable and interesting and he consistently provided guidance, which enabled me to seek a thorough and more accurate solution.

I would also like to thank the rest of my thesis committee: Dr. Alan Brown and Dr. Seongim Choi for their encouragement, insight and thought-provoking questions.

In addition to my committee, I would like to thank Dr. Saad Ragab and Dr. Rakesh Kapania for their technical expertise and advice on the Finite Element Analysis method. Additionally, I would like to show my gratitude to Jim Shaughnessy and team at MAESTRO Marine along with others classmates and parents who helped in general software and technical discussions and proofreading.

This effort has been partially supported by the Defense Advanced Research Project Agency (DARPA) as part of a more comprehensive research project between Brown University, Massachusetts Institute of Technology (MIT), Virginia Tech, Naval Postgraduate School and University of California, Santa Cruz entitled "Scalable Framework for Hierarchical Design under Uncertainty with Application to Marine Vehicles". The project is being developed as part of the DARPA program EQUiPS (Enabling Quantification of Uncertainty in Physical Systems) efforts directed by Dr. Fariba Fahroo as program manager.

Table of Contents

Abstract.....	ii
General Audience Abstract.....	iii
Acknowledgements.....	iv
List of Figures.....	vii
List of Tables.....	x
1. Introduction.....	1
1.1 High-Speed Vessels.....	2
1.2 Small Water Plane Area Twin Hull (SWATH).....	3
1.3 Foil-Supported Vessels.....	5
1.3.1 Fully-Submerged Hydrofoils.....	5
1.3.2 Surface-Piercing Hydrofoils.....	6
1.4 Alternative Design Methods and Processes.....	7
1.4.1 Spiral Model Design Method.....	8
1.4.2 Waterfall Model Design Method.....	9
1.4.3 Set Based Design (SBD).....	10
2. Advanced Marine Vehicle Structural (AMVS) Modules Scope and Objectives.....	1
2.1 Operational Requirements.....	1
2.2 Multi-Fidelity Approach.....	3
2.2.1 Low-Fidelity Physics Structural Analysis Method.....	3
2.2.2 High-Fidelity Physics Structural Analysis Method.....	7
3. Structure Design and Assessment AMVS Module (Low-Fidelity Method).....	7
3.1 Frame and Cross-Sectional Geometry Definition.....	9
3.2 Loads, Boundary Conditions, and Stresses.....	11
3.3 Reference Vessel Substructure Breakdown.....	13
3.3.1 Substructure 1: Forward Struts with Wing-Shaped Superstructure.....	14
3.3.2 Substructure 2: Aft Struts with Wing-Shaped Superstructure.....	18
3.3.3 Substructure 3: Torpedo-Shaped Hull.....	22
3.4 Hogging and Sagging Slamming Loading Condition.....	31
3.5 Input Variable Range, Data Generation, and Feasibility Constraints.....	41

3.5.1	Buoyancy Mode Results	45
3.5.2	Flying Mode Results	46
3.5.3	Hogging Condition Results	46
3.5.4	Sagging Condition Results	46
4.	Structure Design and Assessment Module (High-Fidelity Method)	47
4.1	Geometry Mesh Creation	47
4.2	Material Properties, Loads and Boundary Conditions	53
4.3	Buoyancy Mode Results	58
4.4	Flying Mode Results	64
4.5	Hogging Condition Results	67
4.6	Sagging Condition Results	70
5.	HY2-SWATH Multi-Fidelity Model Analysis and Future Work	73
5.1	Multi-Fidelity Model Analysis	73
5.2	Future Work	80
6.	Conclusions	82
7.	References	85
8.	APPENDIX A: Buoyancy Mode Variable Sweep Data	87
9.	APPENDIX B: Buoyancy Mode Histogram Plots	88
10.	APPENDIX C: Buoyancy Mode Variable Sensitivity Plots	90
11.	APPENDIX D: Flying Mode Variable Sweep Data	91
12.	APPENDIX E: Flying Mode Histogram Plots	92
13.	APPENDIX F: Flying Mode Variable Sensitivity Plots	94
14.	APPENDIX G: Hogging Condition Variable Sweep Data	95
15.	APPENDIX H: Hogging Condition Histogram Plots	96
16.	APPENDIX I: Hogging Condition Variable Sensitivity Plots	98
17.	APPENDIX J: Sagging Condition Variable Sweep Data	99
18.	APPENDIX K: Sagging Condition Histogram Plots	100
19.	APPENDIX L: Sagging Condition Variable Sensitivity Plots	102
20.	Appendix M: HY2-SWATH Structural Improvement Modifications	103

List of Figures

Figure 1: HY2-SWATH Specialty Groups	2
Figure 2: Unconventional Torpedo-Shaped Hull for SWATH Vessels with Minimum Drag [7] ...	4
Figure 3: Comparison of Different Waterline Areas [8].....	4
Figure 4: Fully-Submerged Boeing Hydrofoil Vessel [6]	6
Figure 5: Surface Piercing Hydrofoil Vessel [6]	7
Figure 6: Spiral Model Design Process - Adaptable to Ship Design [9]	8
Figure 7: Waterfall Model Design Process [9]	9
Figure 8: Set-Based Design Process [15].....	10
Figure 9: HY2-SWATH Specialty Groups	14
Figure 10: Displacement and Foilborne Operating Conditions	2
Figure 11: Frame Element with Degrees of Freedom.....	5
Figure 12: Cross-Section of Hull	10
Figure 13: Cross-Section of Strut	10
Figure 14: 3D Image of the Whole Reference Vessel.....	13
Figure 15: Whole Reference Vessel (Looking Aft)	13
Figure 16: Profile View of Reference Vessel	14
Figure 17: Top View of the Reference Vessel.....	14
Figure 18: Forward Struts with Elements, Loads, and Boundary Conditions	15
Figure 19: Forward Struts Element Cross-Sections	16
Figure 20: Forward Struts Frame and Deflected Frame	17
Figure 21: Forward Struts Frame and Scaled Moment	17
Figure 22: Forward Struts Frame and Scaled Shear	17
Figure 23: Aft Struts with Elements, Loads, and Boundary Conditions.....	19
Figure 24: Aft Struts Element Cross-Sections	20
Figure 25: Aft Struts Frame and Deflected Frame.....	21
Figure 26: Aft Struts Frame and Scaled Moment	21
Figure 27: Aft Struts Frame and Scaled Shear.....	21
Figure 28: Hull with Elements, Loads, and BCs (Buoyancy Mode)	22
Figure 29: Hull Bezier Curve.....	23
Figure 30: Hull Element Cross-Sections.....	25
Figure 31: Hull Frame and Deflected Frame	26
Figure 32: Hull Frame and Scaled Moment.....	26

Figure 33: Hull Frame and Scaled Shear	26
Figure 34: Hull with Elements, Loads, and BCs (Flying Mode)	29
Figure 35: Hull Frame and Deflected Frame	29
Figure 36: Hull Frame and Scaled Moment.....	29
Figure 37: Hull Frame and Scaled Shear	29
Figure 38: Hogging [14]	32
Figure 39: Sagging [14]	32
Figure 40: Long. Slamming Pressure Distribution Factor for High Speed Mode [14]	34
Figure 41: Hull with Elements, Loads, and BCs (Hogging Mode).....	35
Figure 42: Hull Frame and Deflected Frame	36
Figure 43: Hull Frame and Scaled Moment.....	36
Figure 44: Hull Frame and Scaled Shear	36
Figure 45: Hull with Elements, Loads, and BCs (Sagging Mode).....	39
Figure 46: Hull Frame and Deflected Frame	39
Figure 47: Hull Frame and Scaled Moment.....	39
Figure 48: Hull Frame and Scaled Shear	39
Figure 49: Shell Plating Conversion to Mesh	48
Figure 50: Internal Structure Converted to Mesh	48
Figure 51: Rhino Cutting Planes Example.....	49
Figure 52: Rhino Loft Example	49
Figure 53: Node Discontinuities	50
Figure 54: MAESTRO Model Mesh.....	52
Figure 55: MAESTRO Free Edge Correction.....	52
Figure 56: Aluminum 7075 Material Properties	53
Figure 57: Concentrated Forces	54
Figure 58: Distributed Forces	54
Figure 59: Flying Mode Restraints (Only Hull Shown)	55
Figure 60: Hogging Condition Restraints (Only Hull Shown)	56
Figure 61: Sagging Condition Restraints (Only Hull Shown)	56
Figure 62: Buoyancy Mode Load Balancing Outputs	57
Figure 63: Buoyancy Weight Summary.....	57
Figure 64: Profile View Showing Waterline.....	58
Figure 65: MAESTRO Reference Model Displacement Results (Buoyancy Mode).....	59
Figure 66 : Max Displacement Node Location (Buoyancy)	59

Figure 67: Von Mises Stress on Shell Plating and Internal Structure (Buoyancy)	61
Figure 68: Zoomed Highest Stress Element (Buoyancy).....	62
Figure 69: Longitudinal and Transverse Shear (Buoyancy Mode)	63
Figure 70: Longitudinal and Transverse Bending Moment (Buoyancy Mode)	64
Figure 71: MAESTRO Reference Model Displacement Results (Flying Mode)	65
Figure 72 : Max Displacement Node Location (Flying).....	65
Figure 73: Von Mises Stress on Shell Plating and Internal Structure (Flying).....	66
Figure 74: Zoomed Highest Stress Element (Flying)	67
Figure 75: MAESTRO Reference Model Displacement Results (Hogging Condition)	68
Figure 76: Max Displacement Node Location (Hogging)	68
Figure 77: Von Mises Stress on Shell Plating and Internal Structure (Hogging)	69
Figure 78: Zoomed Highest Stress Element (Hogging).....	70
Figure 79: MAESTRO Reference Model Structural Displacement Results (Sagging Condition)	71
Figure 80: Max Displacement Node Location (Sagging)	71
Figure 81: Von Mises Stress on Shell Plating and Internal Structure (Sagging)	72
Figure 82: Zoomed Highest Stress Element (Sagging).....	73
Figure 83: AMVS Von Mises Stress Histograms	76
Figure 84: MAESTRO Von Mises Stress Histograms.....	79
Figure 85: MAESTRO Structural Reinforcement Example	81
Figure 86: Improved MAESTRO Reference Model Displacement Results (Buoyancy Mode)..	103
Figure 87: VM Stress on Improved Shell Plating and Internal Structure (Buoyancy Mode)	104
Figure 88: Improved MAESTRO Reference Model Displacement Results (Flying Mode).....	105
Figure 89: VM Stress on Improved Shell Plating and Internal Structure (Flying Mode).....	106
Figure 90: Improved MAESTRO Reference Model Disp. Results (Hogging Condition)	107
Figure 91: VM Stress on Improved Shell Plating and Internal Structure (Hogging Condition)..	108
Figure 92: Improved MAESTRO Reference Model Disp. Results (Sagging Condition).....	109
Figure 93: VM Stress on Improved Shell Plating and Internal Structure (Sagging Condition)...	110

List of Tables

Table 1: Loads Applied.....	12
Table 2: Forward Struts Element Geometry Outputs.....	16
Table 3: Forward Struts Global Node Displacement and Reaction Forces	18
Table 4: Forward Struts Stress and Failure Analysis	18
Table 5: Aft Struts Element Geometry Outputs.....	20
Table 6: Aft Struts Global Node Displacement and Reaction Forces.....	21
Table 7: Aft Struts Stress and Failure Analysis	22
Table 8: Hull Element Geometry Outputs	24
Table 9: Hull Global Node Displacement and Reaction Forces (Buoyancy Mode)	27
Table 10: Hull Stress and Failure Analysis (Buoyancy Mode).....	28
Table 11: Hull Global Node Displacement and Reaction Forces (Flying Mode).....	30
Table 12: Hull Stress and Failure Analysis (Flying Mode)	31
Table 13: Hull Global Node Displacement and Reaction Forces (Hogging Mode)	37
Table 14: Hull Stress and Failure Analysis (Hogging Mode).....	38
Table 15: Hull Global Node Displacement and Reaction Forces (Sagging Mode)	40
Table 16: Hull Stress and Failure Analysis (Sagging Mode).....	41
Table 17: Material Property Parametric Inputs.....	42
Table 18: Stiffener Count Parametric Input.....	42
Table 19: Buoyancy Mode Operating Condition Constraints.....	43
Table 20: Flying Mode Operating Condition Constraints	43
Table 21: Hogging and Sagging Condition Constraints	44
Table 22 : Shear and Bending Moment Summary Results (Buoyancy Mode)	64
Table 23: AMVS Max Displacement Results Summary	73
Table 24: AMVS Principal Stress Results Summary.....	74
Table 25: AMVS Max Von Mises Stress Results Summary	74
Table 26: AMVS Von Mises Stress Statistics	74
Table 27: MAESTRO Max Displacement Results Summary.....	76
Table 28: MAESTRO Max Von Mises Stress Results Summary.....	77
Table 29: MAESTRO Von Mises Stress Statistics	77
Table 30: Stresses in Elements Surrounding the Highest Stress Elements	80

1. Introduction

The complex ship design process is initiated when a capability gap, or need, within an organization or industry is identified. It is currently accomplished by a team of designers, engineers and scientists, often in collaboration with government, industry and the academia. An innovative ship design requires extensive research in the initial design phases to identify a set of requirements which clearly describe a design to fill the identified capability gap. Due to the parametric nature of ship design, establishing requirements and use of traditional design methodologies, such as Spiral and Waterfall, fail to capture the necessary detail to design something as complex as a ship [2]. The iterative steps in these methodologies of capturing this detail results in schedule delays, cost overruns and design rework or redesign. Ships and their numerous systems are too large and complex to be adequately designed using these single point solution methods without eliminating feasible design options very early in the design process. The early eliminated designs could be optimal solutions but they are never explored [2]. Due to project schedule, resource, and cost constraints; eliminated design options are never returned to for further investigation and development or vetting. On 11 May 2004, Representative Duncan Hunter, Chairman of the House Armed Services Committee stated “The lack of discipline in both the requirements development process and the systems design and demonstration process are making new ships unaffordable.”[3] Poorly established requirements drive up the design and development process time and cost as it requires more negotiation and re-work or redesign to accomplish a final product that meets the requirements and to fill the capability gap(s) identified. The SBD methodology has been shown to resolve the requirement-design dilemma by identifying a set of feasible design solutions that satisfy the desired requirements. The feasible solutions are then systematically refined and ranked to converge on a preferred design(s), based on trade-off analysis of risk, cost, quality and intended effectiveness of the design solution options.

The fundamental focus for this thesis was on the development of a parametrically modifiable AMVS module using a low-fidelity structural analysis method implemented using a numerical 2D Finite Element Analysis (FEA) applied to the concept ultra-high-speed Unmanned Surface Vehicle (USV) Hybrid Hydrofoil SWATH (HY2-SWATH). To verify the AMVS module accuracy, a high-fidelity structural analysis was implemented in MAESTRO to analyze the reference marine model and provide a comparison baseline. The comparison baseline will provide useful information for future refinement and accuracy enhancement of the AMVS module. This thesis shows that the AMVS module can be implemented in the SBD methodology in conjunction with other marine vehicle analysis modules for the total ship design of the HY2-SWATH. It also validates that there are feasible design choices for the structural arrangement.

The AMVS module is one of three modules being created for the HY2-SWATH. Figure 1 shows that in addition to the structure, the aerodynamics and the hydro-statics/dynamics are considered in the design process. Parametrically-modifiable modules are being created by other scientists on the team, at Massachusetts Institute of Technology (MIT), to consider the aerodynamics and hydro-statics/dynamics of the vessel. Figure 1 shows the division of labor in the HY2-SWATH project.

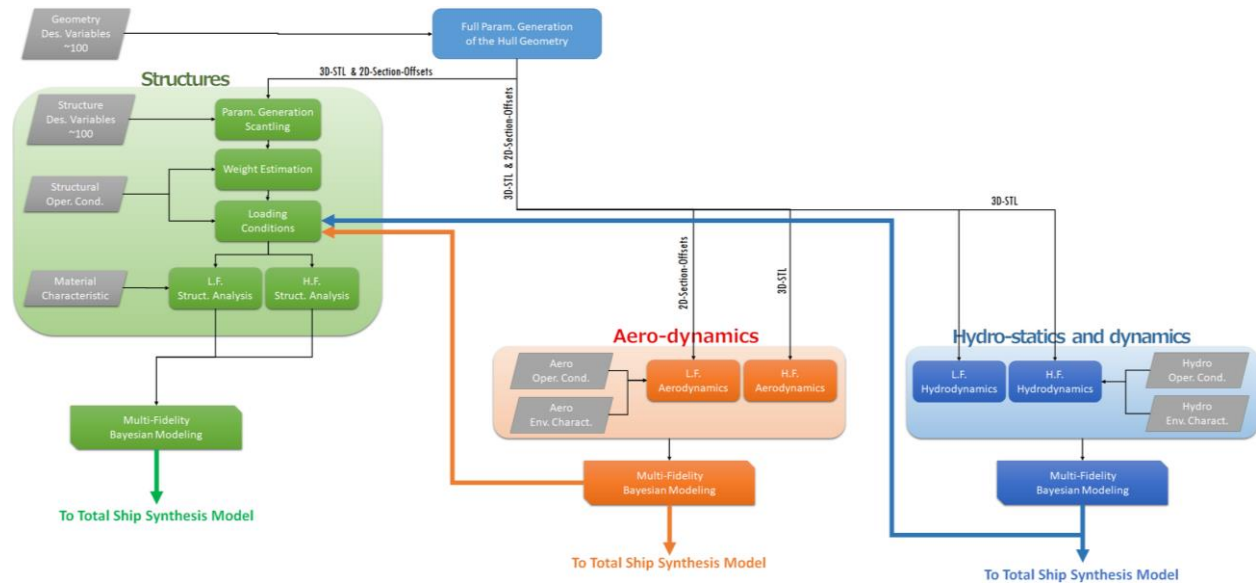


Figure 1: HY2-SWATH Specialty Groups

Together, the major disciplines involved in the HY2-SWATH’s design are considered.

- In displacement mode the hydrodynamics in calm water (total resistance), motions and loads in irregular waves, powering and propulsion, internal arrangements and weight estimation, intact and damage stability are analyzed.
- In the foil-borne mode, the aerodynamics of the emerged sections (e.g. struts, wing-shaped superstructure, turbojets) of the vessel are considered as well as the hydrodynamics of the submerged sections of the vessel (e.g. propulsion motors, torpedo-shaped hulls, and struts).

1.1 High-Speed Vessels

A high speed marine vessel, as defined by the International Maritime Organization’s (IMO) International Code of Safety for High-Speed Craft (HSC), is “...a craft capable of a maximum speed equal to or exceeding: $3.7\bar{V}^{0.1667} (m/s)$ where: \bar{V} = displacement corresponding to the design waterline

(m^3).”[5] In terms of the volumetric Froude Number, $F_{N_V} = \frac{velocity}{gravity^{0.5} * \nabla^{0.1667}}$, a displacement vessel is considered “fast” when $F_{N_V} \geq 1.2$ and in terms of the length Froude Number, $F_{N_L} = \frac{velocity}{\sqrt{velocity*length}}$, a vessel is considered “fast” when $F_{N_L} \geq 0.4$, corresponding to the so called hull speed. The HY2-SWATH design falls in to the high-speed vessel category using any of these definitions. This has practical design implications due to the different requirements set by classification societies with respect to safety and structural strength.

When discussing vessels it is important to differentiate between different hull form typologies by their operational speed because the hydrodynamic characteristics change based on the hull type and operating speeds. For example, at vessel operational speeds greater than 50 knots, hydrodynamic cavitation needs to be considered in order to implement a suitable design of any lifting surface. In the context of the HY2-SWATH, that is meant to reach speed in excess of 100 knots, this means when operating the vessel in foilborne mode, the hydrofoils need to be optimized and implemented in the form of super-cavitating hydrofoils [4]. Additionally, the physics of slamming (and related low order models used to calculate slamming pressures in practical naval architecture) pressures changes based on the speed of the vessel. The slamming pressure and applicable equations implemented in the HY2-SWATH’s design are discussed in detail in Section 3.4.

1.2 Small Water Plane Area Twin Hull (SWATH)

The HY2-SWATH uses a torpedo-shaped SWATH hullform. A SWATH is a type of marine vessel with two hulls, also referred to as demihulls, which are submerged under the surface of water and provide buoyancy and volume capacity for fuel and propulsion systems. The demihulls can be shaped optimally for a designed cruise speed and because they are below the surface of the water, are less affected by wave action thus reducing the drag. Figure 2, illustrates how the geometry of a hull can be optimized at different Froude Numbers i.e. for different vessel designed operational speeds.

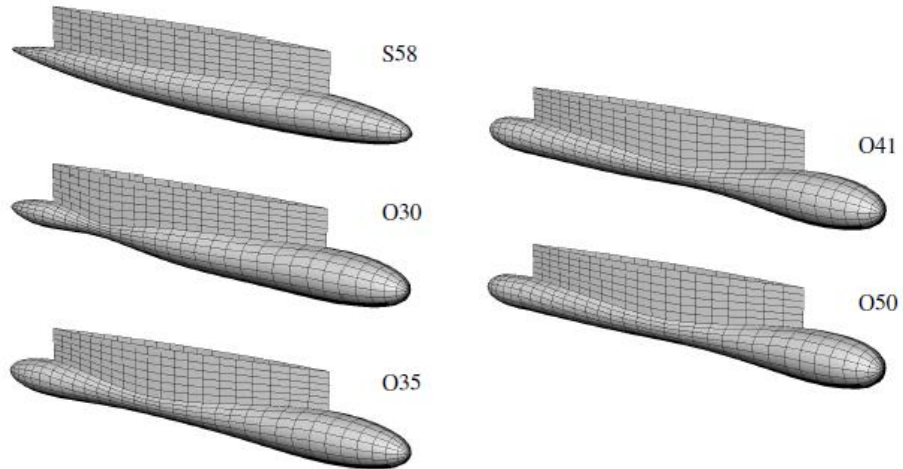


Figure 2: Unconventional Torpedo-Shaped Hull for SWATH Vessels with Minimum Drag [7]

Specifically, Figure 2 shows hull forms optimized for different Froude Numbers ranging from low speeds ($F_r = 0.30$) to high speeds ($F_r = 0.40$). Appended to the hulls are single or twin struts which rise above the water and support the upper platform.

Figure 3, provides a comparison of wetted-surface areas between a monohull, catamaran, and a SWATH. The monohull has the largest wetted-surface area and the SWATH has the smallest wetted-surface area.

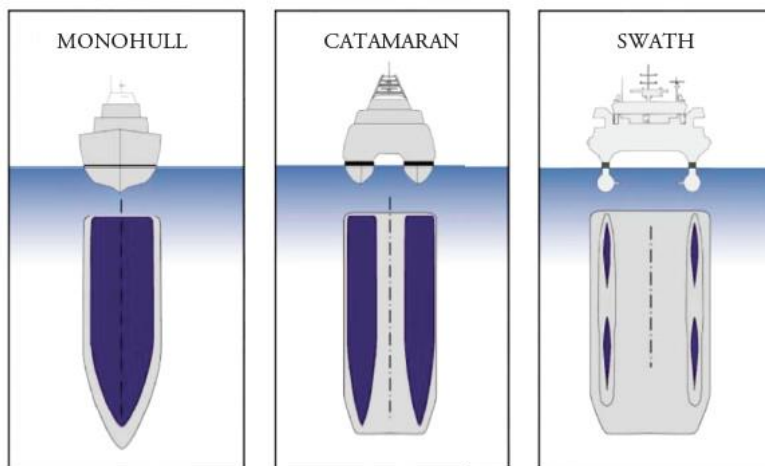


Figure 3: Comparison of Different Waterline Areas [8]

The benefit of smaller waterline area is in the smaller wave excitation forces, which ultimately means lower motion in rough seas. However, smaller waterline areas lower the hydrostatic restoring forces, so

the vessel will have less hydrostatic capability to react to external roll/pitch moments and vertical forces. Figure 3 shows that a SWATH resembles a catamaran but with added benefit of better seakeeping characteristics in head sea conditions when compared with a catamaran or equivalent monohull [8]. Traditional SWATH vessels are typically affected by a higher wave-making resistance, compared to equivalent catamarans or monohulls. This handicap can be overcome with non-conventional hull forms as first demonstrated by Brizzolara [7] and as represented in Figure 3. Additionally, similar to a catamaran, the advantageous seakeeping characteristics can be lost if there are resonant vertical motions caused by current sea state, speed and heading [6]. Due to the unique structural geometric design, SWATHs are far more complex vessels than conventional catamarans.

1.3 Foil-Supported Vessels

In its foilborne mode, the HY2-SWATH engages its hydrofoils to lift the vessel out of the water which reduces the drag and allows the vessel to increase its speed from its displacement mode design speed (8-20 knots) to its foilborne mode design speed (120+ knots). The characteristic of having two operational modes is why the vessel is classified as a hybrid. Foil-supported vessels, i.e. hydrofoil-supported vessels, use similar design theory as plane wings. However, an airfoil and a hydrofoil's purpose is the same; to provide a lift force to the craft. As a ship increases speed, the hydrofoil lifts the ship's hull(s) out of the water in order to decrease drag and allow for further increase of vessel speed. Hydrofoils can be attached to any hull type e.g. monohull, catamaran, SWATH, etc. Hydrofoils can be subdivided in to two subcategories: fully-submerged hydrofoils and surface-piercing hydrofoils.

1.3.1 Fully-Submerged Hydrofoils

Fully-submerged hydrofoils, generally inverted T-shaped, are fully submerged under water and remain fully submerged while the vessel is in foilborne mode. As discussed in Section 1.2, because the hydrofoil remains fully submerged, there is less drag due to wave making actions. The majority of fully-submerged hydrofoil (e.g. those developed by Boeing) is outfitted with flaps, similar to an airplane wing, which are activated with a control system to stabilize the vessel in heave, pitch, and roll motions. The active control system makes the vessel's ride smoother than the surface-piercing hydrofoil's passive stabilization feature.

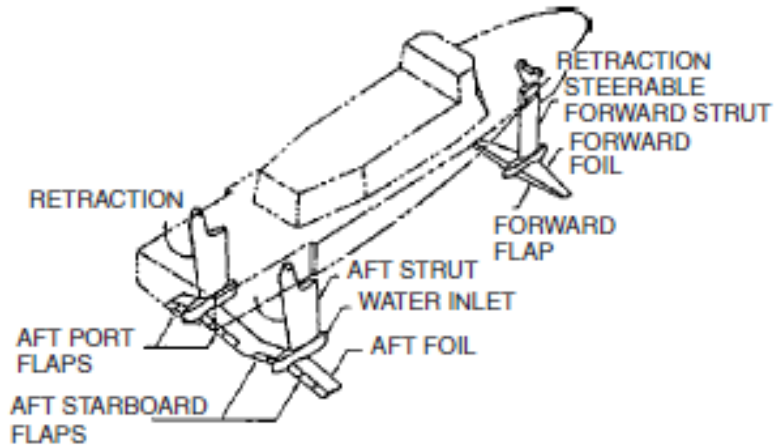


Figure 4: Fully-Submerged Boeing Hydrofoil Vessel [6]

Figure 4 shows what the fully-submerged hydrofoils look like on vessel. The vessel contains one hydrofoil towards the bow of the ship and one continuous hydrofoil towards the aft of the ship. This specific arrangement of hydrofoils is known as the “canard” configuration and is suitable when the center of gravity is located in the aft part of the vessel.

1.3.2 Surface-Piercing Hydrofoils

Surface-piercing hydrofoils, generally V-shaped, are shaped so that the main portion of the hydrofoil is submerged under water, providing lift, with a small portion of the foil which rises above the surface when in foilborne mode. Figure 5 provides an image of a traditional surface-piercing hydrofoil, as those developed in Russia and Italy by Rodriquez shipyard.



Figure 5: Surface Piercing Hydrofoil Vessel [6]

The surface-piercing hydrofoil is self-stabilizing with respect to the vertical position, heel, and trim making the surface-piercing hydrofoil the simpler of the two hydrofoil subcategories to implement. Due to the inclined shape of the hydrofoil, a larger foil area is required to provide the same lift at a given vessel's speed and weight [6].

An in depth analysis was conducted by Pruner [4] which resulted in equipping the HY2-SWATH with two sets of deployable super-cavitating surface-piercing hydrofoils with negative dihedral angle with respect to the free surface. This configuration ensures the vessel can be adequately supported and provides minimized resistance and good inherent dynamic stability, as demonstrated in a new study by Williams and Brizzolara [18].

1.4 Alternative Design Methods and Processes

The purpose of design is for the ultimate specification and procurement of a product, system or service for the customer. For the procurement of complex products, a formal process is often implemented to ensure that the customer actually receives what they wanted. There are many different design processes that provide structured approaches for making decisions as the design progresses, instructions, procurement of materials, etc. all in order to produce a final product that meets the customer's requirements.

Sections 1.4.1 and 1.4.2 briefly describe the Spiral Model Design Method and Waterfall Model Design Method, two traditional design methods used to organize the development process of the product,

system, or service. Section 1.4.3 describes the Set Based Design Method approach to product and system procurement and the advantages it offers over the traditional design methods. In the following sections, the use of the word “product” refers to a system(s), service(s) and/or product(s).

1.4.1 Spiral Model Design Method

The Spiral Model design is an iterative design process that consists of four main phases. Starting from quadrant II and moving clockwise. In Figure 6, the four phases are: design, evaluation/risk analysis, development/testing, and planning with stakeholder participation and approval. While Figure 6 specifically references software design, all of the total ship design processes at a high level are essentially the same. Any minor variances between the design processes can be easily modified and adapted for ship design.

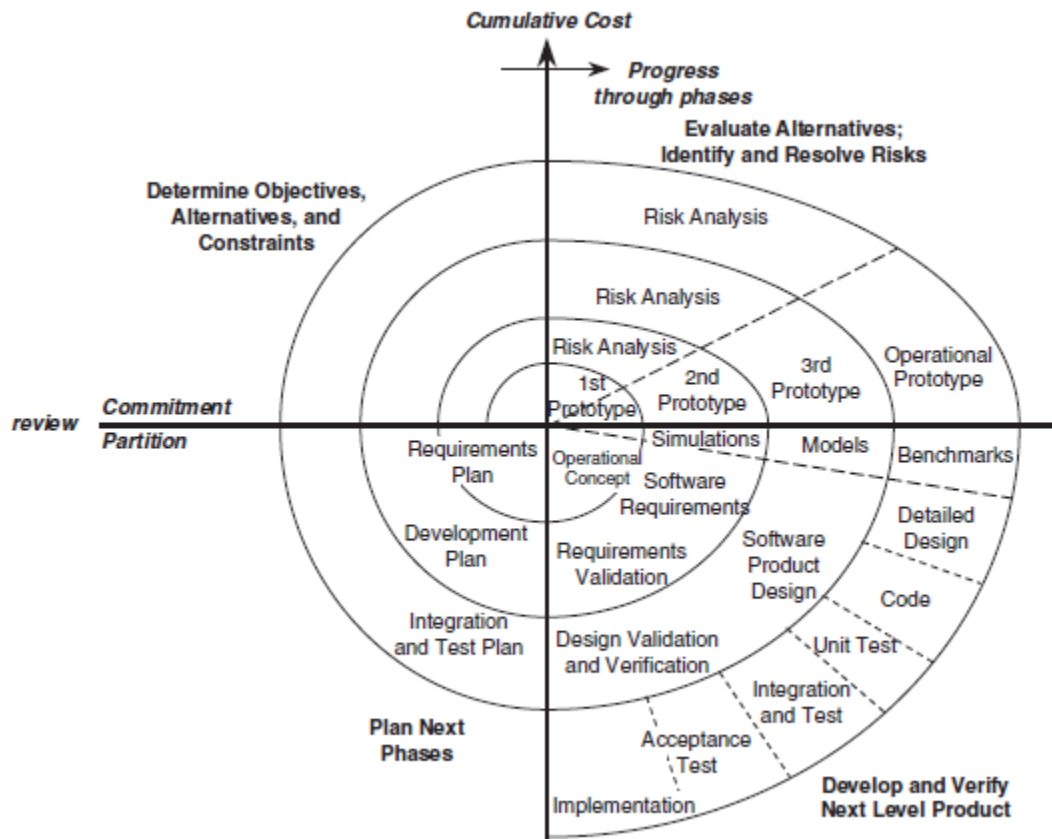


Figure 6: Spiral Model Design Process - Adaptable to Ship Design [9]

The process is iteratively repeated, moving radially outward until the final product has been developed with cost being proportional to the circle’s radius. The main concept behind this design process is to identify and mitigate risks associated with cost, schedule, and performance to develop

partially operational prototypes or proof of concept, rapidly. Rapid prototyping allows for the development of improved requirements and increased product functionality [9]. The ultimate goal of the Spiral Model design process is to develop a single product/system and refine the product for increased functionality as stakeholders generate new and improved detailed requirements.

1.4.2 Waterfall Model Design Method

The Waterfall Model design method is a step-by-step evolution of typical life-cycle phases with progress flow primarily in one direction. Similar to Figure 6, Figure 7 provides an example of the life-cycle phases as applied to ship software systems development but is extendable to any product/system development including ship hardware design. It shows that iteration is only permitted between adjacent phases and product design only moves forward to the next phase when the preceding phase has been reviewed and verified.

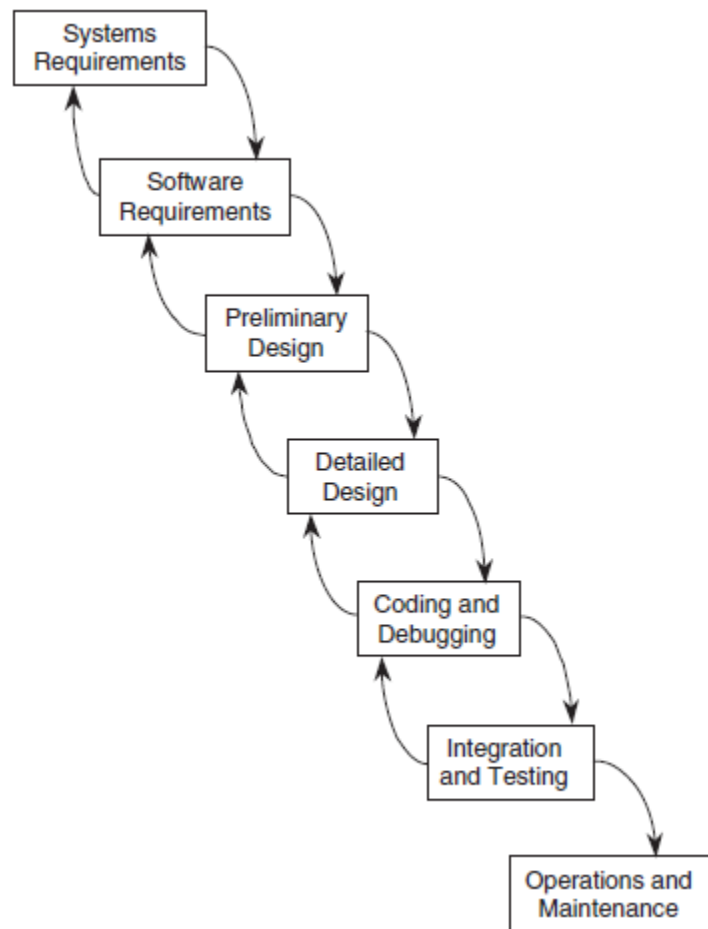


Figure 7: Waterfall Model Design Process [9]

The design process is initiated with product/system requirements definition and refinement. Once requirements have been reviewed and verified with relevant stakeholders, the next step is to design the system followed by testing/sea trials and deployment. The final step is to maintain and service the product or ship as in our case.

1.4.3 Set Based Design (SBD)

SBD is a design methodology, like the spiral model design method and waterfall model design method; all with the intended purpose of producing a product for the customer. Unlike the aforementioned traditional methodologies, which identify a single solution through continuous iterative refinement, the SBD methodology implements the process in reverse. This is a major variance. SBD identifies multiple feasible solutions of the design as a whole and works to eliminate infeasible solutions or badly dominated solutions [13]. Bernstein thoroughly describes the SBD process in “Design Methods in the Aerospace Industry: Looking for Evidence of Set-Based Practices” [15] and provided Figure 8 which shows a simplified diagram of the SBD process.

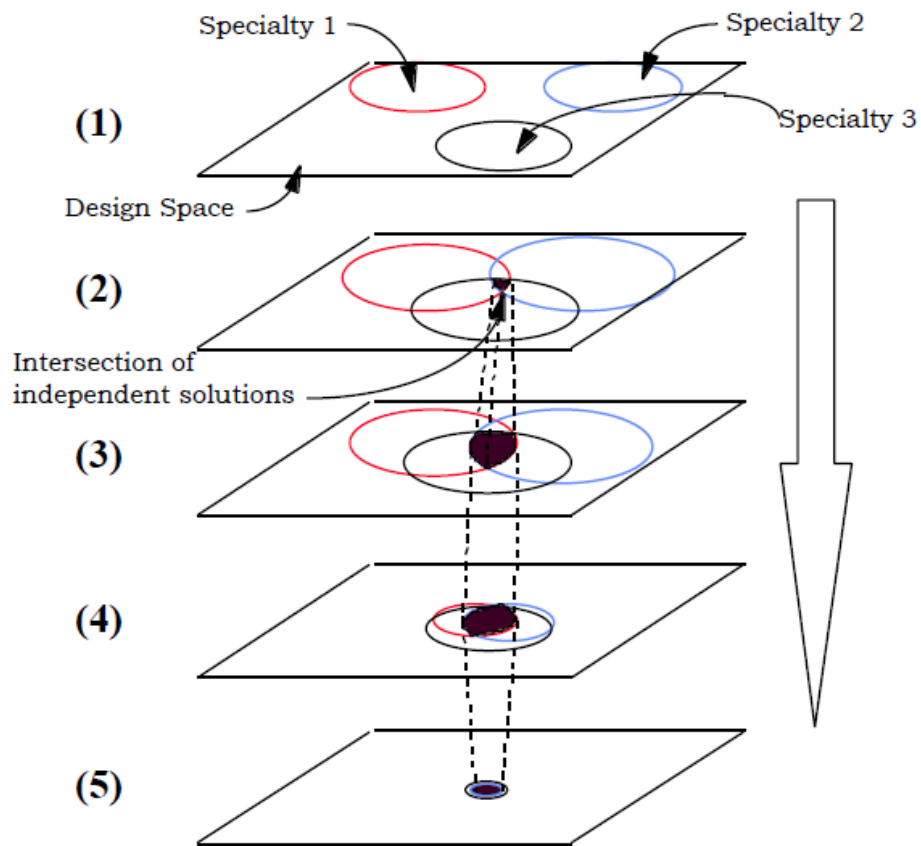


Figure 8: Set-Based Design Process [15]

SBD is summarized in three steps or phases as follows:

1. Explore the design space (Figure 8: step (1))
2. Identify overlapping solution set regions (Figure 8: step (2))
3. Refine feasible design regions (Figure 8: step (3) – step (5))

The first task of SBD is to explore the design space. A design space contains all possible solutions to the design problem. The design space is bounded by current and future-potential capabilities. Once the requirements have been established which define the objectives and capability gap(s) the final product is to fill. Various specialty groups (functional groups, domains, disciplines) concurrently work to identify all possible product solutions and alternatives to accomplish the objectives to meet the requirements. The solutions identified within a specialty are known as solution sets. The boundaries on the solution sets are restricted by constraints, physical or governing parameter minimum and maximum ranges as delineated in the product requirements specification by the client or stakeholder. At this phase, the goal is to identify and expand as many possible solutions that will satisfy the product requirements.

As more solutions are identified, the solution sets become larger and begin to overlap with other solution sets. To develop a feasible ship design solution, all specialty domains must be coordinated and function harmoniously. Step two of SBD is to identify the overlapped regions. The overlapped regions are known as feasible solutions because they meet all the stated requirements of each specialty discipline and could feasibly be matured into a final product. However, in SBD, the final solution is identified through elimination of infeasible solutions. At this step, the non-overlapping solution regions can be eliminated as a final product must satisfy the requirements for all solution domains.

After step two has been completed, the remaining balance is the feasible solutions to each domain specialty. Step three works to refine the feasible design region. The specialty groups work to add detail to the remaining designs to ensure their continued feasibility [15]. The iterative refinement process is continued until a single design or set of non-dominated designs remain. When there are multiple, often conflicting, objectives to be accomplished by a product, multiple optimal solutions can be identified by prioritizing and optimizing towards one of the multiple objectives. Optimizing towards one of multiple objectives means that no single solution can simultaneously provide the optimal solution for all objectives. Then trade-offs between objectives will result in the existence of numerous optimal solutions capable of achieving the objectives to different degrees. A non-dominated solution refers to one of the optimal solutions to the set of objectives. An example of two conflicting objectives is the objective of providing a low cost product versus a product outfitted with all the optional accessories.

The major advantages of the SBD process include:

1. Gaining a comprehensive understanding of the design space

2. Design solution validation and improved quality through converging (overlapping) specialty group solution sets
3. Mitigation of design rework
4. Flexibility in solution options

The SBD process requires the investigation and identification of many creative and objective design solution options, by various specialty groups, and their refinement. Refinement through overlapping solution sets serves as a form of checks and balances. The overlapping regions represent converging solutions, validated through scrutiny by different technical design methods. Refinement through elimination of infeasible solutions requires a thorough understanding of the potential forms and capabilities a range of product solutions can provide in order to cross-reference the solutions with the requirements in order to identify their inconsistencies to classify the designs as infeasible.

Since designs are only eliminated if infeasible, there is no need to return to eliminated design options for rework since they have been declared as infeasible. This minimizes impact to schedule, cost and resources. Principally, the process of elimination via infeasibility, as opposed to single solution selection, allows flexibility for a variety of vetted future design solutions.

The major disadvantages of the SBD process include:

1. Requires a method to quickly generate numerous design variations
2. Method to refine solution options

Each specialty group involved in the design of a product must identify a range of design solutions to adequately explore the design space and ensure overlap with other specialty group solution sets. Often the number of design solutions could be in the hundreds or thousands. To identify many designs, a computer program is created; in which input parameters can be varied to quickly output a design i.e. a what-if analysis. The creation of such a computer code initially takes a greater amount of time in the early phases of the product's design. Often, many different computer codes, or modules, may be created to output design solutions within the realm of each specialty group. The modules are often written for analysis of the specific product and requirements in question and are not general enough for reuse in the design of another product with different requirements.

Initial refinement through solution set convergence and infeasible solution removal may not immediately converge to a single final solution. Further refinement of the remaining valid solution options must take place to reveal a final solution. The current literature research on SBD are often vague and do not provide a concise direction on how to conduct the final stage(s) of refinement. Singer et. al. [2] suggest at this point to switch to point design methods; deferring to stakeholders' preferences and expertise. Brown et. al. [13] suggest a slight deviation from SBD by conducting a multi-objective optimization to establish a Pareto frontier of non-dominated solutions. This is a slight deviation from

traditional SBD because it seeks to select the best of solutions through specific objectives as opposed to seeking to eliminate the poorer solutions through specific objectives. Gretna [1] and Bernstein [15] do not elaborate on an additional refinement; assuming solution set convergence and physically infeasible solutions elimination will result in a single final solution.

To apply the SBD process to HY2-SWATH, the design space exploration was tasked to four specialty groups (Structures, Aerodynamics, Hydro-statics, and Hydro-dynamics) that are worked concurrently to identify feasible solution sets, as shown in Figure 9. Each specialty group worked to create parametrically-modifiable modules that will be integrated into a global software manager which will automate the domain minimum and maximum parameters.

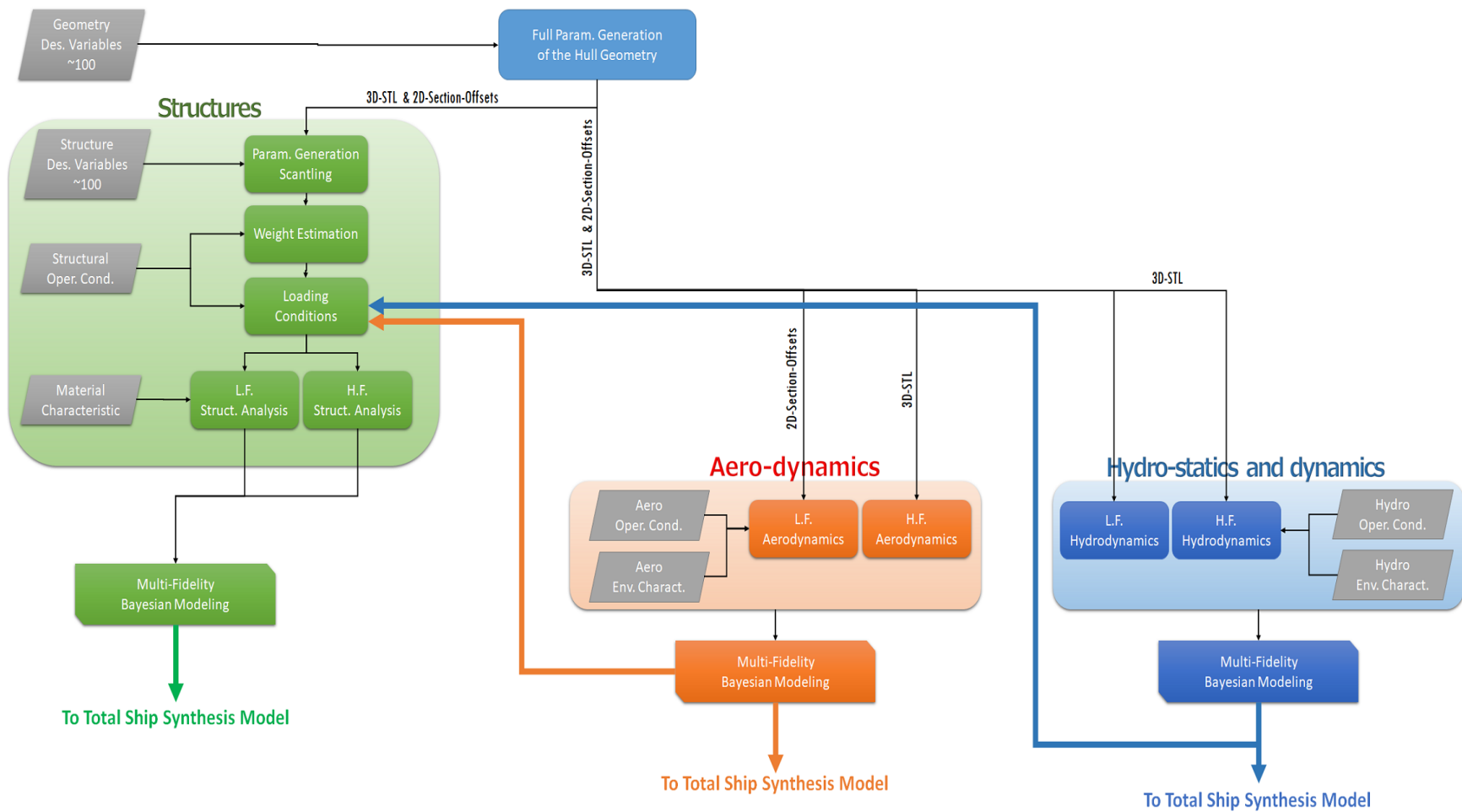


Figure 9: HY2-SWATH Specialty Groups

The domain specialty research focus of this thesis is for the parametric generation structural module. The structural module inputs are easily and automatically varied to generate many structural designs of the ultra-high-speed hydrofoil SWATH and their associated structural analysis solutions. The module is described in detail in Section 3 and Section 4.

2. Advanced Marine Vehicle Structural (AMVS) Modules Scope and Objectives

AMVS module is essential in the overall design framework, Figure 9, of the vessel used to create the structural layout of advanced marine vehicles; in this case, the HY2-SWATH. The AMVS module also contains an analysis module to assess the structural integrity of the HY2-SWATH and to determine if any aspects of the structure fails. For this paper, AMVS module was used to analyze the stresses the vessel will experience in accordance with the vessel's operating modes and environment conditions including displacement mode, foilborne mode, hogging, sagging, and slamming. The vessel's operational requirements are discussed in Section 2.1.

The AMVS module is parametrically modifiable as a function of designer input variables so that many geometric variations of the HY2-SWATH are automatically generated, presented, and analyzed. The AMVS module can be integrated with other ship domain analysis modules in a global system software manager. Collectively, the modules will be used in the Set Based Design (SBD) methodology for the total ship design and analysis of this advance marine vehicle.

2.1 Operational Requirements

The HY2-SWATH operates in two different cruise speeds of ~8-25 knots and ~120+ knots. It is difficult to optimize a single hull form configuration of a vessel which is optimized for two extremely different cruise speeds and thus the vessel operates in one of two modes: displacement mode or foilborne mode. Figure 10 shows the vessel with the hydrofoils retracted and in displacement mode as well as the hydrofoils deployed and in foilborne mode.

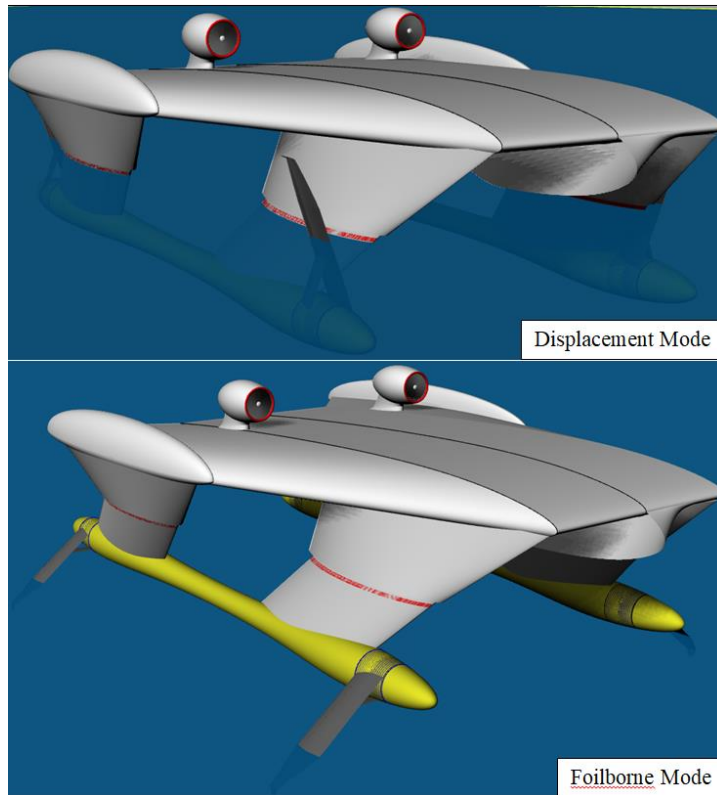


Figure 10: Displacement and Foilborne Operating Conditions

In displacement mode, the vessel uses its two motor-driven propellers to cruise at speeds between 8 - 25 knots. The torpedo-shaped twin hulls have been optimally shaped to minimize resistance at cruise speeds. In its displacement mode, the vessel is capable of operating in sea states up to three i.e. significant wave heights of 1.67 – 4.08 ft. or 0.5 – 1.25 m. The hogging, sagging and slamming stresses on the HY2-SWATH are considered due to these higher sea states.

In foilborne mode, the vessel uses its two turbo jet engines to provide thrust and its four super-cavitating hydrofoils and wing-shaped superstructure to provide lift to raise the hulls out of the water in order to cruise at 120+ knots. The vessel is capable of transporting a three to five metric tonne payload, 500 nautical miles at top speed. Additionally, the vessel is capable of accomplishing a 5 day mission.

Both modes of vessel operation were considered and analyzed. Specific areas of development and testing were necessary in the overall structural design and in the dynamic behavior of the vessel. Structurally, the vessel's design had to be lightweight but capable of handling the material stresses and fatigue in both operating modes. The vessel's twin hulls, struts, superstructure, and the hydrofoils are designed with sufficient strength, enough to support the weight of the fully loaded vessel in foilborne mode, yet hydro and aerodynamic enough to minimize drag and resistance.

2.2 Multi-Fidelity Approach

A multi-fidelity model analysis approach was implemented to analyze the structure of the reference marine model. A high-fidelity model offers the advantage of greater correlation to full-scale sea trial results while the low-fidelity model offers the advantage of reduced computational time. The disadvantage of the high-fidelity model is that it is not always possible to develop a sophisticated high-fidelity model due to the lack of specific information required setting up a detailed model and complex mathematical models characterized by long computational times. It is useful to represent the sophisticated high-fidelity model with a simplified, lower-fidelity model characterized by sufficient fidelity to represent the complex geometries and capture local effects but with a shorter computational time. “Sufficient fidelity” is accomplished by using simplified mathematical models and formulas which have demonstrated similar behavior to full-scale trial results. In addition, “sufficient fidelity” is accomplished by modeling all major aspects of the design that may significantly impact the results, as determined through professional discussions. Thus, the multi-fidelity design analysis approach mitigates expensive and time consuming-full scale trials by using low-fidelity analysis to quickly explore the design space; integrated with high-fidelity analysis for increased accuracy [13].

The fundamental focus for this thesis was on the development of a parametrically modifiable AMVS module using a low-fidelity structural analysis method implemented using a numerical 2D Finite Element Analysis (FEA) applied to the HY2-SWATH. To verify the AMVS module accuracy, a high-fidelity structural analysis was implemented in MAESTRO to analyze the reference marine model and provide a comparison baseline.

2.2.1 Low-Fidelity Physics Structural Analysis Method

This section provides a general background theory on the low-fidelity physics selected and implemented in the AMVS product module. The Euler-Bernoulli finite element method was selected for implementation of the low-fidelity structural analysis. Euler-Bernoulli beam theory is a special case of Timoshenko beam theory which is often used to calculate the load-carrying and elastic deflection characteristics of rods, beams or frames. The difference between Euler-Bernoulli beam theory and Timoshenko beam theory is in their respective assumptions. Euler-Bernoulli assumes plane sections remain plane i.e. the finite element cross-sections are perpendicular the bending line. Timoshenko beam theory allows rotation between cross-section and bending line. The Euler-Bernoulli assumption is valid for the analysis of vessel because it covers the case for small deflections. Large deflections are not acceptable in ship design and result in clearly infeasible solutions which are directly eliminated from the feasible space.

Finite element method is a numerical method, like finite difference method, for solving differential equations but is more general and powerful in its application. In the finite element method, a domain is divided into subdomains, called finite elements, and an approximate solution is developed over each element. The division of the domain into subdomains offers the advantage of accurate representation of dissimilar material properties and complex geometries. The sub-domain captures the local effects within each element, and together, provides an accurate representation of the total solution [10].

“The three fundamental steps of the finite element method... are:

1. Divide the whole domain into parts (both to represent the geometry and the solution of the problem).
2. Over each part, seek an approximation to the solution as a linear combination of nodal values and approximation functions, and derive the algebraic relations among nodal values of the solution over each part.
3. Assemble the parts and obtain the solution to the whole.” [10]

There are three inherent sources of error in the finite element solution:

1. Due to the approximation of the domain, i.e. geometric region over which the equations are solved.
2. Due to the approximation of the solution i.e. use of approximating polynomial interpolating functions in the element equation derivation.
3. Due to numerical computation e.g. numerical integration and computer round-off errors. [10]

Figure 11 shows an ordinary un-deformed and deformed frame element with two nodes, three degrees of freedom per node, displacements in the x and y-axis directions, and where external concentrated forces and moments act. This frame element is the fundamental element used in this method and is the superposition of a bar element and a beam element. Thus, the frame element takes on the characteristics of both the bar and beam element, allowing for axial and transverse forces and bending moments to be developed in the members [10].

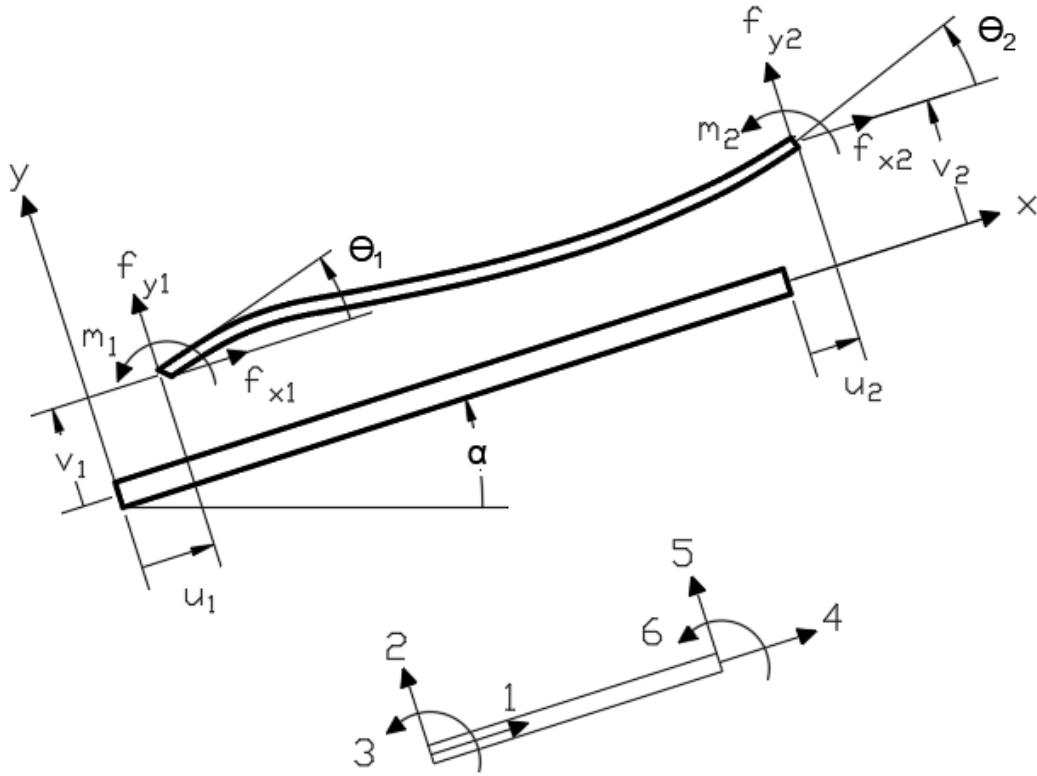


Figure 11: Frame Element with Degrees of Freedom

The Euler-Bernoulli frame element equations, in the local element reference framed (denoted by the subscript/superscript “e”), are given by the element equations:

$$[\bar{K}]^e \{\bar{\Delta}\}^e = \{\bar{F}\}^e \quad \text{Equation 1}$$

Equation 1 is the algebraic element equation of the Euler-Bernoulli differential equation. The element stiffness matrix $[\bar{K}]^e$ and force vector $\{\bar{F}\}^e$ are derived using the Hermite cubic interpolation functions and have the final form as shown in Equation 2 and Equation 4.

$$[\bar{K}]^e = \frac{2E_e I_e}{L_e^3} \begin{pmatrix} \frac{A_e L_e^2}{2I_e} & 0 & 0 & -\frac{A_e L_e^2}{2I_e} & 0 & 0 \\ 0 & 6 & -3L_e & 0 & -6 & -3L_e \\ 0 & -3L_e & 2L_e^2 & 0 & 3L_e & L_e^2 \\ -\frac{A_e L_e^2}{2I_e} & 0 & 0 & \frac{A_e L_e^2}{2I_e} & 0 & 0 \\ 0 & -6 & 3L_e & 0 & 6 & 3L_e \\ 0 & -3L_e & L_e^2 & 0 & 3L_e & 2L_e^2 \end{pmatrix} \quad \text{Equation 2}$$

E_e = Element elastic modulus

A_e = Element cross-sectional area

I_e = Element second moment of area

L_e = Element length

Equation 3 shows the element nodal degrees of freedom, which follows and corresponds to the ordered forces and moments listed in the force vector $\{\bar{F}\}^e$ (Equation 4). Displacement and force vector components are visually indicated in Figure 11.

$$\{\bar{\Delta}\}^e = \begin{pmatrix} u_1 \\ v_1 \\ \theta_1 \\ u_2 \\ v_2 \\ \theta_2 \end{pmatrix}^e \quad \text{Equation 3}$$

u_i = Node axial displacement

v_i = Node transverse displacement

θ_i = node rotation angle

$$\{\bar{F}\}^e = \begin{pmatrix} f_{x1} \\ f_{y1} \\ m_1 \\ f_{x2} \\ f_{y2} \\ m_2 \end{pmatrix}^e + \begin{pmatrix} \bar{Q}_1 \\ \bar{Q}_2 \\ \bar{Q}_3 \\ \bar{Q}_4 \\ \bar{Q}_5 \\ \bar{Q}_6 \end{pmatrix}^e \quad \text{Equation 4}$$

f_{yi} = distributed transverse element force

f_{xi} = distributed axial element force

m_i = pure moment

\bar{Q}_i = force and moment boundary conditions

Equation 1 - Equation 4 are represented in the element's local coordinate system and must be transformed in to a global coordinate system of the entire frame. The local element reference frame equations are related to a global coordinates by a transformation matrix as show in Equation 5.

$$[T]^e = \begin{pmatrix} \cos(\alpha_e) & \sin(\alpha_e) & 0 & 0 & 0 & 0 \\ -\sin(\alpha_e) & \cos(\alpha_e) & 0 & 0 & 0 & 0 \\ 0 & 0 & 1 & 0 & 0 & 0 \\ 0 & 0 & 0 & \cos(\alpha_e) & \sin(\alpha_e) & 0 \\ 0 & 0 & 0 & -\sin(\alpha_e) & \cos(\alpha_e) & 0 \\ 0 & 0 & 0 & 0 & 0 & 1 \end{pmatrix} \quad \text{Equation 5}$$

The final element matrices in the global reference frame are obtained by Equation 6.

$$[T]^T [\bar{K}]^e [T]^e [T]^e \{\bar{\Delta}\}^e = [T]^T \{\bar{F}\}^e \quad \text{Equation 6}$$

Next, the element matrices are assembled into a global matrix equation based on a connectivity matrix describing how the element end nodes interface with one another. Finally, boundary conditions are applied and the resulting equations are solved for the unknown nodal displacements and forces.

2.2.2 High-Fidelity Physics Structural Analysis Method

The high-fidelity structural analysis of the reference HY2-SWATH was conducted using MAESTRO. MAESTRO is a commercial 3D modeling software used to structurally design, analyze and evaluate floating structures. A model can be built using a combination of coarse/fine and quad/triangular meshes. The software calculates the displacements and stresses on a model using the FEA method and evaluates the structural failure modes using different methodologies including:

1. ALPS/ULSAP
2. ALPS/HULL (hull girder ultimate strength)
3. ABS High Speed Naval Craft (HSNC) and Offshore Buckling Guide
4. US Navy NVR criteria

MAESTRO can also be set up to analyze many different loading scenarios, including the loading cases analyzed in the AMVS module; such as hydro-static loads, hydro-dynamic loads, hogging and sagging wave conditions [16].

3. Structure Design and Assessment AMVS Module (Low-Fidelity Method)

The Euler-Bernoulli theory described in Section 2.2.1 was implemented in a MATLAB 2D Finite Element Analysis (FEA) code written by Dr. Saad Ragab [17]. This code was converted from MATLAB to Mathematica and adapted and enhanced to allow for analysis of the HY2-SWATH. Modifications include, but not limited to, the addition of code to:

1. Create and element cross-sections (described in Section 3.1)
 - a. Calculate element area
 - b. Calculate element inertias
 - c. Calculate element volumes
 - i. Material volume (structural weight)
 - ii. Enclosed volume (buoyancy and fuel)
2. Analyze three interdependent frames in various operational conditions (described in Section 3.3)
 - a. Generate deflection, shear and bending moment plots
 - b. Calculate bending stress, shear stress, and principle stresses
 - i. Apply a safety factor
 - ii. Compare principle stresses against material yield stresses for structure failure analysis
 - c. Calculate frame center of gravity and total center of gravity of the three interdependent frames
 - d. Incorporate DNVGL rules (described in Section 3.4)
3. Calculate buoyancy and trim the vessel when necessary
4. Generate histograms for assistance in visualization and interpretation of results (described in Section 3.5)
5. Generate input variable sensitivity plots (described in Section 3.5)

The AMVS module is parametrically modifiable. The whole module has been written generically to allow varied inputs; effectively generating a new vessel structure and enable analysis of its associated structural properties each time inputs are modified and the code is executed. Numerous variations of the vessel structure can be analyzed as required in the design space exploration of the Set Based Design approach.

The AMVS module sets up a frame structure, subdivided into a collection of finite elements. It then determines and calculates the geometry and associated geometric properties of each element cross-section. Finally, force/moment loads and boundary conditions are applied to the structure and the code calculates stresses and determines whether there is a structural failure. Sections 3.1, 3.2, and 3.3 elaborate on the process with a specific example using the original dimensions of the reference HY2-SWATH, as described in the thesis “Design of a Supercavitating Hydrofoil for Ultra-High Speed Vessel with Numerical Methods” [4].

The HY2-SWATH was divided into three frames and analyzed in the buoyancy mode, flying mode, hogging and sagging conditions. The hogging and sagging conditions include analysis of

slamming forces and are discussed in Section 3.4. Once the module was tested using the reference HY2-SWATH, several design variables were selected for variation and a variable sweep was conducted to expand and explore the design space. After data generation, constraints were applied and the design space was refined based on clearly feasible designs. The variable sweep, data generation and constraints are further discussed in Section 3.5.

3.1 Frame and Cross-Sectional Geometry Definition

Initial setup requires a frame to be generated as a collection of finite frame elements connected at the end nodes via a connectivity matrix. The number of elements per frame can be varied with more elements being used in areas of dissimilar material properties, element geometries, variations in applied loads and areas of structural interest. Once an element frame is created, the AMVS module calculates the moment of inertia, cross-sectional area of each element, element structural weight, and element volumes.

Separately, other scientists on the on the HY2-SWATH team run Computational Fluid Dynamic (CFD) software to create aerodynamically and hydrodynamically feasible vessel geometries for the wing-shaped superstructure, forward struts, aft struts and torpedo-shaped twin hulls as a component of the larger ship design framework. Cross-sections of these structures are provided at the determined element locations. The code is set up to analyze any cross-sectional shape provided. Figure 12 and Figure 13 are cross-sections of the hull and strut, respectively, and are used to aid in the following explanation of structure creation.

The AMVS module takes the cross-sectional element shape (blue line) and generate an outer shell plating (red line) given a parametrically defined element thickness. Due to the dimensions of Figure 13, the original blue cross-section line is overshadowed by the red outer shell line. Then AMVS module generates internal stiffeners. The number of stiffeners per element can be specified as well as the dimensions, e.g. height and thickness, of each individual stiffener within an element. To conclude element geometry generation, internal ring stiffeners (black line), i.e. girders, are generated. The ring stiffeners contribute to the element weight and are shaped the same as the element cross-section they support. Similar to the stiffeners, the number of ring stiffeners and dimensions, e.g. thickness and depth, of the ring stiffeners can be parametrically specified per element.

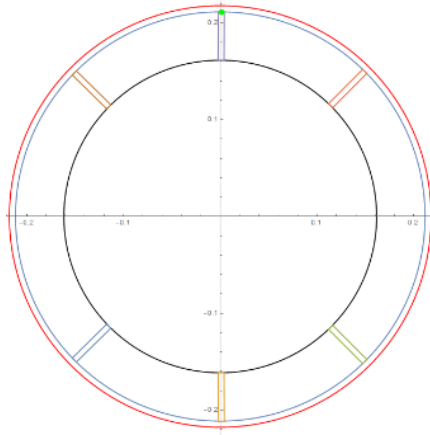


Figure 12: Cross-Section of Hull

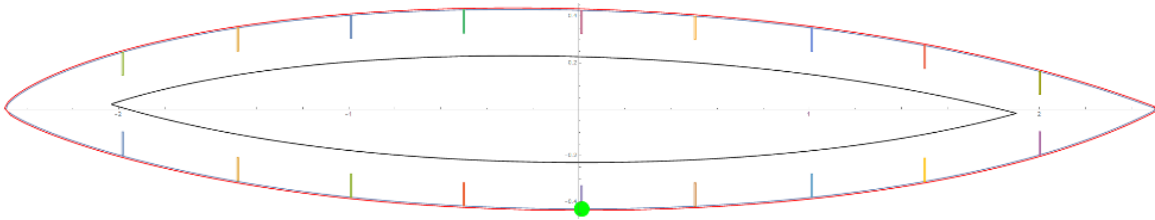


Figure 13: Cross-Section of Strut

Once the cross-sectional geometry of each element was completed, the element cross-sectional structural area and volume, moment of inertia, structural weight, and element buoyancy provided were calculated. Buoyancy is only provided if the element is submerged in water. These values are then exported to the stress calculation portion of the AMVS module. The general equations used are applicable to any shaped provided and are described below.

Equation 7 allows for the calculation of a polygon's area using the coordinates of the polygon's vertices. For curved shapes, as shown in Figure 12 and Figure 13, a sufficient number of data points needs to be used to define the shape vertices to provide sufficient polygon area accuracy.

$$\text{Polygon Area} = \text{abs}\left(\frac{\sum_{i=1}^{n-1}(x_i y_{i+1} - y_i x_{i+1})}{2}\right) \quad \text{Equation 7}$$

n= number of coordinates defining the polygon

Similar to Equation 7, Equation 8 is used to calculate the moment of inertia for any polygon using the coordinates of the polygon's vertices.

$$I_x = \frac{1}{12} \sum_{i=1}^n (y_i^2 + y_i y_{i+1} + y_{i+1}^2) (x_i y_{i+1} - x_{i+1} y_i) \quad \text{Equation 8}$$

$$I_y = \frac{1}{12} \sum_{i=1}^n (x_i^2 + x_i x_{i+1} + x_{i+1}^2) (x_i y_{i+1} - x_{i+1} y_i)$$

n= number of coordinates defining the polygon

The material structural volume of the each element was calculated using Equation 9.

$$\text{Struc. Vol.} = \left(\sum_i^m A_{stiff.} + A_{shell} \right) * \text{length of element} + \sum_j^n Vol_{ring\ stiff.} \quad \text{Equation 9}$$

m = number of stiffeners

n = number of ring stiffeners

3.2 Loads, Boundary Conditions, and Stresses

Once the geometry and associated geometric properties have been calculated, loads and boundary conditions are applied. The AMVS module allows for concentrated forces, applied in global coordinate system in the horizontal and vertical directions, and pure moments to be applied to element end nodes. Uniform distributed loads can be applied to elements with the load applied transversely to the element in element local coordinates. The specific loads due to machinery, electrical cables and piping, fuel, etc. were calculated and described by Pruner [4] in the development of reference HY2-SWATH, and are summarized in Table 1. Since some of structural values were estimated by Pruner [4], and the dimensions of the vessel structure are parameter inputs in the AMVS module and therefore are subject to change, they are recalculated by AMVS module. The calculated load values have been noted in Table 1.

Table 1: Loads Applied			
Load	Quantity	Mass (Each, MT)	Reference Vessel Weight (Each, N)
Electric Motor	2	0.255 + 5% allowance	2,316.67
Payload	1	5	49,030
Wing-Superstructure	1	Calc. + 5% allowance	76,262.8
Cables and Pipes	1	0.65+ 5% allowance	6,692.6
Struts	1	Calc. + 5% allowance	43,672.6
Hull	2	Calc. + 5% allowance	15,799.75
Fore foil	2	1.535 + 5% allowance	15,804.8
Aft foil	2	1.57 + 5% allowance	16,165.2
Rotating Mech. Fore	2	0.125 +5% allowance	1,287.04
Rotating Mech. Aft	2	0.125 + 5% allowance	1,287.04
Elec. Nav. Equip.	1	0.5 + 5% allowance	5,148.15
Liquids	1	0.3 + 5% allowance	2,941.8
Fuel	1	Calculated	157,502.0
Gas Turbines	2	1.5 + 5% allowance	15,444.5
Genset	2	0.75 + 5% allowance	7,722.23

Boundary conditions are applied at global nodes and can be changed to include pinned ends, clamped ends, and rollers in the global x and z directions. Finally, all the geometric properties, loads, and boundary conditions are assembled in to a matrix using the finite element method and nodal displacements, rotations, reaction forces, reaction moments, bending stress, shear stress, principal stresses, and element failure determination are calculated. The formulas used to calculate the stresses have been summarized in the below.

$$\sigma_{bending} = \frac{Max(moment\ over\ element) * y}{Inertia} \quad \text{Equation 10}$$

$$\tau_{xy} = \frac{Max(Shear\ over\ element)*(A_{shell}*y-centroid)}{Inertia*shell\ thickness} \quad \text{Equation 11}$$

$$\sigma_1 = \frac{\sigma_{bending} + \sigma_y}{2} + \sqrt{\left(\frac{\sigma_{bending} - \sigma_y}{2}\right)^2 + \tau_{xy}^2} \quad \text{Equation 12}$$

$$\sigma_2 = \frac{\sigma_{bending} + \sigma_y}{2} - \sqrt{\left(\frac{\sigma_{bending} - \sigma_y}{2}\right)^2 + \tau_{xy}^2} \quad \text{Equation 13}$$

$$\tau_{12} = \sqrt{\left(\frac{\sigma_{bending} - \sigma_y}{2}\right)^2 + \tau_{xy}^2} \quad \text{Equation 14}$$

3.3 Reference Vessel Substructure Breakdown

The HY2-SWATH vessel large and complex, to implement the AMVS module and obtain an accurate representation of the vessel, the vessel was divided into three interdependent substructures. When the substructures are analyzed together, an accurate structure analysis of the whole vessel is obtained. The three substructures were as follows:

1. forward two struts connected via the wing-shaped superstructure
2. aft two struts connected via the wing-shaped superstructure
3. torpedo-shaped demi-hull

The below figures provide different views of vessel and help to clarify how the vessel was divided into substructures.

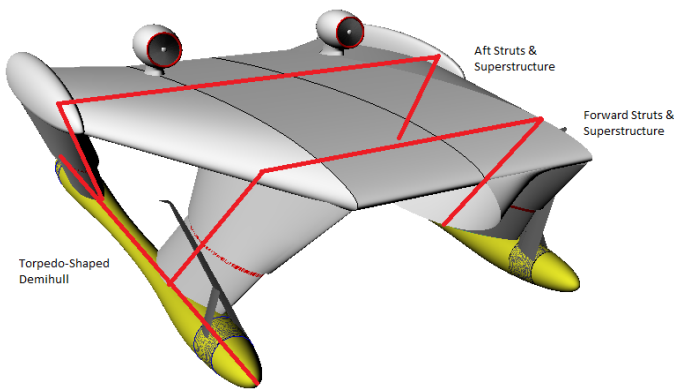


Figure 14: 3D Image of the Whole Reference Vessel

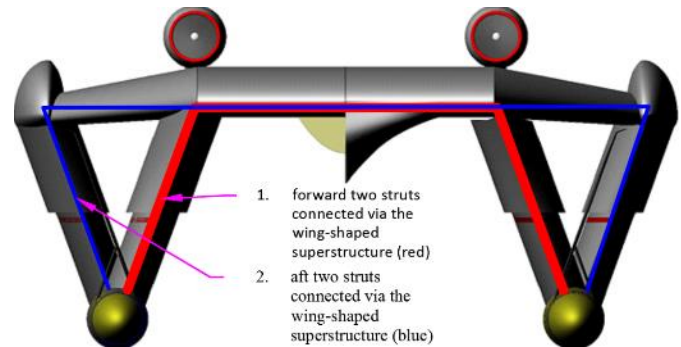


Figure 15: Whole Reference Vessel (Looking Aft)

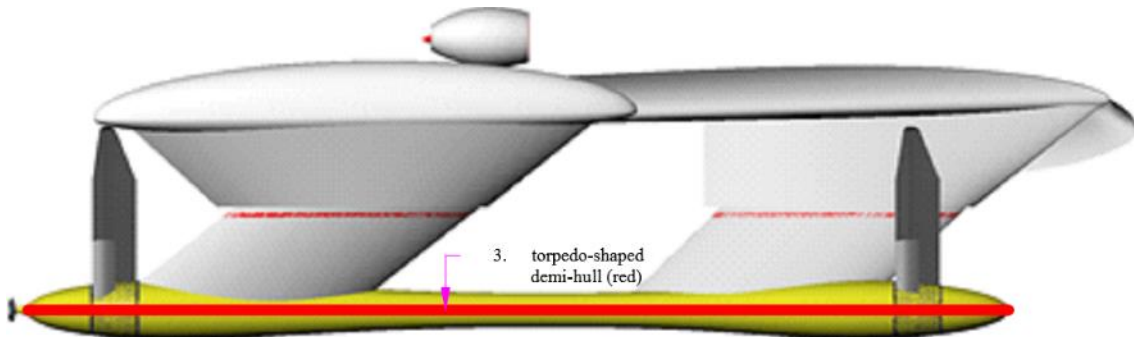


Figure 16: Profile View of Reference Vessel

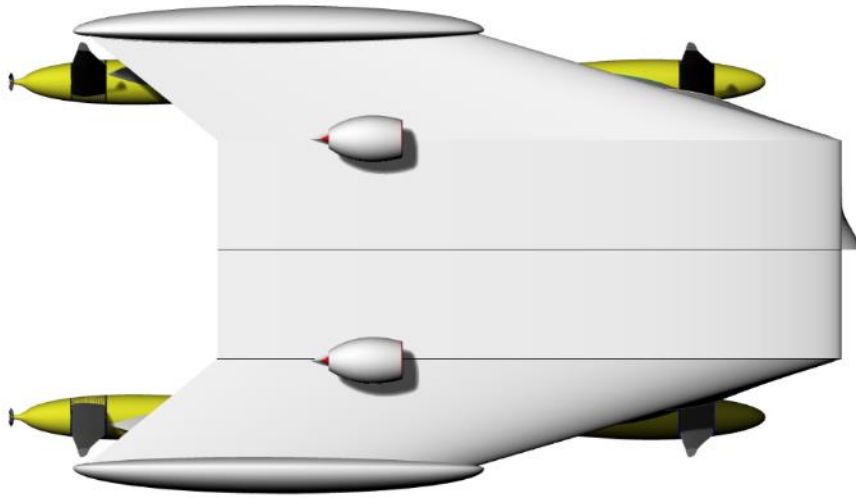


Figure 17: Top View of the Reference Vessel

Figure 14 shows the whole vessel with several lines which trace out, red lines, the three different substructures and how they are interconnected. Figure 15 shows the forward view of the whole vessel, looking aft, and shows substructures 1 and 2, as defined above, highlighted in red and blue. This is the primary view used for the analysis of these two substructures. Figure 16 shows the profile view of the vessel and the primary view for analysis of substructure 3, as defined above. Figure 17 is the top view of the vessel and helps to visualize the vessel.

Through regular discussions of the HY2-SWATH, structural details were progressively incorporated in to AMVS module calculations. To include the structural details and effectively describe the vessel, the number of elements used in each frame was increased accordingly. Sections 3.3.1 - 3.3.3 describe the frames and the elements determined necessary for analysis.

3.3.1 Substructure 1: Forward Struts with Wing-Shaped Superstructure

For the forward two struts substructure refer to Figure 18 for reference.

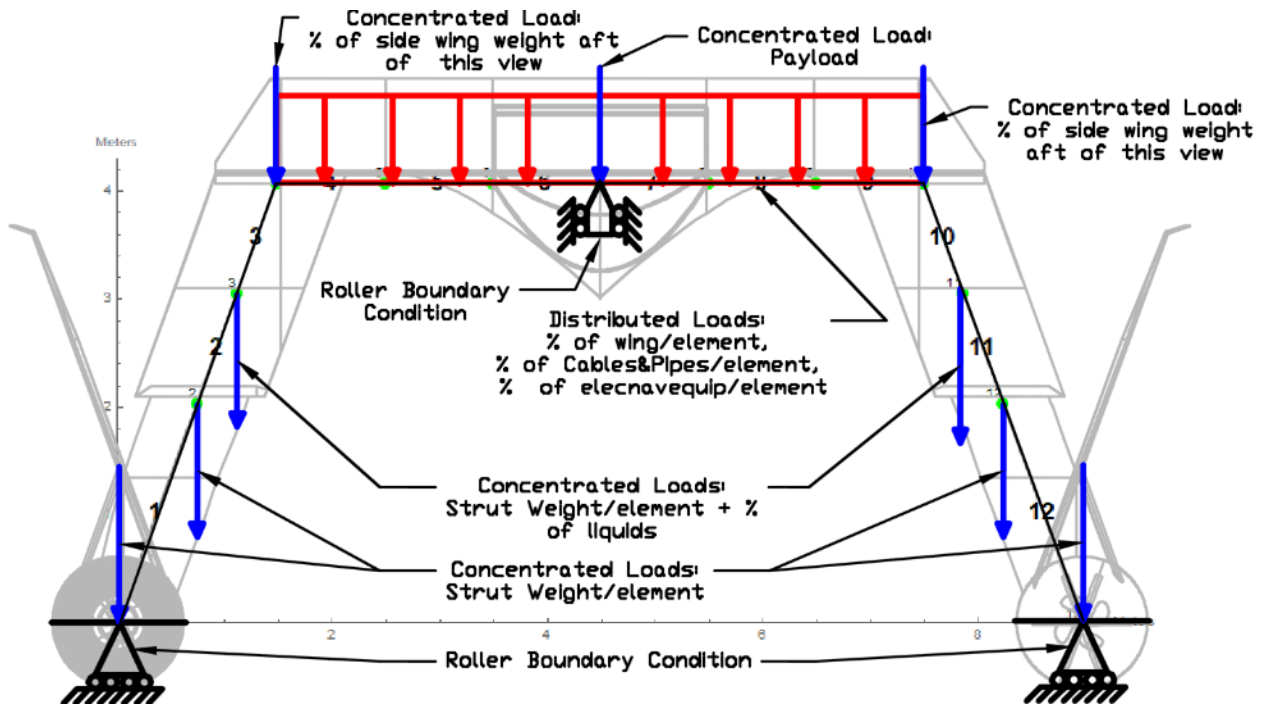


Figure 18: Forward Struts with Elements, Loads, and Boundary Conditions

This substructure was divided into 12 elements and together forms a frame. Each of the elements, global nodes, loads, and boundary conditions have been labeled and overlaid with the forward two struts drawing. Note, the aft two struts have been removed from this view to allow for better visualization. The lower struts are defined by one element each. The cross-sectional area along the length of the elements is constant. The upper struts are defined by two elements each since the upper struts are tapered and the cross-sectional area changes. The wing-shaped superstructure is defined by six elements. The element nodes are defined by the changes in cross-sectional areas to create space for the payload.

The frame has been loaded with several concentrated loads and a distributed load. The weight of each element is calculated based on the geometry properties. The weight of the strut elements have been applied as concentrated vertical loads at the node through which the entire element's weight will act. The payload is applied as a concentrated load at the center of the wing. From Figure 14 - Figure 17, it can be seen that there is a part of the superstructure that runs aft of the forward struts and connects to the aft struts to each other, i.e. the swept portion of the wing-shaped superstructure. A percentage of this structure's weight has been applied as concentrated loads at nodes 4 and 10, where the struts meet the superstructure. The percentage of the wing weight is determined as a function of the position of center of gravity of these elements in substructure 2. A percentage of the weight of the elements defining the superstructure, elements 4-9, have been applied as distributed loads across the span of the superstructure.

The percentage of these elements' weight is also determined as a function of the position of the center of gravity's location.

Figure 19 shows the element cross-sections with their respective outer shells, stiffeners, and ring stiffeners generated. While each of the elements appear to be the same dimensions, the scale on the axes varies. The struts do not have the same dimensions as the wing superstructure. Table 2 shows the elements' geometry properties which are used to calculate the deflections, rotations, moments, shears, and stresses.

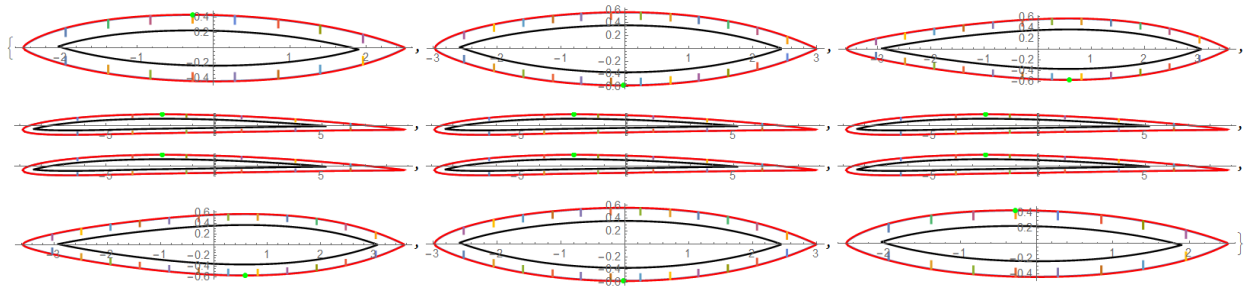


Figure 19: Forward Struts Element Cross-Sections

Table 2: Forward Struts Element Geometry Outputs												
	Centroid X (m)	Centroid Y (m)	Total Stiffener Area (m ²)	Ring Stiffener Area (m ²)	Total Shell Area (m ²)	Shell Area + Stiffener Area (m ²)	Ring Vol. (m ³)	Element Material Volume (m ³)	Element Enclosed Volume (m ³)	Structural Weight (kg)	Element Buoyancy (kg)	Residual Buoyancy (kg)
Element 1	2.490	-0.0040	0.010	1.845	0.061	0.071	0.013	0.131	5.247	368.932	5399.47	5030.54
Element 2	2.973	-0.0025	0.014	2.273	0.073	0.088	0.017	0.105	4.925	294.701	0	0
Element 3	3.575	-0.0033	0.014	2.696	0.087	0.101	0.020	0.141	6.874	396.762	0	0
Element 4	8.863	0.1902	0.007	6.370	0.211	0.218	0.047	0.265	10.946	744.307	0	0
Element 5	8.863	0.1902	0.007	6.370	0.211	0.218	0.047	0.265	10.946	744.307	0	0
Element 6	8.863	0.1902	0.007	6.370	0.211	0.218	0.047	0.265	10.946	744.307	0	0
Element 7	8.863	0.1902	0.007	6.370	0.211	0.218	0.047	0.265	10.946	744.307	0	0
Element 8	8.863	0.1902	0.007	6.370	0.211	0.218	0.047	0.265	10.946	744.307	0	0
Element 9	8.863	0.1902	0.007	6.370	0.211	0.218	0.047	0.265	10.946	744.307	0	0
Element 10	3.575	-0.0033	0.014	2.696	0.087	0.101	0.020	0.141	6.874	396.762	0	0
Element 11	2.973	-0.0025	0.014	2.273	0.073	0.088	0.017	0.105	4.925	294.701	0	0
Element 12	2.490	-0.0040	0.010	1.845	0.061	0.071	0.013	0.131	5.247	368.932	5399.47	5030.54

Figure 20, Figure 21, and Figure 22, show the how the substructure deflects, the bending moment and the shear forces due to the applied loads. Note the element deflection, has been magnified for visibility, and the element moment and shear have been scaled and superimposed on the initial frame. The deflection magnification is an input to AMVS module and can be modified easily. Also, the

superimposition of the element moments and element shears on to the frame is done automatically for each frame analyzed.

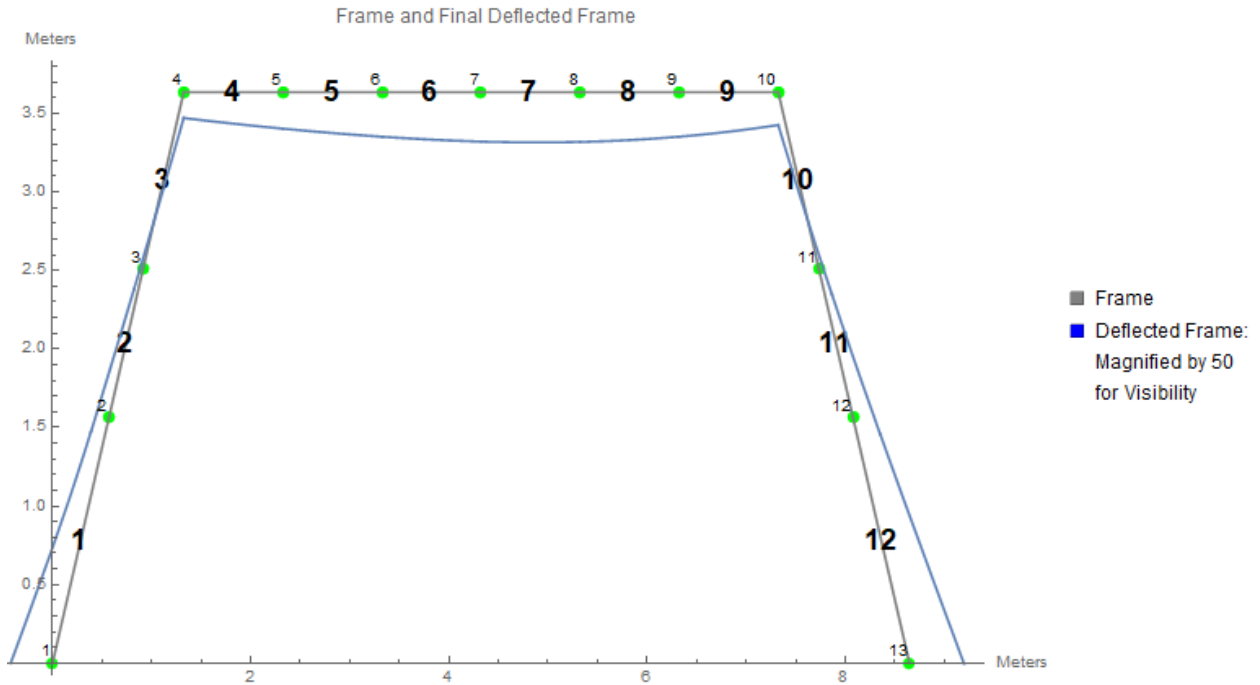


Figure 20: Forward Struts Frame and Deflected Frame

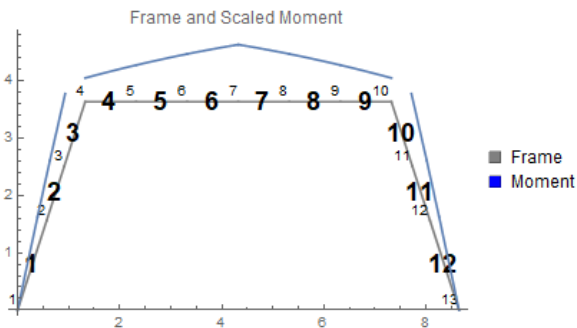


Figure 21: Forward Struts Frame and Scaled Moment

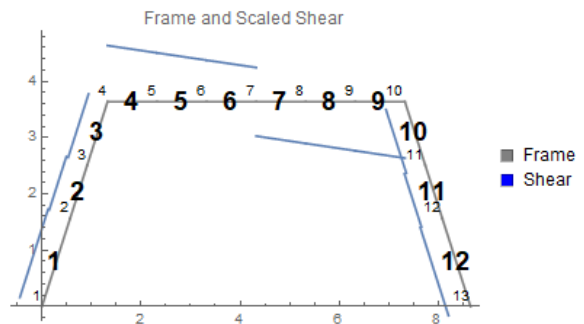


Figure 22: Forward Struts Frame and Scaled Shear

	Horizontal Displacement, u (m)	Vertical Displacement, v (m)	Rotation, Θ (rad.)	Horizontal Force, F_x (N)	Vertical Force, F_z (N)	Moment, M_y (Nm)
Global Node 1	-0.00776	0.00000	0.00344	0.00000	58001.5000	0.00000
Global Node 2	-0.00323	-0.00177	0.00187	0.00000	0.00000	0.00000
Global Node 3	-0.00160	-0.00241	0.00158	0.00000	0.00000	0.00000
Global Node 4	0.00000	-0.00303	0.00127	0.00000	0.00000	0.00000
Global Node 5	0.00000	-0.00415	0.00097	0.00000	0.00000	0.00000
Global Node 6	0.00000	-0.00495	0.00061	0.00000	0.00000	0.00000
Global Node 7	0.00000	-0.00533	0.00012	0.00000	0.00000	0.00000
Global Node 8	0.00000	-0.00511	-0.00054	0.00000	0.00000	0.00000
Global Node 9	0.00000	-0.00428	-0.00109	0.00000	0.00000	0.00000
Global Node 10	0.00000	-0.00295	-0.00153	0.00000	0.00000	0.00000
Global Node 11	0.00200	-0.00219	-0.00201	0.00000	0.00000	0.00000
Global Node 12	0.00405	-0.00142	-0.00231	0.00000	0.00000	0.00000
Global Node 13	0.00784	0.00000	-0.00250	0.00000	58001.5000	0.00000

	Total Stiffener Ix (m ⁴)	Total Ix (m ⁴)	Bending Stress, σ_x (Pa)	Shear Stress, τ_{xy} (Pa)	σ_1 (Pa)	SF*Abs(σ_1) > σ_{yield}	σ_2 (Pa)	SF*Abs(σ_2) > σ_{yield}	τ_{max} (Pa)	SF*Abs(τ_{max}) > τ_{yield}
Element 1	0.00089	0.00762	1748050	-98785	1753620	FALSE	-5564.75	FALSE	879590	FALSE
Element 2	0.00235	0.01605	1735470	-53198	1737100	FALSE	-1629.19	FALSE	869366	FALSE
Element 3	0.00225	0.01805	2149060	-51010	2150270	FALSE	-1210.07	FALSE	1075740	FALSE
Element 4	0.00069	0.02165	2509480	-255855	2535300	FALSE	-25820.0	FALSE	1280560	FALSE
Element 5	0.00069	0.02165	3276210	-223255	3291350	FALSE	-15143.6	FALSE	1653250	FALSE
Element 6	0.00069	0.02165	3922160	-190656	3931410	FALSE	-9245.94	FALSE	1970330	FALSE
Element 7	0.00069	0.02165	3922160	158056	3928520	FALSE	-6359.07	FALSE	1967440	FALSE
Element 8	0.00069	0.02165	3276210	190656	3287270	FALSE	-11057.7	FALSE	1649160	FALSE
Element 9	0.00069	0.02165	2509480	223255	2529190	FALSE	-19707.1	FALSE	1274450	FALSE
Element 10	0.00225	0.01805	2149060	51010	2150270	FALSE	-1210.07	FALSE	1075740	FALSE
Element 11	0.00235	0.01605	1735470	-53198	1737100	FALSE	-1629.19	FALSE	869366	FALSE
Element 12	0.00089	0.00762	1748050	-98785	1753620	FALSE	-5564.75	FALSE	879590	FALSE

Table 3 and Table 4 are generated outputs. Table 3 shows the element displacements, rotation, reaction forces and reaction moments due the loading conditions. Table 4 shows the stress, shear stress, and principal stress calculation results. A safety factor (SF) of 6 was applied to the principle stresses and compared with the yield stresses to determine if the element failed. An output of “False” indicates that the element did not fail due to the stresses. It is important to see that the table only displays “False” for the reference HY2-SWATH substructure frame.

3.3.2 Substructure 2: Aft Struts with Wing-Shaped Superstructure

The aft two struts substructure frame is set up in a similar way as the forward two struts. Figure 23 can be used to reference the setup.

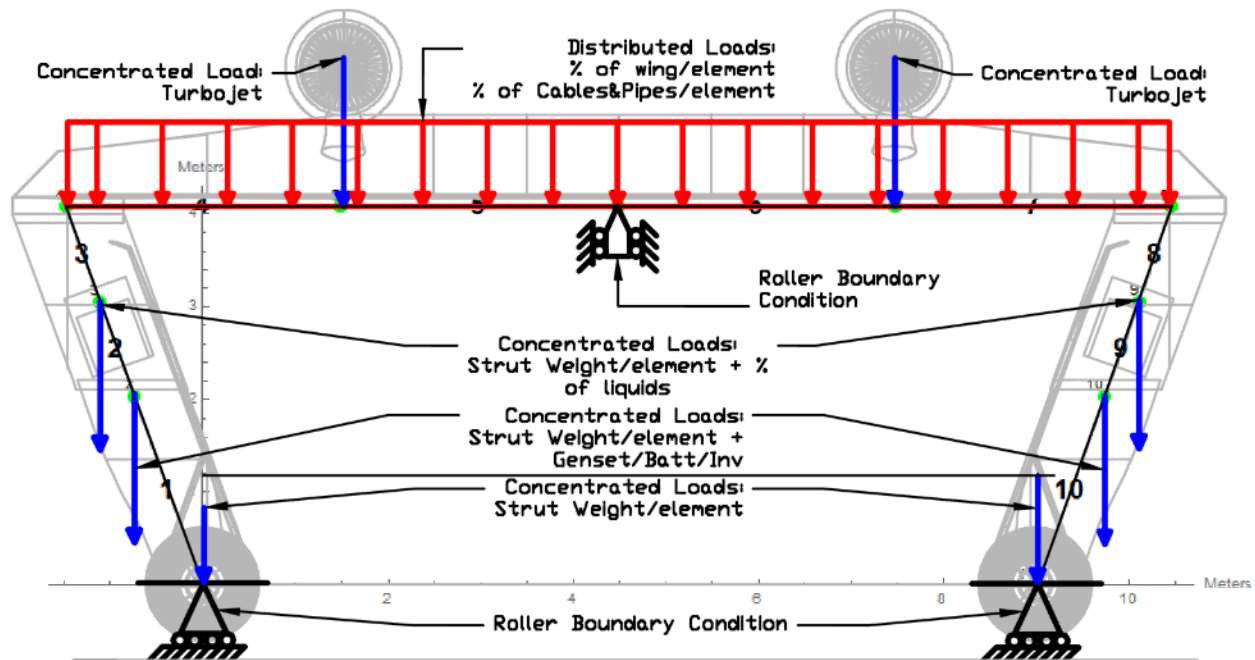


Figure 23: Aft Struts with Elements, Loads, and Boundary Conditions

This substructure was divided into 10 elements and together forms the substructure frame. Each of the elements, global nodes, loads, and boundary conditions have been labeled and overlaid with the forward aft struts drawing. Note, the forward two struts have been removed from this view for better visualization. The lower struts are defined by one element each. The cross-sectional area along the length of the elements is constant. The upper struts are defined by two elements each since the upper struts are tapered and the cross-sectional area changes. The wing-shaped superstructure is defined by four elements. The element nodes are defined by the changes in cross-sectional areas and concentrated load locations.

The frame has been loaded with several concentrated loads and a distributed load. The weight of each element is calculated based on the geometry properties. The weight of the strut elements have been applied as concentrated vertical loads at the node through which the entire element's weight will act. The turbojets have been applied as concentrated loads as placed on the reference vessel and shown in Figure 23. A percentage of weight of the superstructure and cables and piping has been as distributed loads over the span of the superstructure, elements 4-7. The percentage of the weight is determined as a function of the center of gravity of the elements' location.

Figure 24 - Figure 27 and Table 5 - Table 7 show the same information as described in Figure 19 - Figure 22 and Table 2- Table 4 as applied to aft strut substructure frame.

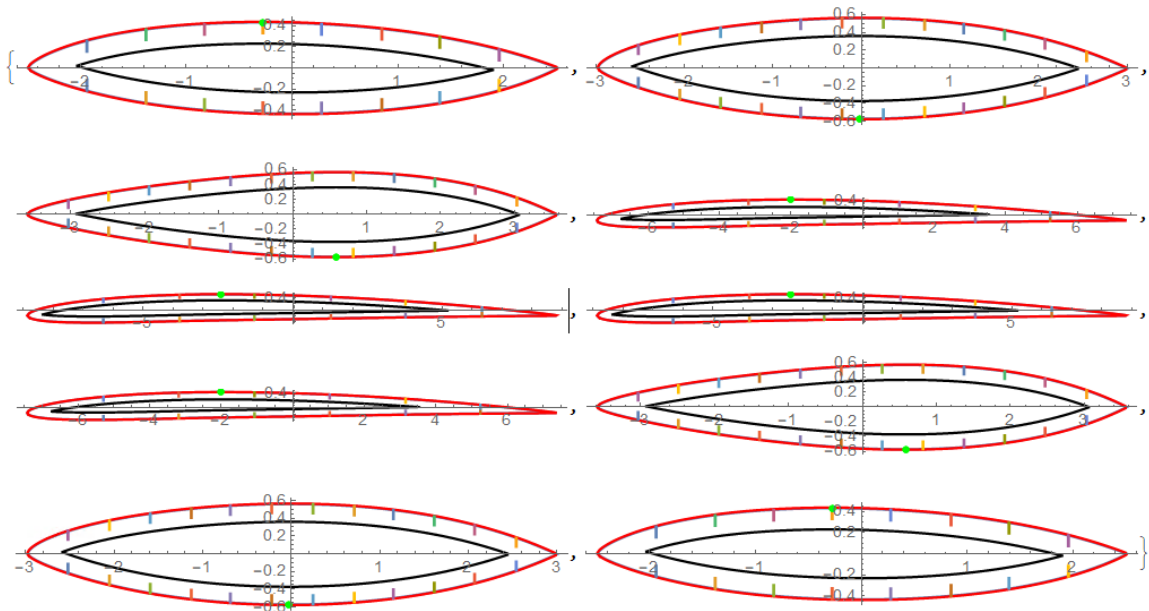


Figure 24: Aft Struts Element Cross-Sections

Table 5: Aft Struts Element Geometry Outputs

	Centroid X (m)	Centroid Y (m)	Total Stiffener Area (m ²)	Ring Stiffener Area (m ²)	Total Shell Area (m ²)	Shell Area + Stiffener Area (m ²)	Ring Vol. (m ³)	Element Material Volume (m ³)	Element Enclosed Volume (m ³)	Structural Weight (kg)	Element Buoyancy (kg)	Residual Buoyancy (kg)
element 1	2.490	-0.0040	0.010	1.845	0.061	0.071	0.013	0.131	5.247	368.932	5399.47	5030.54
element 2	2.973	-0.0025	0.014	2.273	0.073	0.088	0.017	0.105	4.925	294.701	0	0
element 3	3.575	-0.0033	0.014	2.696	0.087	0.101	0.020	0.141	6.874	396.762	0	0
element 4	7.415	0.1544	0.007	5.162	0.176	0.183	0.038	0.523	19.809	1470.48	0	0
element 5	8.863	0.1902	0.007	6.370	0.211	0.218	0.140	0.795	32.838	2232.92	0	0
element 6	8.863	0.1902	0.007	6.370	0.211	0.218	0.140	0.795	32.838	2232.92	0	0
element 7	7.415	0.1544	0.007	5.162	0.176	0.183	0.038	0.523	19.809	1470.48	0	0
element 8	3.575	-0.0033	0.014	2.696	0.087	0.101	0.020	0.141	6.874	396.762	0	0
element 9	2.973	-0.0025	0.014	2.273	0.073	0.088	0.017	0.105	4.925	294.701	0	0
element 10	2.490	-0.0040	0.010	1.845	0.061	0.071	0.013	0.131	5.247	368.932	5399.47	5030.54

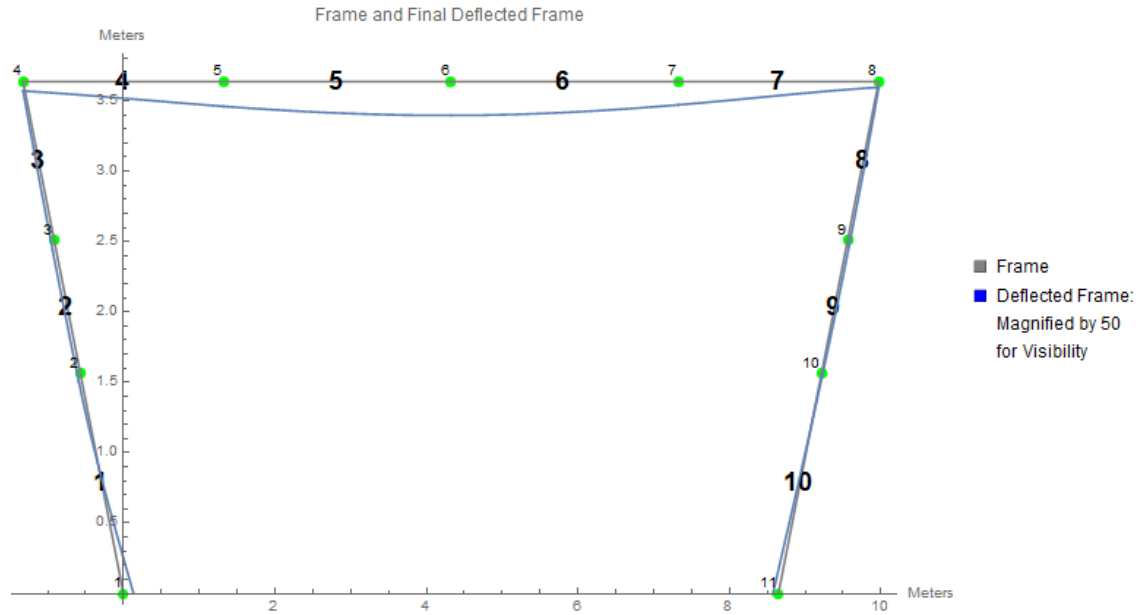


Figure 25: Aft Struts Frame and Deflected Frame

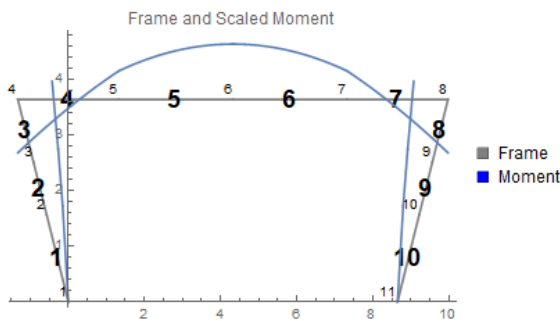


Figure 26: Aft Struts Frame and Scaled Moment

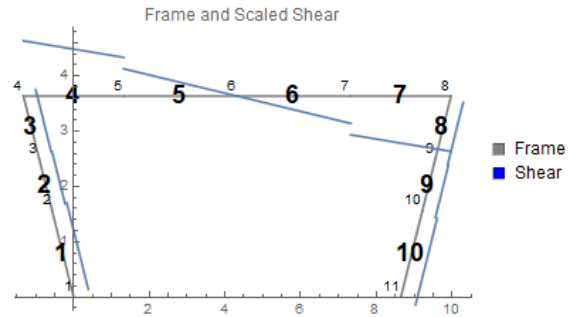


Figure 27: Aft Struts Frame and Scaled Shear

Table 6: Aft Struts Global Node Displacement and Reaction Forces

	Horizontal Displacement, u (m)	Vertical Displacement, v (m)	Rotation, Θ (rad.)	Horizontal Force, F_x (N)	Vertical Force, F_z (N)	Moment, M_y (Nm)
Global Node 1	0.00301	0.00000	-0.00293	0.00000	91102.30000	0.0000
Global Node 2	-0.00019	-0.00137	-0.00040	0.00000	0.00000	0.0000
Global Node 3	-0.00034	-0.00148	0.00006	0.00000	0.00000	0.0000
Global Node 4	0.00000	-0.00141	0.00055	0.00000	0.00000	0.0000
Global Node 5	0.00000	-0.00343	0.00073	0.00000	0.00000	0.0000
Global Node 6	0.00000	-0.00450	-0.00009	0.00000	0.00000	0.0000
Global Node 7	0.00000	-0.00276	-0.00099	0.00000	0.00000	0.0000
Global Node 8	0.00000	-0.00003	-0.00076	0.00000	0.00000	0.0000
Global Node 9	0.00057	-0.00020	-0.00026	0.00000	0.00000	0.0000
Global Node 10	0.00067	-0.00020	0.00006	0.00000	0.00000	0.0000
Global Node 11	0.00031	0.00000	0.00034	0.00000	91102.30000	0.0000

	Total Stiffener Ix (m ⁴)	Total Ix (m ⁴)	Bending Stress, σ_x (Pa)	Shear Stress, τ_{xy} (Pa)	σ_1 (Pa)	SF*Abs(σ_1) > σ_{yield}	σ_2 (Pa)	SF*Abs(σ_2) > σ_{yield}	τ_{max} (Pa)	SF*Abs(τ_{max}) > τ_{yield}
Element 1	0.00089	0.00762	0	158910	158910	FALSE	-158910	FALSE	158910	FALSE
Element 2	0.00235	0.01605	1775350	79417	1778890	FALSE	-3545.49	FALSE	891219	FALSE
Element 3	0.00225	0.01805	2413080	78631	2415640	FALSE	-2559.50	FALSE	1209100	FALSE
Element 4	0.00043	0.01366	1761400	-616360	1955660	FALSE	-194257.	FALSE	1074960	FALSE
Element 5	0.00069	0.02165	2632880	-228448	2652560	FALSE	-19674.8	FALSE	1336120	FALSE
Element 6	0.00069	0.02165	2632880	0	2632880	FALSE	0.00	FALSE	1316440	FALSE
Element 7	0.00043	0.01366	1761400	434054	1862560	FALSE	-101153	FALSE	981854	FALSE
Element 8	0.00225	0.01805	2413080	-78631	2415640	FALSE	-2559.50	FALSE	1209100	FALSE
Element 9	0.00235	0.01605	1775350	-79417	1778890	FALSE	-3545.49	FALSE	891219	FALSE
Element 10	0.00089	0.00762	0	-158910	158910	FALSE	-158910	FALSE	158910	FALSE

As was the case in Table 4, Table 7 also only displays “False” for the stress comparison to the yield stress. The display of only “false” indicates that this reference HY2-SWATH substructure frame does not fail structurally either.

3.3.3 Substructure 3: Torpedo-Shaped Hull

The torpedo-shaped hull was analyzed by the AMVS module under two different loading conditions. The two loading conditions are buoyancy mode, and flying mode. Buoyancy mode is when the hydrofoils are retracted and the vessel is stationary or traveling between 8 - 25 knots. Flying mode is when the hydrofoils are deployed and vessel is traveling at 120+ knots. Figure 28 and Figure 34 can be used to reference the setup.

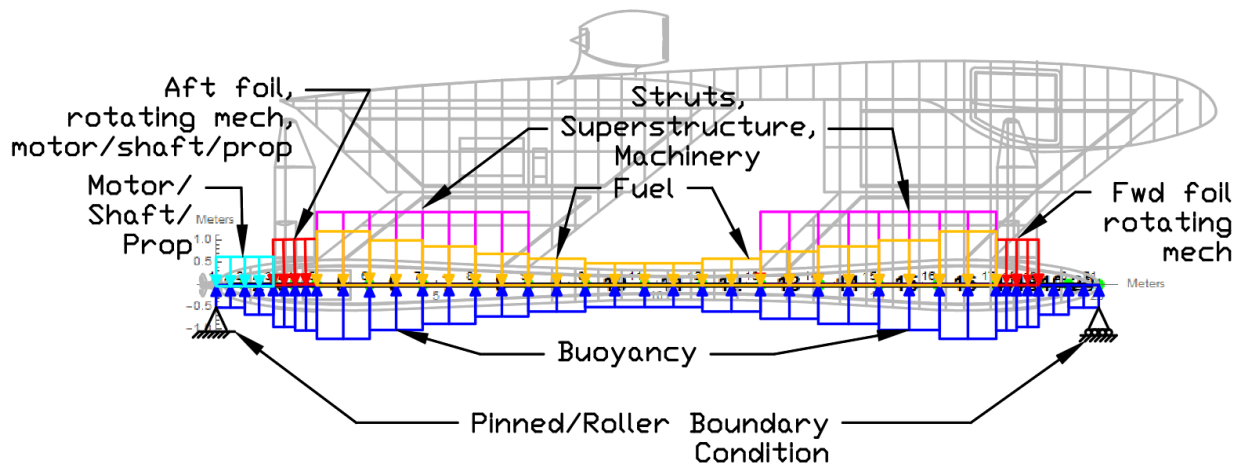


Figure 28: Hull with Elements, Loads, and BCs (Buoyancy Mode)

For both of these loading conditions the frame was constructed using 20 elements. This frame required more elements than the other two substructure frames due the changes in loading conditions across the length of the substructure and due to the variation in hull shape i.e. cross-sectional shape across the length of the hull.

In this case, the reference vessel hull was derived and provided in the form of a data points and used to generate a Bezier curve, Figure 29.

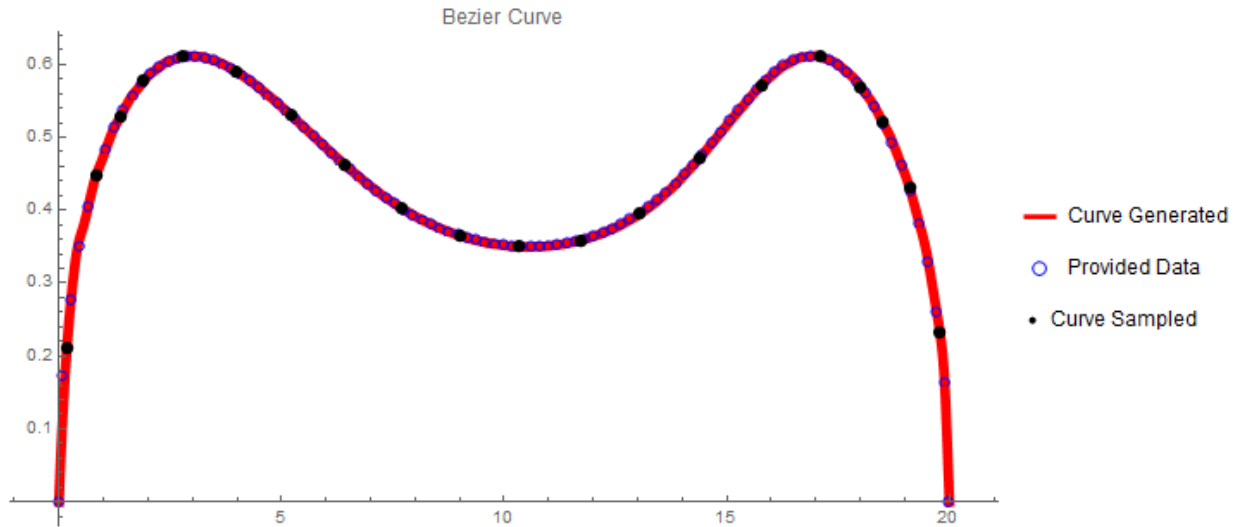


Figure 29: Hull Bezier Curve

The blue circles on the curve are the data points obtained from the reference vessel model. The red line is a Bezier curve generated using the data points and the black dots are where the curve was sampled, at the midpoint of each element, to obtain the input radius of the hull cross-sections for each element. The code has been setup to generate ellipse-shaped hull cross-sections; however, the original reference vessel used circular cross-sections as shown in Figure 30. Note, there are many cross-sections shown in Figure 30. To show them all, the images are shown as the same size and appear to have the same diameter, however, specific inspection of the x- and y-axis will show that they all have different diameters and are in accordance with the y-axis values of the black dots (curve sampled) shown in the Bezier Curve (Figure 29). Additionally, elements 3, 4, 17, and 18 do not have the inner black line representing the ring stiffener. These elements are the forward and aft boundaries of the hydrofoils and have been designed and calculated as watertight bulkheads.

After the obtaining the element cross-sections the frame is loaded using several distributed loads. The elements are numbered from left to right, stern to bow, and as oriented in Figure 28 and Figure 34. In the buoyancy mode loading condition, all elements are submerged under water and loaded with the

elements respective upward buoyancy distributed force as determined by the cross-section volume multiplied by the element length. Elements 1-4 are loaded down with the motor/shaft/prop machinery. Elements 3 - 4 are additionally loaded with the aft foil and aft rotating mechanism. In the reference vessel case, elements 5-16 are filled with jet propulsion fuel as permitted by internal element volume availability. The elements containing fuel is a parametric input. Elements 5 - 8 and 13 - 16 are additionally loaded with the weight of the struts, superstructure, and machinery. Elements 5 - 8 are loaded as determined by the reaction forces calculated from the aft strut substructure analysis. Similarly, elements 13-16 are loaded as determined by the reaction forces calculated from the forward strut substructure analysis. Lastly, elements 17-18 are loaded with the fore foil and forward foil rotating mechanism.

The flying mode loading condition has been loaded exactly the same, however, the hulls are no longer submerged under water and therefore the buoyancy force has been removed. Additionally, simple support boundary conditions have been located on global nodes 4 and 17, as hydrofoils will support the whole vessel and provide an upward force.

Table 8: Hull Element Geometry Outputs

	Centroid X (m)	Centroid Y (m)	Total Stiffener Area (m ²)	Ring Stiffener Area (m ²)	Total Shell Area (m ²)	Shell Area + Stiffener Area (m ²)	Ring Vol. (m ³)	Element Material Volume (m ³)	Element Enclosed Volume (m ³)	Structural Weight (kg)	Element Buoyancy (kg)	Residual Buoyancy (kg)
element 1	0.212	0.0000	0.002	0.059	0.008	0.010	0.000	0.007	0.096	19.1958	99.228	80.0322
element 2	0.447	0.0000	0.002	0.133	0.017	0.019	0.001	0.013	0.419	36.8134	430.748	393.935
element 3	0.528	0.0000	0.002	0.877	0.020	0.022	0.006	0.017	0.439	47.9009	451.947	404.046
element 4	0.577	0.0000	0.002	1.047	0.022	0.024	0.008	0.019	0.523	53.9018	538.523	484.621
element 5	0.611	0.0000	0.002	0.184	0.023	0.025	0.001	0.031	1.434	87.422	1475.12	391.969
element 6	0.590	0.0000	0.002	0.178	0.022	0.024	0.001	0.030	1.339	84.6901	1377.89	363.869
element 7	0.530	0.0000	0.002	0.159	0.020	0.022	0.001	0.027	1.084	76.7882	1115.5	288.43
element 8	0.462	0.0000	0.002	0.137	0.026	0.028	0.001	0.035	0.835	97.5478	859.724	193.622
element 9	0.402	0.0000	0.002	0.119	0.031	0.033	0.001	0.044	0.708	122.488	728.488	134.299
element 10	0.365	0.0000	0.002	0.107	0.028	0.030	0.001	0.040	0.586	111.924	603.434	103.426
element 11	0.350	0.0000	0.002	0.102	0.027	0.029	0.001	0.038	0.541	107.718	556.931	92.1533
element 12	0.359	0.0000	0.002	0.105	0.027	0.029	0.001	0.039	0.567	110.129	583.363	98.5453
element 13	0.395	0.0000	0.002	0.116	0.030	0.032	0.001	0.044	0.694	122.26	714.011	129.982
element 14	0.471	0.0000	0.002	0.140	0.027	0.029	0.001	0.039	0.965	110.123	993.1	225.572
element 15	0.571	0.0000	0.002	0.172	0.022	0.023	0.001	0.032	1.398	91.0453	1438.04	377.765
element 16	0.611	0.0000	0.002	0.184	0.023	0.025	0.001	0.034	1.594	96.7783	1639.89	436.055
element 17	0.569	0.0000	0.002	1.016	0.021	0.023	0.007	0.019	0.497	52.1386	511.507	459.368
element 18	0.520	0.0000	0.002	0.850	0.020	0.021	0.006	0.016	0.416	46.2725	428.485	382.212
element 19	0.431	0.0000	0.002	0.127	0.016	0.018	0.001	0.013	0.410	37.4358	422.169	384.733
element 20	0.233	0.0000	0.002	0.065	0.009	0.011	0.000	0.008	0.123	21.9333	126.9	104.967

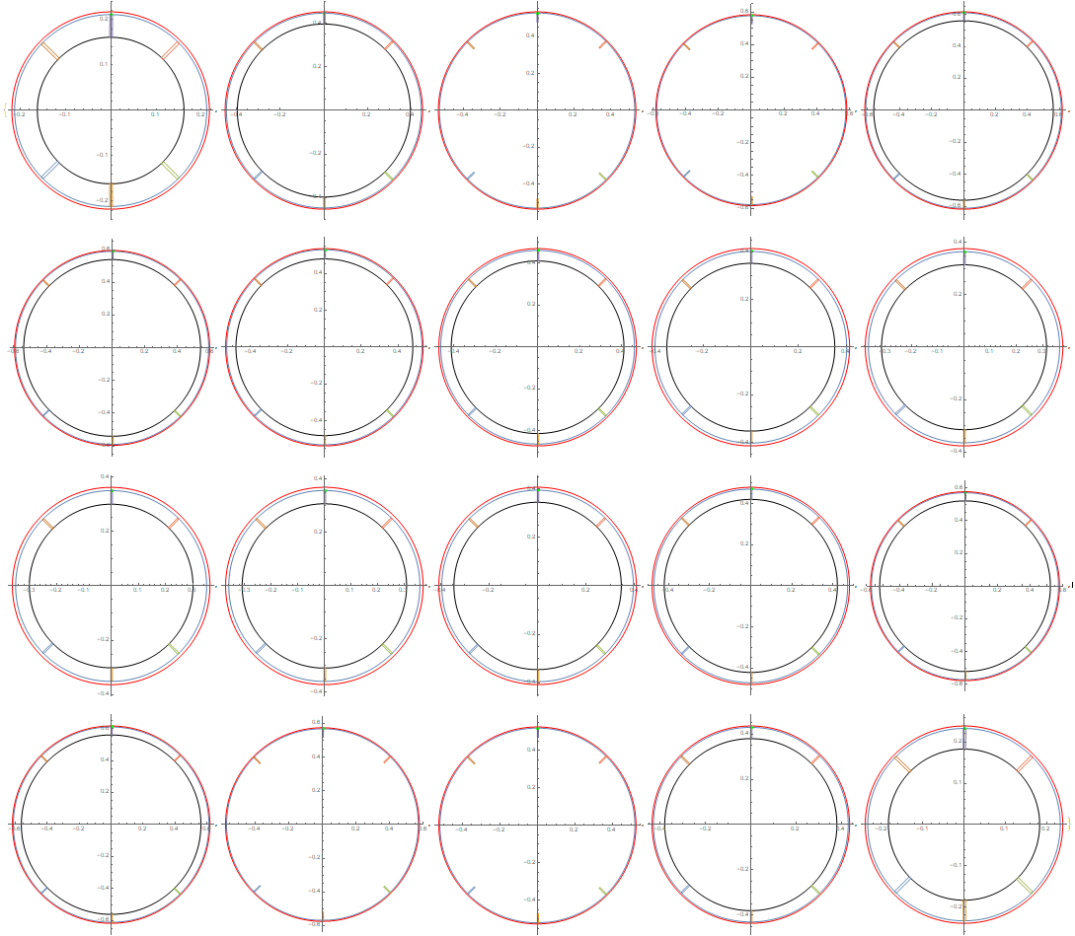


Figure 30: Hull Element Cross-Sections

Buoyancy Mode Results

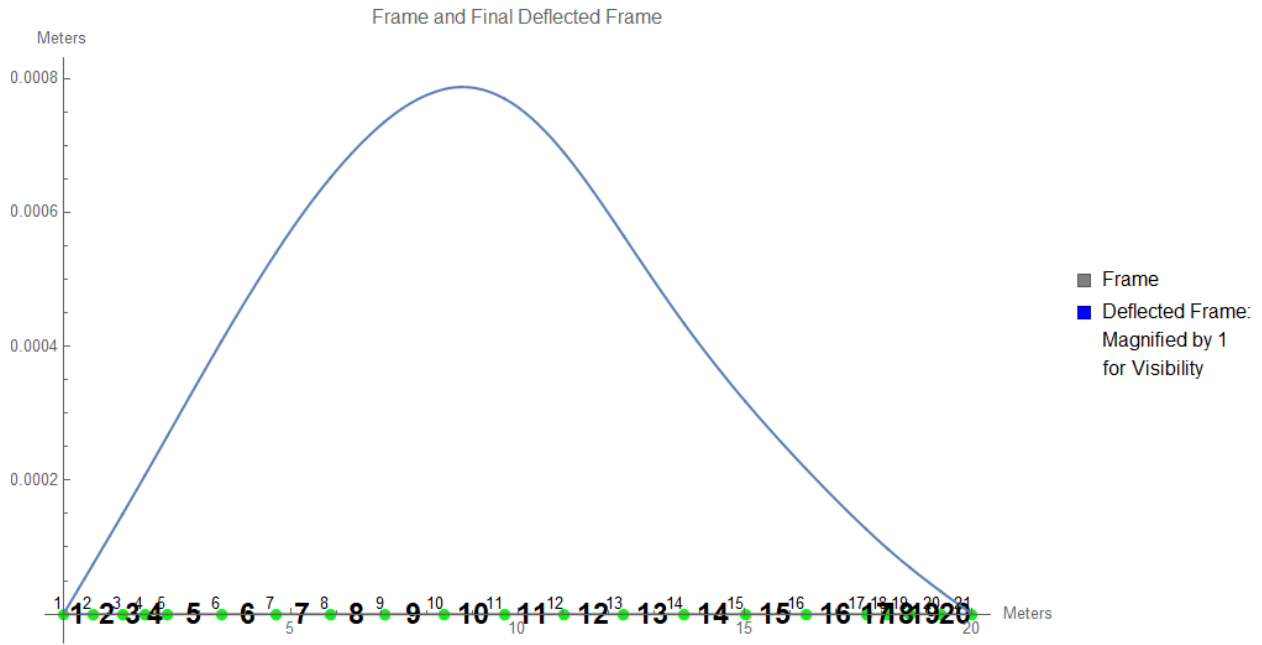


Figure 31: Hull Frame and Deflected Frame

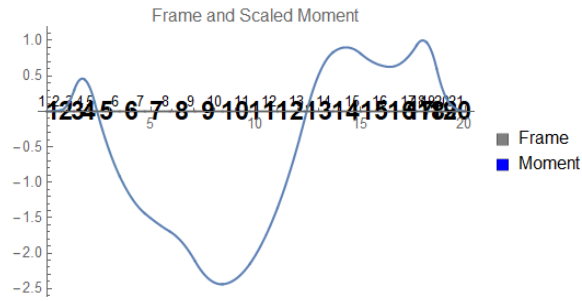


Figure 32: Hull Frame and Scaled Moment

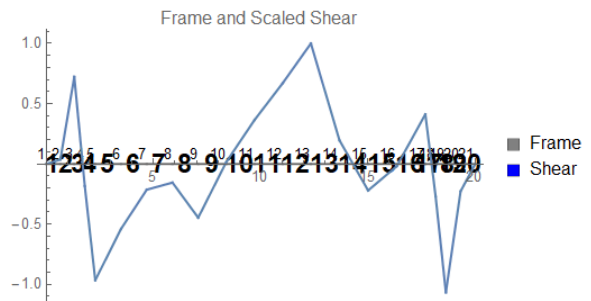


Figure 33: Hull Frame and Scaled Shear

Table 9: Hull Global Node Displacement and Reaction Forces (Buoyancy Mode)						
	Horizontal Displacement, u (m)	Vertical Displacement, v (m)	Rotation, Θ (rad.)	Horizontal Force, F_x (N)	Vertical Force, F_z (N)	Moment, M_y (Nm)
Global Node 1	0	0.00000	-0.00011	0	0	0
Global Node 2	0	0.00007	-0.00011	0	0	0
Global Node 3	0	0.00015	-0.00012	0	0	0
Global Node 4	0	0.00021	-0.00012	0	0	0
Global Node 5	0	0.00027	-0.00012	0	0	0
Global Node 6	0	0.00041	-0.00012	0	0	0
Global Node 7	0	0.00054	-0.00010	0	0	0
Global Node 8	0	0.00065	-0.00008	0	0	0
Global Node 9	0	0.00074	-0.00006	0	0	0
Global Node 10	0	0.00078	-0.00002	0	0	0
Global Node 11	0	0.00077	0.00004	0	0	0
Global Node 12	0	0.00069	0.00008	0	0	0
Global Node 12	0	0.00056	0.00010	0	0	0
Global Node 13	0	0.00043	0.00009	0	0	0
Global Node 14	0	0.0003	0.000	0	0	0
Global Node 15	0	0.0002	0.000	0	0	0
Global Node 16	0	0.0001	0.000	0	0	0
Global Node 17	0	0.0001	0.000	0	0	0
Global Node 18	0	0.0001	0.000	0	0	0
Global Node 19	0	0.0000	0.000	0	0	0
Global Node 20	0	0.0000	0.000	0	0	0
Global Node 21	0	0.00000	-0.00011	0	0	0

Table 10: Hull Stress and Failure Analysis (Buoyancy Mode)

	Total Stiffener Ix (m ⁴)	Total Ix (m ⁴)	Bending Stress, σ_x (Pa)	Shear Stress, τ_{xy} (Pa)	σ_1 (Pa)	SF*Abs(σ_1) > σ_{yield}	σ_2 (Pa)	SF*Abs(σ_2) > σ_{yield}	τ_{max} (Pa)	SF*Abs(τ_{max}) > τ_{yield}
Element 1	0.000042	0.00023	32752.30	0	32752	FALSE	0.00	FALSE	16376.20	FALSE
Element 2	0.000214	0.00193	177903.00	0	177903	FALSE	0.00	FALSE	88951.30	FALSE
Element 3	0.000303	0.00312	200956.00	0	200956	FALSE	0.00	FALSE	100478.00	FALSE
Element 4	0.000365	0.00403	166016.00	0	166016	FALSE	0.00	FALSE	83008.10	FALSE
Element 5	0.000411	0.00474	41681.10	0	41681	FALSE	0.00	FALSE	20840.60	FALSE
Element 6	0.000382	0.00429	323929.00	0	323929	FALSE	0.00	FALSE	161965.00	FALSE
Element 7	0.000306	0.00315	622459.00	0	622459	FALSE	0.00	FALSE	311230.00	FALSE
Element 8	0.000229	0.00309	651340.00	0	651340	FALSE	0.00	FALSE	325670.00	FALSE
Element 9	0.000171	0.00273	799204.00	0	799204	FALSE	0.00	FALSE	399602.00	FALSE
Element 10	0.000139	0.00206	976961.00	0	976961	FALSE	0.00	FALSE	488481.00	FALSE
Element 11	0.000127	0.00183	669588.00	0	669588	FALSE	0.000	FALSE	334794.00	FALSE
Element 12	0.000133	0.00196	43116.90	0	43117	FALSE	0.000	FALSE	21558.50	FALSE
Element 13	0.000164	0.00259	325543.00	0	325543	FALSE	0.000	FALSE	162772.00	FALSE
Element 14	0.000238	0.00327	333987.00	0	333987	FALSE	0.000	FALSE	166993.00	FALSE
Element 15	0.000358	0.0039	304773.00	0	304773	FALSE	0.000	FALSE	152386.00	FALSE
Element 16	0.000411	0.0047	308032.00	0	308032	FALSE	0.000	FALSE	154016.00	FALSE
Element 17	0.000354	0.0039	378577.00	0	378577	FALSE	0.000	FALSE	189288.00	FALSE
Element 18	0.000294	0.0030	435446.00	0	435446	FALSE	0.000	FALSE	217723.00	FALSE
Element 19	0.000197	0.0017	385440.00	0	385440	FALSE	0.000	FALSE	192720.00	FALSE
Element20	0.000052	0.0003	179186.00	0	179186	FALSE	0.000	FALSE	89593.00	FALSE

As was the case in Table 4 and Table 7, Table 10 also only displays “False” for the stress comparison to the yield stress. The display of only “false” indicates that this reference HY2-SWATH substructure frame does not fail in buoyancy mode either.

Flying Mode Results

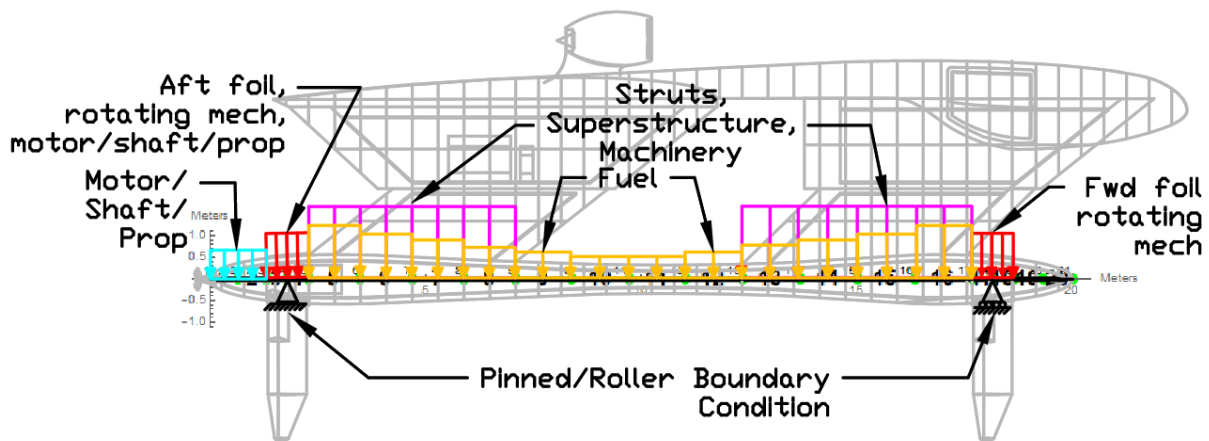


Figure 34: Hull with Elements, Loads, and BCs (Flying Mode)

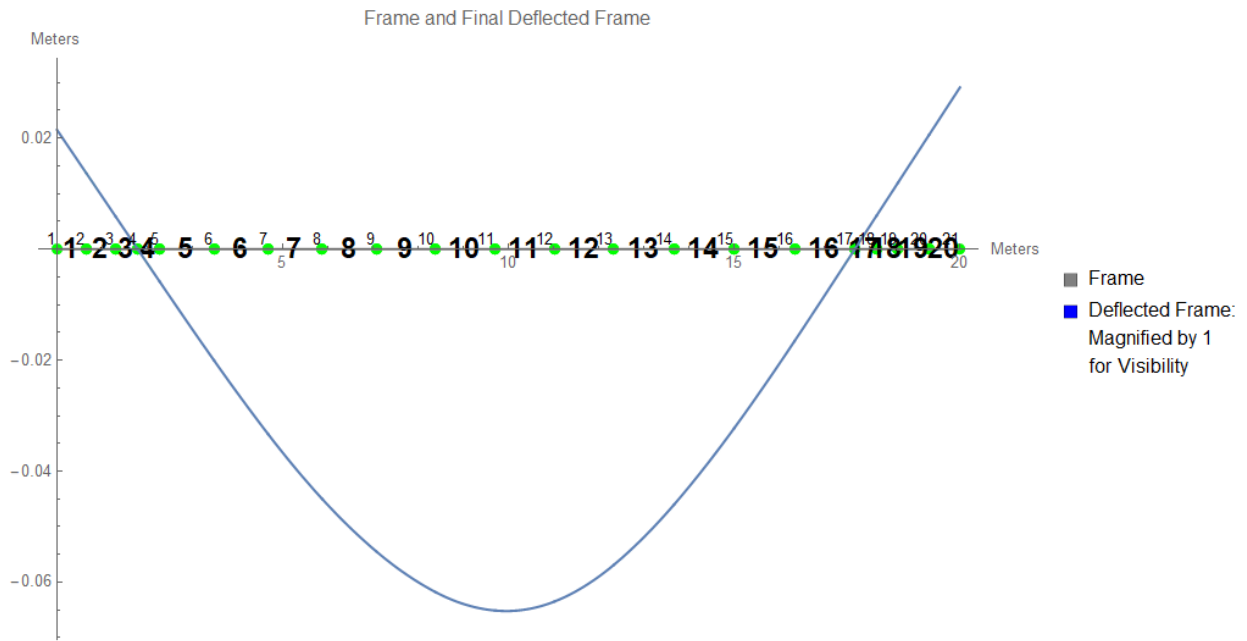


Figure 35: Hull Frame and Deflected Frame

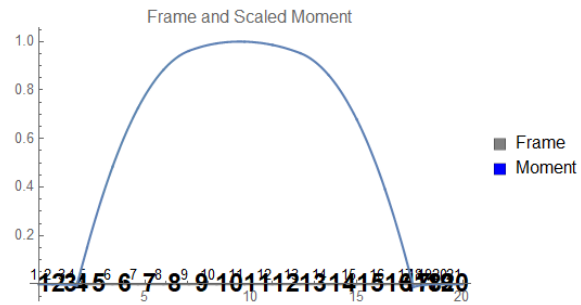


Figure 36: Hull Frame and Scaled Moment

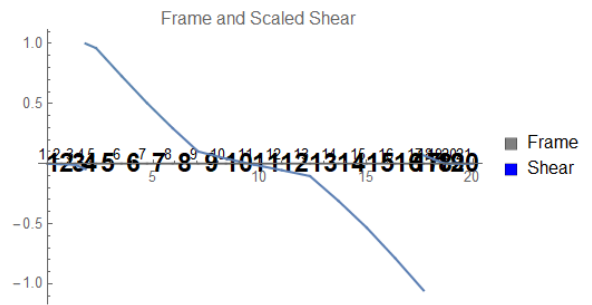


Figure 37: Hull Frame and Scaled Shear

Table 11: Hull Global Node Displacement and Reaction Forces (Flying Mode)						
	Horizontal Displacement, u (m)	Vertical Displacement, v (m)	Rotation, Θ (rad.)	Horizontal Force, F_x (N)	Vertical Force, F_z (N)	Moment, M_y (Nm)
Global Node 1	0	0.021481	0.012019	0	0	0.000000
Global Node 2	0	0.013685	0.012021	0	0	0.000000
Global Node 3	0	0.005888	0.012023	0	0	0.000000
Global Node 4	0	0.000000	0.012026	0	135970	0.000000
Global Node 5	0	-0.005881	0.011976	0	0	0.000000
Global Node 6	0	-0.020028	0.011522	0	0	0.000000
Global Node 7	0	-0.033324	0.010575	0	0	0.000000
Global Node 8	0	-0.045023	0.008865	0	0	0.000000
Global Node 9	0	-0.054481	0.006869	0	0	0.000000
Global Node 10	0	-0.061804	0.004263	0	0	0.000000
Global Node 11	0	-0.065096	0.000744	0	0	0.000000
Global Node 12	0	-0.063470	-0.003210	0	0	0.000000
Global Node 12	0	-0.056872	-0.006812	0	0	-0.000003
Global Node 13	0	-0.046013	-0.009419	0	0	0.000000
Global Node 14	0	-0.032223	-0.011178	0	0	-0.000004
Global Node 15	0	-0.016561	-0.012203	0	0	0.000004
Global Node 16	0	0.000000	-0.012512	0	146277	-0.000020
Global Node 17	0	0.005991	-0.012507	0	0	-0.000054
Global Node 18	0	0.011981	-0.012506	0	0	-0.000029
Global Node 19	0	0.020553	-0.012505	0	0	-0.000003
Global Node 20	0	0.029125	-0.012504	0	0	0.000002
Global Node 21	0	0.021481	0.012019	0	0	0.000000

Table 12: Hull Stress and Failure Analysis (Flying Mode)

	Total Stiffener Ix (m ⁴)	Total Ix (m ⁴)	Bending Stress, σ_x (Pa)	Shear Stress, τ_{xy} (Pa)	σ_1 (Pa)	SF*Abs(σ_1) > σ_{yield}	σ_2 (Pa)	SF*Abs(σ_2) > σ_{yield}	τ_{max} (Pa)	SF*Abs(τ_{max}) > τ_{yield}
Element 1	0.000042	0.000228	0.0	0.00000	0	FALSE	0	FALSE	0.00	FALSE
Element 2	0.000214	0.001927	37920.5	0.00001	37921	FALSE	0	FALSE	18960.20	FALSE
Element 3	0.000303	0.003117	117249.0	0.00002	117249	FALSE	0	FALSE	58624.60	FALSE
Element 4	0.000365	0.004029	8610060.0	-0.00175	8610060	FALSE	0	FALSE	4305030	FALSE
Element 5	0.000411	0.004742	24757600.0	-0.00151	24757600	FALSE	0	FALSE	12378800	FALSE
Element 6	0.000382	0.004291	39689200.0	-0.00122	39689200	FALSE	0	FALSE	19844600	FALSE
Element 7	0.000306	0.003150	59114900.0	-0.00104	59114900	FALSE	0	FALSE	29557400	FALSE
Element 8	0.000229	0.003087	57173700.0	-0.00054	57173700	FALSE	0	FALSE	28586900	FALSE
Element 9	0.000171	0.002729	58118700.0	-0.00018	58118700	FALSE	0	FALSE	29059400	FALSE
Element 10	0.000139	0.002060	70420000.0	-0.00009	70420000	FALSE	0	FALSE	35210000	FALSE
Element 11	0.000127	0.001827	76147200.0	0.00002	76147200	FALSE	0	FALSE	38073600	FALSE
Element 12	0.000133	0.001958	71787100.0	0.00012	71787100	FALSE	0	FALSE	35893600	FALSE
Element 13	0.000164	0.002588	57743500.0	0.00019	57743500	FALSE	0	FALSE	28871800	FALSE
Element 14	0.000238	0.003266	49406800.0	0.00055	49406800	FALSE	0	FALSE	24703400	FALSE
Element 15	0.000358	0.003910	39391300.0	0.00095	39391300	FALSE	0	FALSE	19695700	FALSE
Element 16	0.000411	0.004740	19969700.0	0.00123	19969700	FALSE	0	FALSE	9984850	FALSE
Element 17	0.000354	0.003860	218900.0	-0.00013	218900	FALSE	0	FALSE	109450	FALSE
Element 18	0.000294	0.002978	43610.7	-0.00008	43611	FALSE	0	FALSE	21805.30	FALSE
Element 19	0.000197	0.001726	13231.6	-0.00001	13232	FALSE	0	FALSE	6615.78	FALSE
Element20	0.000052	0.000300	0.001821	-0.00001	0	FALSE	0	FALSE	0.0009	FALSE

To continue with the trend, Table 12 also only displays “False” for the stress comparison to the yield stress. The display of only “false” indicates that this reference HY2-SWATH substructure frame does not fail in flying mode.

3.4 Hogging and Sagging Slamming Loading Condition

Slamming loads are much more significant than global bending moment for smaller crafts (indicatively having lengths less than 50 m). Slamming events happen when a ship is heaving and pitching and a portion of the hull emerges and re-enters the water, inducing an extreme pressure on the vessel’s point of re-entry. Hogging and Sagging conditions describe specific wave-induced forces that act on a marine vessel. Hogging is when tensile bending stresses occur at the midship upper deck and compression bending stresses occur at the bottom of the vessel. Sagging is the opposite of hogging, and

is when there are tensile bending stresses in the bottom and compression bending stresses at the upper deck [6]. Figure 38 and Figure 39 show the load distribution along the hull beam due to hogging and sagging forces.

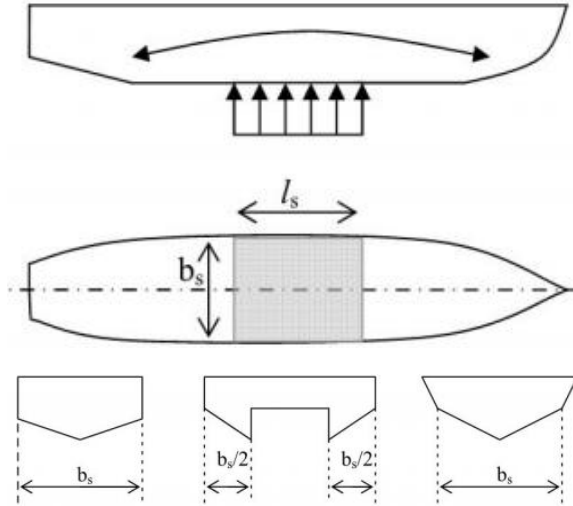


Figure 38: Hogging [14]

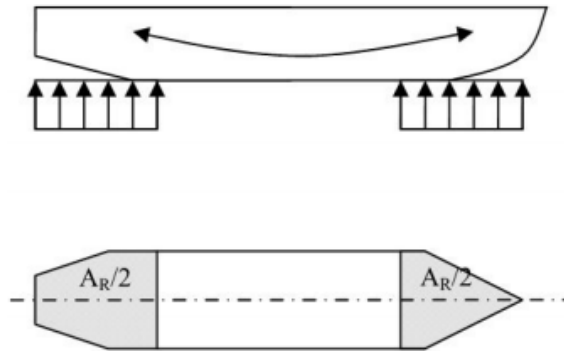


Figure 39: Sagging [14]

The hogging and sagging slamming load condition is an idealized load condition in which the hydrostatic forces due to waves (hogging/sagging) and the hydrodynamic forces due to slamming impact pressures have been combined to simulate the worst-case-scenario the HY2-SWATH may encounter. Designing with consideration to this load condition will minimize the risk of structural failure. The hogging and sagging slamming pressures were used to calculate the minimum required hull shell thickness in accordance with DNVGL High Speed, Light Craft and Naval Surface Craft Part 3 Chapters 1-3, i.e. using Figure 38 through Figure 40 and Equation 15 through Equation 20 [14].

Equation 15 defines the vertical acceleration as a function of the velocity and significant wave height. The design shape of the twin hulls is unique and therefore the DNVGL does not have a specific

formula for calculating the equivalent deadrise angle as required in the vertical acceleration equation. Therefore deadrise angle of the rounded twin hull was taken to be 10°, the minimum allowed, because it would result in a larger vertical acceleration and ultimately, a more robust design.

$$a_{cg} = \frac{k_h g_0}{1650} * \left(\frac{H_s}{B_{WL2}} + 0.084 \right) * (50 - \beta_{cg}) * \left(\frac{V}{\sqrt{L}} \right)^2 * \frac{L * B_{WL2}}{\Delta} \left(\frac{m}{s^2} \right) \quad \text{Equation 15}$$

H_s = significant wave height in m

β_{cg} = deadrise angle at LCG in degrees

= minimum 10°

= maximum 30°

B_{WL2} = waterline breadth at L/2 in m

For twin- and multi hull vessels the total breadth of hulls (exclusive tunnels) shall be used

g_0 = standard acceleration of gravity = 9.81 m/s²

k_h = hull type factor

= 0.7 for Foil assisted hull or SWATH

The slamming pressure acts over the shaded area, A_R , in Figure 38 and Figure 39 and was calculated in accordance with Equation 16.

$$A_R = k * \Delta * \frac{(1+0.2 \frac{a_{cg}}{g_0})}{T} (m^2) \quad \text{Equation 16}$$

k = 0.7 for hogging

k = 0.6 for sagging

Δ = displacement in tonnes

T = fully loaded draught in m with the craft floating in calm water

The longitudinal extension of the slamming reference area, l_s , was calculated using Equation 17. This length was used to apply a series of pinned boundary conditions on each element's end nodes that fell within the calculated length.

$$l_s = \frac{A_R}{b_s} \quad \text{Equation 17}$$

b_s = breadth of slamming reference area

The slamming pressure was calculated using Equation 18.

$$p_{sl} = 1.3 k_l \left(\frac{\Delta}{nA}\right)^{0.3} T_o^{0.7} \frac{50 - \beta_x}{50 - \beta_{cg}} a_{cg} \left(\frac{kN}{m^2}\right) \quad \text{Equation 18}$$

k_l =longitudinal distribution factor calculated using Figure 40

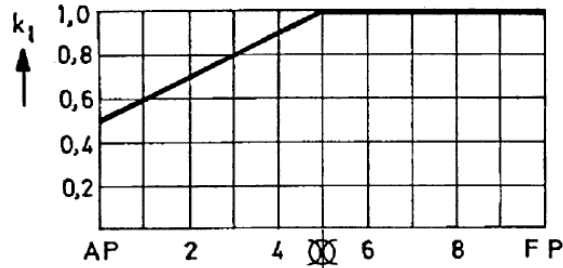


Figure 40: Long. Slamming Pressure Distribution Factor for High Speed Mode [14]

n = number of hulls, 1 for monohulls, 2 for catamarans

A = design load area for element considered in m^2

For plating A shall not be taken greater than $2.5s^2$

T_o = draught at $L/2$ in m at normal operation condition at service speed

β_x = deadrise angle in degrees at transverse section considered (minimum 10° , maximum 30°)

β_{cg} = deadrise angle in degrees at LCG (minimum 10° , maximum 30°)

Equation 19 and Equation 20 were used to calculate the required minimum hull shell thickness. As stated previously, the nominal allowable bending stress in Equation 19 is defined for specific steel grades and in Equation 20 is defined for specific aluminum grades with specific consideration taken for different materials. As the materials investigated in this project are all stronger than the steel and aluminum grades considered by the DNVGL rules, the strongest steel and strongest aluminum associated nominal allowable bending stresses were used for this calculation. The titanium used was considered as “steel” in this calculation. These assumptions would again yield conservative estimates for the hull shell thickness and a safer, more design.

$$t = \frac{15.8k_a k_r s \sqrt{p_{sl}}}{\sqrt{\sigma}} \text{ (mm)} \quad \text{Equation 19}$$

k_a = correction factor for aspect ratio of plate field

$$= (1.1 - 0.25 s/l)^2$$

$$= \text{maximum } 1.0 \text{ for } s/l = 0.4$$

$$= \text{minimum } 0.72 \text{ for } s/l = 1.0$$

$$k_r = (1 - 0.5 \text{ s/r})$$

= correction factor for curved plates

r = radius of curvature in mm

σ = nominal allowable bending stress in N/mm² due to lateral pressure

$$t = \frac{22.4 k_a k_r s \sqrt{p_{sl}}}{\sqrt{\sigma}} \text{ (mm)}$$

Equation 20

k_a = correction factor for aspect ratio of plate field

$$= (1.1 - 0.25 \text{ s/l})^2$$

= maximum 1.0 for s/l = 0.4

= minimum 0.72 for s/l = 1.0

$$k_r = (1 - 0.5 \text{ s/r})$$

= correction factor for curved plates

r = radius of curvature in m

σ = nominal allowable bending stress in N/mm² due to lateral pressure

Once the DNVGL rules for calculating hogging and sagging had been implemented in the AMVS module the code was run and the results for the both hogging and sagging for the reference vessel hull have been provided below.

Hogging Mode Results

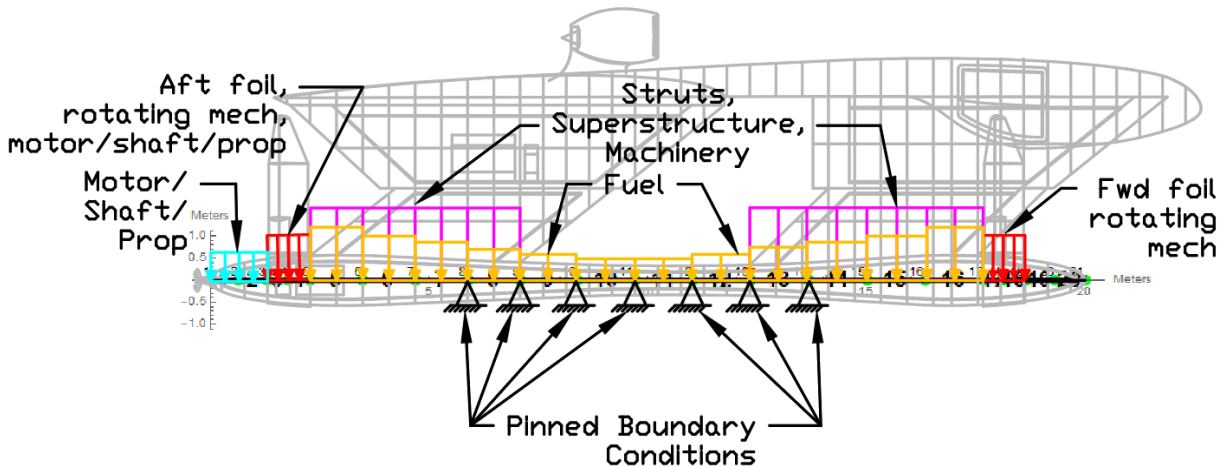


Figure 41: Hull with Elements, Loads, and BCs (Hogging Mode)

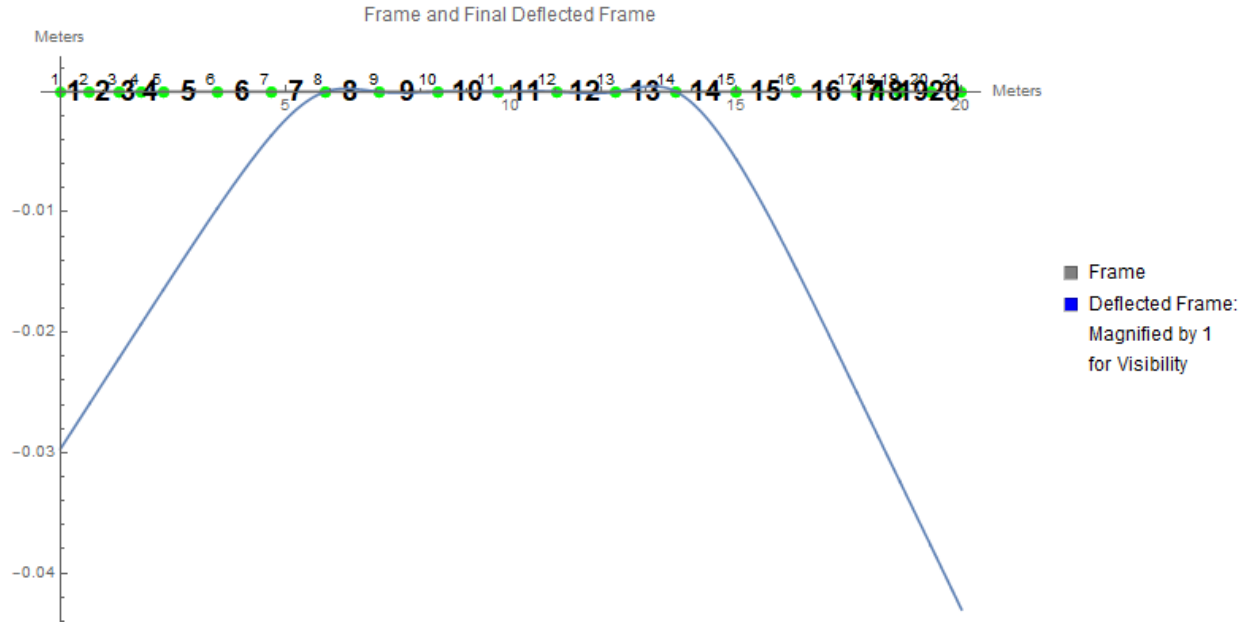


Figure 42: Hull Frame and Deflected Frame

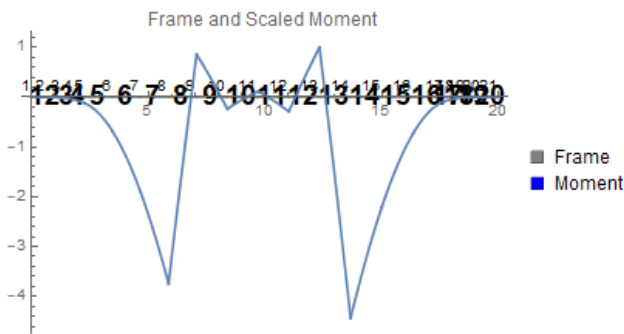


Figure 43: Hull Frame and Scaled Moment

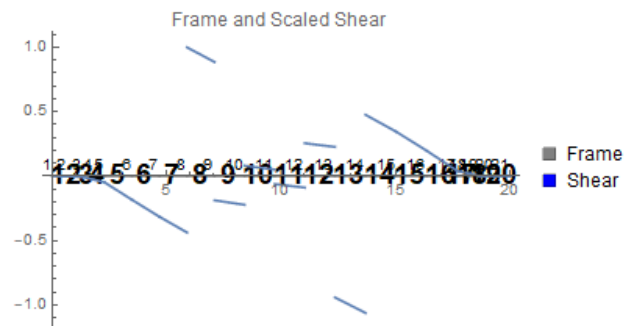


Figure 44: Hull Frame and Scaled Shear

Table 13: Hull Global Node Displacement and Reaction Forces (Hogging Mode)						
	Horizontal Displacement, u (m)	Vertical Displacement, v (m)	Rotation, Θ (rad.)	Horizontal Force, F_x (N)	Vertical Force, F_z (N)	Moment, M_y (Nm)
Global Node 1	0	-0.0296679	-0.00581	0	-1.0391E-09	2.09866E-10
Global Node 2	0	-0.0259025	-0.0058	0	6.63931E-09	-1.0804E-08
Global Node 3	0	-0.0221432	-0.00579	0	-7.9259E-07	2.03948E-07
Global Node 4	0	-0.0193093	-0.00578	0	5.07018E-07	3.09439E-07
Global Node 5	0	-0.0164847	-0.00575	0	1.52015E-06	-5.8475E-07
Global Node 6	0	-0.00969765	-0.00549	0	4.29538E-06	-4.1176E-06
Global Node 7	0	-0.00363598	-0.00444	0	-0.000016063	2.6663E-06
Global Node 8	0	1.15034E-15	-0.00126	0	1264000	1.06977E-05
Global Node 9	0	8.69758E-15	0.000368	0	-944312	-7.8992E-07
Global Node 10	0	4.05185E-18	-0.0001	0	266459	-2.5771E-06
Global Node 11	0	-7.0104E-19	-9.1E-06	0	-99399.7	1.85379E-07
Global Node 12	0	9.0332E-20	0.000154	0	302849	-3.8431E-07
Global Node 12	0	0	-0.00059	0	-1027680	-1.2877E-07
Global Node 13	0	-8.0669E-20	0.001993	0	1352670	-8.8574E-08
Global Node 14	0	-0.00564058	0.006003	0	3.49537E-08	-5.5292E-08
Global Node 15	0	-0.0147814	0.007444	0	-3.1729E-07	8.41719E-08
Global Node 16	0	-0.0249682	0.007732	0	1.27446E-07	1.62081E-07
Global Node 17	0	-0.028677	0.007752	0	-2.51543E-06	5.54802E-07
Global Node 18	0	-0.0323916	0.007758	0	1.76208E-06	8.13966E-07
Global Node 19	0	-0.037711	0.007761	0	5.65173E-07	2.37879E-07
Global Node 20	0	-0.0430323	0.007763	0	4.62655E-08	1.26156E-08
Global Node 21	0	-0.0296679	-0.00581	0	-1.0391E-09	2.09866E-10

Table 14: Hull Stress and Failure Analysis (Hogging Mode)

	Total Stiffener Ix (m ⁴)	Total Ix (m ⁴)	Bending Stress, σ_x (Pa)	Shear Stress, τ_{xy} (Pa)	σ_1 (Pa)	SF*Abs(σ_1) > σ_{yield}	σ_2 (Pa)	SF*Abs(σ_2) > σ_{yield}	τ_{max} (Pa)	SF*Abs(τ_{max}) > τ_{yield}
Element 1	4.19078E-05	0.000227733	1.949E-07	9.15483E-17	1.94962E-07	FALSE	0	FALSE	-9.74E-08	FALSE
Element 2	0.000213685	0.00192732	149746	4.33752E-05	149746	FALSE	0	FALSE	74873.2	FALSE
Element 3	0.000303497	0.00311715	463012	7.06312E-05	463012	FALSE	0	FALSE	231506	FALSE
Element 4	0.000365331	0.00402855	1368140	0.000314037	1368140	FALSE	0	FALSE	684069	FALSE
Element 5	0.000410794	0.00474188	3306030	0.00051197	3306030	FALSE	0	FALSE	-1653010	FALSE
Element 6	0.000382328	0.00429111	20371800	0.00208208	20371800	FALSE	0	FALSE	-10185900	FALSE
Element 7	0.000305799	0.00314981	69325100	0.00438321	69325100	FALSE	0	FALSE	34662600	FALSE
Element 8	0.00022859	0.00308664	27764600	-0.0124066	27764600	FALSE	0	FALSE	13882300	FALSE
Element 9	0.000170502	0.00272919	27346300	0.00230977	27346300	FALSE	0	FALSE	13673200	FALSE
Element 10	0.000138557	0.00205957	4359440	-0.00119221	-4359440	FALSE	0	FALSE	2179720	FALSE
Element 11	0.000126764	0.00182683	4715320	0.00099123	-4715320	FALSE	0	FALSE	2357660	FALSE
Element 12	0.000133461	0.00195799	39589100	-0.00391176	-39589100	FALSE	0	FALSE	19794600	FALSE
Element 13	0.000163974	0.0025879	32979900	0.0119958	-32979900	FALSE	0	FALSE	16489900	FALSE
Element 14	0.000238142	0.00326553	68804200	-0.0056968	-68804200	FALSE	0	FALSE	34402100	FALSE
Element 15	0.000357572	0.00391038	23190200	-0.00415889	-23190200	FALSE	0	FALSE	11595100	FALSE
Element 16	0.000410671	0.0047399	2440430	-0.00209323	-2440430	FALSE	0	FALSE	1220220	FALSE
Element 17	0.000354212	0.00385954	864427	-0.00049572	864427	FALSE	0	FALSE	432213	FALSE
Element 18	0.000293639	0.00297849	172217	-0.00030656	172217	FALSE	0	FALSE	86108.3	FALSE
Element 19	0.000197058	0.00172639	52250.9	-3.877E-05	52250.9	FALSE	0	FALSE	26125.4	FALSE
Element 20	5.21918E-05	0.000300422	8.009E-06	-4.496E-05	0.000049143	FALSE	-4.1E-05	FALSE	4.51E-05	FALSE

Sagging Mode Results

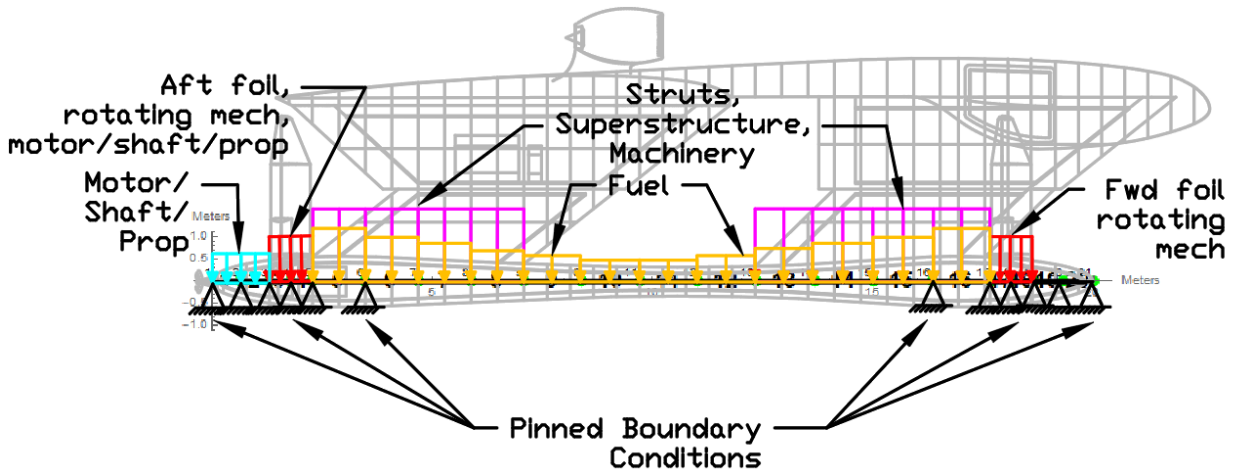


Figure 45: Hull with Elements, Loads, and BCs (Sagging Mode)

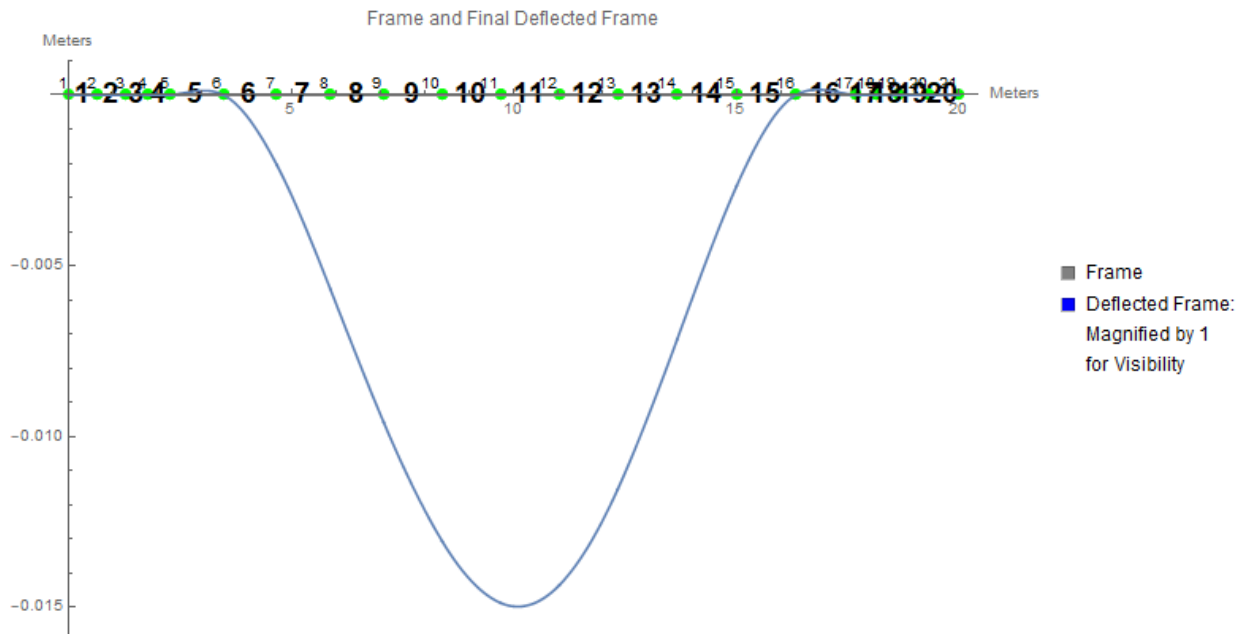


Figure 46: Hull Frame and Deflected Frame

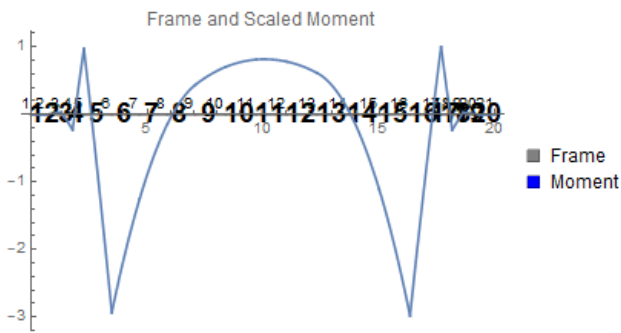


Figure 47: Hull Frame and Scaled Moment

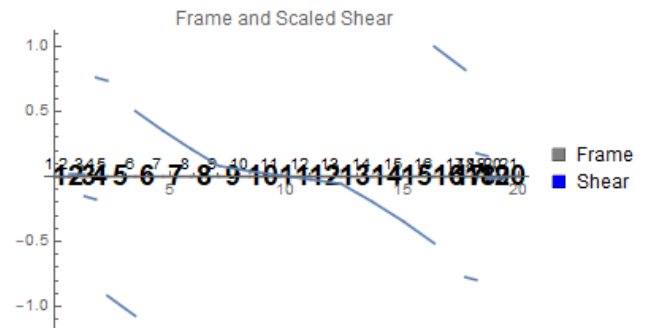


Figure 48: Hull Frame and Scaled Shear

Table 15: Hull Global Node Displacement and Reaction Forces (Sagging Mode)

	Horizontal Displacement, u (m)	Vertical Displacement, v (m)	Rotation, Θ (rad.)	Horizontal Force, F_x (N)	Vertical Force, F_z (N)	Moment, M_y (Nm)
Global Node 1	0	0	-1.8066E-06	0	75.4984	0
Global Node 2	0	-9.1627E-23	5.74319E-06	0	16636.7	-1.1369E-13
Global Node 3	0	1.48702E-22	-1.2571E-05	0	-127997	6.36646E-12
Global Node 4	0	-1.1081E-23	3.48987E-05	0	717998	3.61524E-11
Global Node 5	0	1.9941E-21	-0.00011407	0	-1266000	-4.9113E-11
Global Node 6	0	-1.7889E-19	0.000650104	0	1206830	-1.1532E-09
Global Node 7	0	-0.00204783	0.00250757	0	-2.54659E-09	5.67525E-10
Global Node 8	0	-0.00567774	0.00331261	0	-2.66009E-08	1.3657E-08
Global Node 9	0	-0.00958135	0.00307102	0	7.44185E-08	-5.3678E-09
Global Node 10	0	-0.0130605	0.00215496	0	-1.06404E-07	3.21565E-08
Global Node 11	0	-0.0148667	0.000556584	0	1.33514E-09	4.48363E-08
Global Node 12	0	-0.0143479	-0.00133412	0	1.23062E-06	-7.3477E-07
Global Node 12	0	-0.0115379	-0.00288172	0	-4.63973E-07	-1.1398E-06
Global Node 13	0	-0.00715244	-0.00353855	0	-2.63282E-06	6.49266E-07
Global Node 14	0	-0.00266696	-0.00292362	0	8.00253E-06	-2.8225E-06
Global Node 15	0	-3.3793E-15	-0.00072658	0	1159330	-4.3175E-06
Global Node 16	0	-1.1199E-15	0.000119496	0	-1220520	-1.9225E-07
Global Node 17	0	4.54845E-19	-3.6706E-05	0	746962	1.42706E-05
Global Node 18	0	-4.004E-20	1.36893E-05	0	-131956	1.12243E-06
Global Node 19	0	0	-6.0633E-06	0	13826.4	2.05183E-07
Global Node 20	0	-3.1209E-20	2.75456E-06	0	-606.882	1.38593E-08
Global Node 21	0	0	-1.8066E-06	0	75.4984	0

Table 16: Hull Stress and Failure Analysis (Sagging Mode)

	Total Stiffener Ix (m ⁴)	Total Ix (m ⁴)	Bending Stress, σ_x (Pa)	Shear Stress, τ_{xy} (Pa)	σ_1 (Pa)	SF*Abs(σ_1) > σ_{yield}	σ_2 (Pa)	SF*Abs(σ_2) > σ_{yield}	τ_{max} (Pa)	SF*Abs(τ_{max}) > τ_{yield}
Element 1	4.19078E-05	0.000227733	863.083	-6.651E-06	863.083	FALSE	-5.7E-14	FALSE	431.541	FALSE
Element 2	0.000213685	0.00192732	1893020	-0.00032095	1893020	FALSE	0	FALSE	946510	FALSE
Element 3	0.000303497	0.00311715	1382580	0.00183939	1382580	FALSE	0	FALSE	691290	FALSE
Element 4	0.000365331	0.00402855	32648100	-0.007831	32648100	FALSE	0	FALSE	16324000	FALSE
Element 5	0.000410794	0.00474188	29340600	0.0084614	29340600	FALSE	0	FALSE	14670300	FALSE
Element 6	0.000382328	0.00429111	40202700	-0.0049692	40202700	FALSE	0	FALSE	20101400	FALSE
Element 7	0.000305799	0.00314981	5539350	-0.00425999	5539350	FALSE	0	FALSE	2769680	FALSE
Element 8	0.00022859	0.00308664	15302500	-0.00229463	15302500	FALSE	0	FALSE	7651260	FALSE
Element 9	0.000170502	0.00272919	24258500	-0.0008772	24258500	FALSE	0	FALSE	12129300	FALSE
Element 10	0.000138557	0.00205957	33666300	-0.00054199	33666300	FALSE	0	FALSE	16833200	FALSE
Element 11	0.000126764	0.00182683	36633300	-0.00011755	36633300	FALSE	0	FALSE	18316700	FALSE
Element 12	0.000133461	0.00195799	33472100	0.00030443	33472100	FALSE	0	FALSE	16736000	FALSE
Element 13	0.000163974	0.0025879	21879200	0.000614608	21879200	FALSE	0	FALSE	10939600	FALSE
Element 14	0.000238142	0.00326553	2343630	0.00201422	2343630	FALSE	0	FALSE	1171820	FALSE
Element 15	0.000357572	0.00391038	37735100	0.00360421	37735100	FALSE	0	FALSE	18867500	FALSE
Element 16	0.000410671	0.0047399	30107600	-0.00923683	30107600	FALSE	0	FALSE	15053800	FALSE
Element 17	0.000354212	0.00385954	34445900	0.00817954	34445900	FALSE	0	FALSE	17222900	FALSE
Element 18	0.000293639	0.00297849	337550	-0.0022511	1337550	FALSE	0	FALSE	668776	FALSE
Element 19	0.000197058	0.00172639	1910100	0.000271014	1910100	FALSE	0	FALSE	955048	FALSE
Element20	5.21918E-05	0.000300422	1.076E-05	-8.951E-05	9.51E-05	FALSE	-8.4E-05	FALSE	8.97E-05	FALSE

3.5 Input Variable Range, Data Generation, and Feasibility Constraints

A structural analysis parametric variable input sweep was run for the buoyancy mode, flying mode, hogging and sagging conditions for three groups of inputs. Groups of parametric inputs refer to variables that are associated with each other. For example, the material properties - is a group of four variables: density, yield stress, shear stress, and elastic modulus and must all be modified simultaneously to describe a single material. The three groups of parametric inputs are the material properties, the shell thickness and the number of stiffeners. These inputs were held constant over the three subdomain frames analyzed.

The material properties were modified according to Table 17:

	ρ (kg*m ⁻³)	σ_{yield} (MPa)	τ_{yield} (MPa)	E (GPa)
Aluminum 7075 - T6; 7075 - T651	2810	503	331	71.9
316L Steel	8000	205	370	193
Aluminum 6061 - T6; 6061 - T651	2700	276	207	68.9
AISI Type S20910 Stainless Steel, high strength	7890	725	570	200
Titanium Ti - 6 Al - 4 V (Grade 5), Annealed	4430	880	550	113.8

All of the materials have been verified as materials used in the marine industry, or published research papers have deemed them feasible for their application in the marine industry.

Initially, the shell thickness was modified, keeping the shell thickness constant over each element within all three frame subdomains, from 4 mm to 7 mm in 1 mm increments. However, in the flying mode operational condition, the hull would plastically deform and fail along the midsection line for all materials tested. Figure 35 shows an example of the flying mode condition hull frame, elements, and deflection curve. Based on a “True” value appearing in the principle stress vs yields stress (with safety factor of 6 applied) columns of Table 12, the hull would fail initially at node 11 due to the stress. To prevent the hull from failing, several iterations of the changing the shell thickness of hull frame midship elements, where the hull cross-sectional area is smallest (Figure 16), determined that elements 9-13 required an additional 8mm shell thickness on top of the variable 4-7 mm parametric input shell thickness and elements 8 and 14 required 3mm additional shell thickness. The additional shell thickness applied to these elements, remained a constant on top of any variable input change to the hull shell thickness for all following runs.

The third group of variables that were modified was the number of stiffeners in each frame with each number in the sequence corresponding to the specific number of stiffeners in the element, in accordance with the tables below. These parameter sweep variations provide 60 total runs each of the low-fidelity FEA structural analysis code for the buoyancy mode and flying mode operational conditions.

	Forward Strut Frame Stiffeners	Aft Strut Frame Stiffeners	Hull Frame Stiffeners
Run 1	(8, 12, 12, 6, 6, 6, 6, 6, 6, 12, 12, 8)	(8, 12, 12, 6, 6, 6, 6, 12, 12, 8)	6/element (20 elements)
Run 2	(16, 24, 24, 12, 12, 12, 12, 12, 12, 24, 24, 16)	(16, 24, 24, 12, 12, 12, 12, 24, 24, 16)	12/element (20 elements)
Run 3	(32, 48, 48, 24, 24, 24, 24, 24, 24, 48, 48, 32)	(32, 48, 48, 24, 24, 24, 24, 48, 48, 32)	24/element (20 elements)

After the parameter sweep was completed, feasibility constraints were formulated. The constraints were derived to eliminate infeasible solutions e.g. solutions that result in the HY2-SWATH sinking. The constraints applied have been described in Table 19 and Table 20:

Table 19: Buoyancy Mode Operating Condition Constraints		
1	Buoyancy (initial waterline) > 1.1*weight	Initial waterline provides excess buoyancy. Constraint ensures vessel does not sink.
2	Abs(Trim angle) < 0.5°	Reduced drag, increased fuel efficiency and range
Hull Frame		
3	Max vertical deflection of hull < total hull length *x%	Ensure hull vertical deflection does not cause failure
Forward Struts Frame		
4	Max horizontal deflection < forward starboard strut length *x%	Ensure horizontal deflection of starboard strut does not cause failure
5	Max horizontal deflection < forward port strut length *x%	Ensure horizontal deflection of port strut does not cause failure
6	Max vertical deflection < forward wing span *x%	Ensure forward portion of the wing superstructure vertical deflection does not cause failure
Aft Struts Frame		
7	Max horizontal deflection < aft starboard strut length *x%	Ensure horizontal deflection of starboard strut does not cause failure
8	Max horizontal deflection < aft port strut length *x%	Ensure horizontal deflection of port strut does not cause failure
9	Max vertical deflection < aft wing span *x%	Ensure aft portion of the wing superstructure vertical deflection does not cause failure
Where x = 0.25% and 0.20%		

Table 20: Flying Mode Operating Condition Constraints		
1	Reference vessel weight 49.0335 MT > 1.05*weight.	Hydrofoils sized and angled for vessel weight. Reference vessel weight taken at aluminum 7075-T6, 6mm shell thickness, run 2 suite of stiffeners as defined in the stiffener table above
Hull Frame		

2	Max vertical deflection of hull < total hull length *x%	Ensure hull vertical deflection does not cause failure
Forward Struts Frame		
3	Max horizontal deflection < forward starboard strut length *x%	Ensure horizontal deflection of starboard strut does not cause failure
4	Max horizontal deflection < forward port strut length *x%	Ensure horizontal deflection of port strut does not cause failure
5	Max vertical deflection < forward wing span *x%	Ensure forward portion of the wing superstructure vertical deflection does not cause failure
Aft Struts Frame		
6	Max horizontal deflection < aft starboard strut length *x%	Ensure horizontal deflection of starboard strut does not cause failure
7	Max horizontal deflection < aft port strut length *x%	Ensure horizontal deflection of port strut does not cause failure
8	Max vertical deflection < aft wing span *x%	Ensure aft portion of the wing superstructure vertical deflection does not cause failure
Where x = 0.35% and 0.30%		

Table 21 is similar to Table 19 and Table 20, with the first constraint changed to refine the feasible solutions based on the DNVGL required hull shell thickness needed to withstand slamming loads.

Table 21: Hogging and Sagging Condition Constraints		
1	DNV minimum hull slamming shell thickness < Design hull shell thickness	Ensure the designed hull shell thickness is greater than the hull shell thickness as required by the DNV
Hull Frame		
2	Max vertical deflection of hull < total hull length *x%	Ensure hull vertical deflection does not cause failure
Forward Struts Frame		
3	Max horizontal deflection < forward starboard strut length *x%	Ensure horizontal deflection of starboard strut does not cause failure
4	Max horizontal deflection < forward port strut length *x%	Ensure horizontal deflection of port strut does not cause failure
5	Max vertical deflection < forward wing	Ensure forward portion of the wing superstructure

	span *x%	vertical deflection does not cause failure
Aft Struts Frame		
6	Max horizontal deflection < aft starboard strut length *x%	Ensure horizontal deflection of starboard strut does not cause failure
7	Max horizontal deflection < aft port strut length *x%	Ensure horizontal deflection of port strut does not cause f failure
8	Max vertical deflection < aft wing span *x%	Ensure aft portion of the wing superstructure vertical deflection does not cause failure
Where x = 0.35% and 0.30%		

Histograms of the parameters and constrained parameters were made to graphically show feasible results and are discussed in the following sections. The feasible results are displayed in red in the histograms as a part of the total number of times the parameter was run. Additionally, some variable sensitivity plots were generated to help analyze how the variable changes made, as described above, impact the stresses on the subdomain frames. The variable sweep outputs and associated histograms have been provided in Section 8 - 19, the appendices.

3.5.1 Buoyancy Mode Results

Upon analysis of the buoyancy histograms, Section 9, it was determined what parameters impact the feasibility of the solutions the most. The material type, while potentially offering greater strength, can significantly impact the vessel's weight. Since the size of the hull does not significantly change with each iteration, except due to minor changes in shell thickness, the two steel options and titanium will increase the vessel weight more than the buoyancy the struts and hull permit. The histograms also show that the 4mm shell thickness is the only feasible option as greater shell thicknesses increase the weight greater than the buoyancy allows. As discussed above, the 4 mm feasible shell plating thickness option for hull frame shell thickness means elements 8 and 14 have a shell thickness of 4 + 3 or 7 mm and elements 7 - 13 have a shell thickness of 4 + 8 or 12 mm total while all other elements are at 4 mm. The histograms also show that increasing the number of stiffeners too much causes the vessel weight to increase past the allowable buoyancy. When the deflection is constrained further from 0.25% to 0.20% the feasible aluminum options decrease due to the forward strut horizontal deflection exceeding the constrained allowable amount.

From visual inspection, the sensitivity plots, Section 10, show the general trend as shell thickness increases, or as the number of stiffeners increase, the max principle stresses decreases with an exponential

decay curve trend. This trend is more apparent with the forward and aft strut frames. The hull frame does not show as significant of a stress decrease with increase in shell thickness or stiffeners.

3.5.2 Flying Mode Results

The flying mode operational condition histograms, Section 12, show similar results as the buoyancy mode operational condition histograms. The two steel and titanium material options will increase the vessel weight more than the buoyancy will allow. Increasing the number of stiffeners too much will also increase the vessel weight more than the force provided by the hydrofoils will allow. The histograms also show that the hull frame allowable vertical deflection limits the feasible solutions as compared to the allowable deflections of the forward and aft strut frames. When the deflection is constrained further from 0.35% to 0.30% the feasible aluminum options decrease due to the hull vertical deflection exceeding the constrained allowable amount.

From visual inspection, the sensitivity plots, Section 13, show the general trend as shell thickness increases, or as stiffener number increases, the max principle stresses decreases with an exponential decay curve trend. This trend is more apparent with the forward and aft strut frames. The hull frame does not show as significant of a stress decrease with increase in shell thickness or stiffeners.

3.5.3 Hogging Condition Results

The in the hogging condition with greater applied accelerations, the histograms, Section 15, show that the design solutions are constrained the most by the forward port and starboard strut horizontal deflections. The two aluminum and titanium cases allow more than 0.35% deflection of the total strut length. When further constrained to 0.3% deflection of the total strut length, there are fewer feasible steel solutions. The constraint on DNVGL hull required thickness to resist slamming pressure loads also refines some of the feasible solutions.

As with the buoyancy and flying mode sensitivity plots, the sensitivity plots, Section 16, show the general trend as shell thickness increases, or as stiffener number increases, the max principle stresses decreases with an exponential decay curve trend. The significant difference between hogging condition sensitivity plot and the buoyancy and flying mode sensitivity plots are the magnitude of the stresses. The stresses are much larger in the hogging condition due to increased acceleration as calculated using DNVGL rules. This trend is more apparent with the forward and aft strut frames. The hull frame does not show as significant of a stress decrease with increase in shell thickness or stiffeners.

3.5.4 Sagging Condition Results

The in the sagging condition histograms, Section 18, are identical to the hogging condition histograms and sensitivity plots. The design solutions are constrained the most by the forward port and starboard strut horizontal deflections. The two aluminum and titanium cases allow more than 0.35% deflection of the total strut length. When further constrained to 0.3% deflection of the total strut length, there are fewer feasible steel solutions. The constraint on DNVGL hull required thickness to resist slamming pressure loads also refines some of the feasible solutions.

As with the buoyancy and flying mode sensitivity plots, the sensitivity plots, Section 19, show the general trend as shell thickness increases, or as stiffener number increases, the max principle stresses decreases with an exponential decay curve trend. The significant difference between sagging condition sensitivity plot and the buoyancy and flying mode sensitivity plots are the magnitude of the stresses. The stresses are much larger in the sagging condition due to increased acceleration as calculated using DNVGL rules. This trend is more apparent with the forward and aft strut frames. The hull frame does not show as significant of a stress decrease with increase in shell thickness or stiffeners.

4. Structure Design and Assessment Module (High-Fidelity Method)

The high-fidelity model has been initially created to compare the reference vessel results generated by the AMVS module to the reference vessel modeled in MAESTRO. A future goal, outside the scope of this thesis, is to enhance the high-fidelity module to be parametrically modifiable for automation and inclusion in the SBD process. The HY2-SWATH reference vessel, initially modeled in Rhino, was converted to MAESTRO. This process is described in Section 4.1.

4.1 Geometry Mesh Creation

To conduct a 3D FEA on the reference HY2-SWATH, the model created in Rhino was discretized into a finite element mesh. Since the vessel is symmetrical about the center line, half the model was converted to a mesh and imported in to MAESTRO. MAESTRO allows the half the vessel to be modeled and can apply symmetry to the loads and boundary conditions when calculations are run.

The Rhino reference model consists of the hull, struts and superstructure and was drawn using curves and surfaces. Curves and surfaces can not be imported directly in to MAESTRO and MAESTRO does not currently feature an auto-meshing process. All of the model's external shell plating and internal longitudinal stiffeners, ring stiffeners, and water tight bulkheads were converted to a combination of triangular and quad meshes. This meshing process was primarily manually conducted using Rhino meshing tools and MAESTRO created-Rhino meshing scripts. Figure 49 and Figure 50 show the polysurfaces of the reference HY2-SWATH and the results of the after the vessel was converted to a

mesh. Figure 49 shows the shell plating conversion and Figure 50 shows the internal structure conversion.

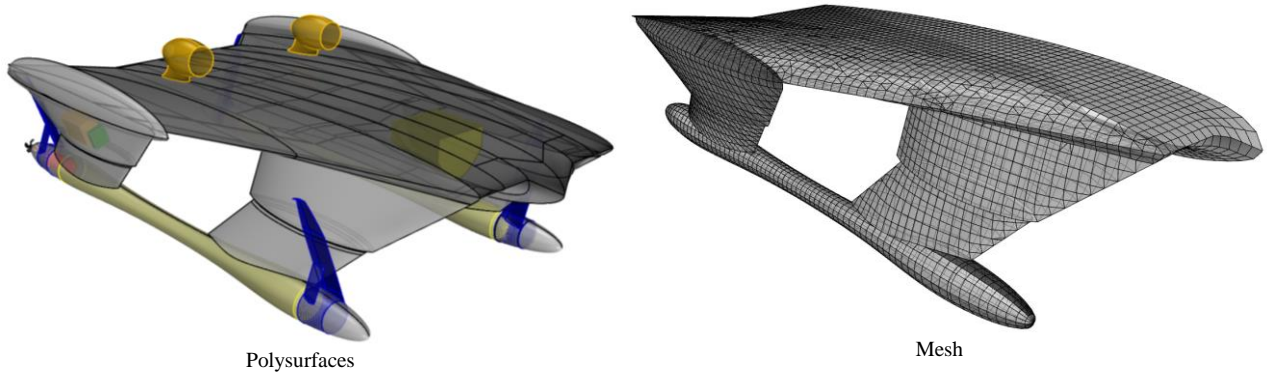


Figure 49: Shell Plating Conversion to Mesh

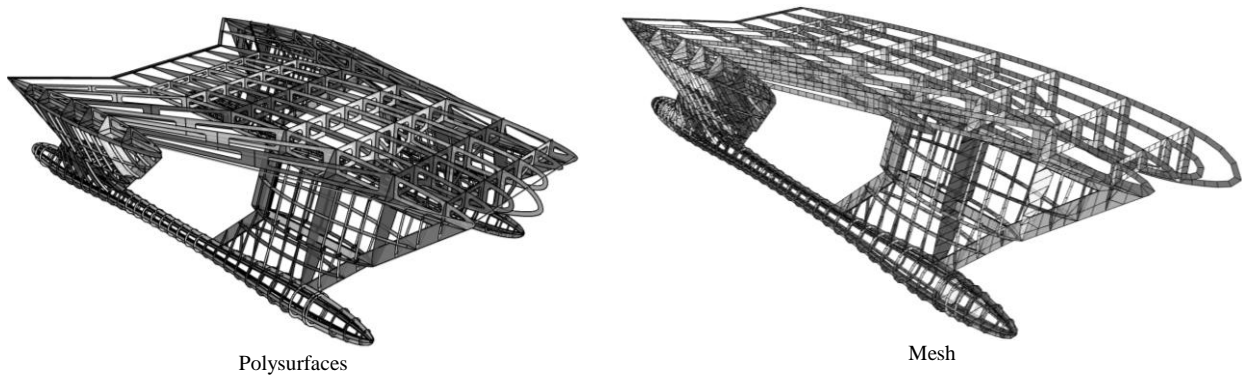


Figure 50: Internal Structure Converted to Mesh

The general Rhino meshing process used is summarized in 14 steps:

1. Duplicate the polysurfaces and place on appropriately named layers.
2. Duplicate the polysurfaces's borders to create line curves.
3. Use horizontal/vertical planes to split the polysurfaces (Figure 51). The number of planes and their spacing will determine how fine or coarse the final mesh displays. In areas of significant curvature, more planes should be used.

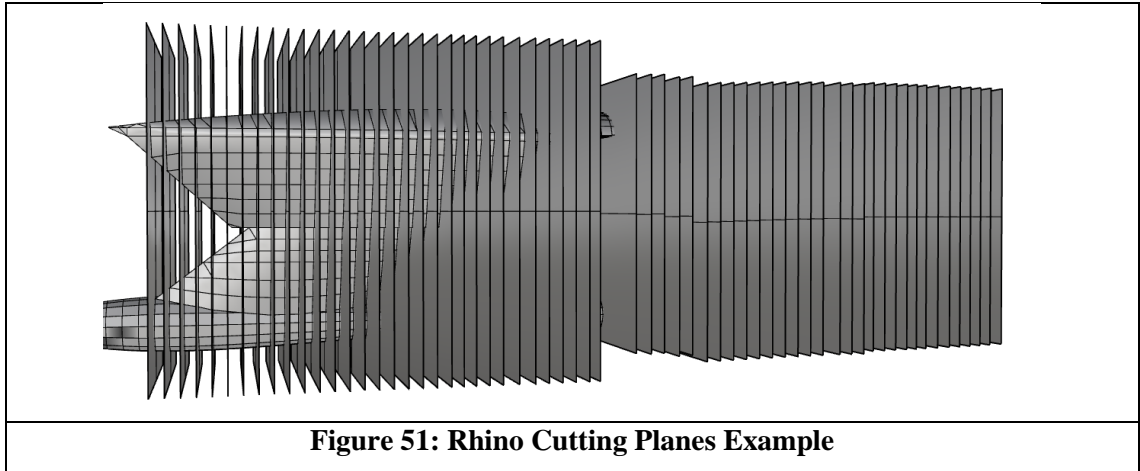


Figure 51: Rhino Cutting Planes Example

4. Delete the polysurfaces, leaving only the line curves.
5. Select all the line curves and use the dropdown menu command Curve → Point Object → Mark Curve Start to create points where each line curve has been split. Use the select duplicate command to delete any duplicate line curves and points.
6. Replace each line curve with polylines using the points. These can be individual line segments, polyline through points (command), or polyline.
7. Loft straight section surfaces through the polylines that represent the structures (Figure 52). This command should be used as much as possible but requires planning and setup of lines and points with specific attention at structure intersections and discontinuities.

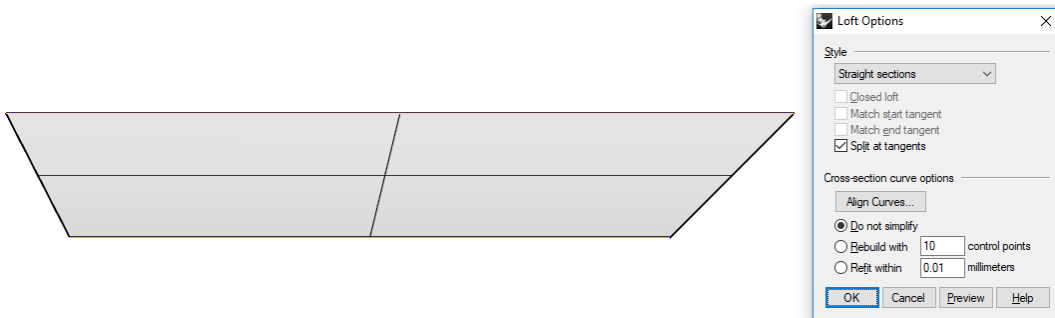


Figure 52: Rhino Loft Example

8. Select and explode any polysurfaces. Select all surfaces and use the dropdown menu command Mesh → From NURBS Control Polygon
9. Join the meshes and use the “weld” command. If adjacent mesh elements do not weld as expected, the mesh points defining the adjacent mesh edges should be checked to ensure the points exactly line up. They can be very difficult to see and may require zooming in far to identify the discontinuity. The top two images of Figure 53 show how a small

discontinuity can result in a free edge. The top left is a zoomed out (left) section of the vessel where there is a free edge due to discontinuity and a zoomed in section (right) of how the nodes are not connected. The bottom image shows the maximum zoom required to see the discontinuity causing a free edge.

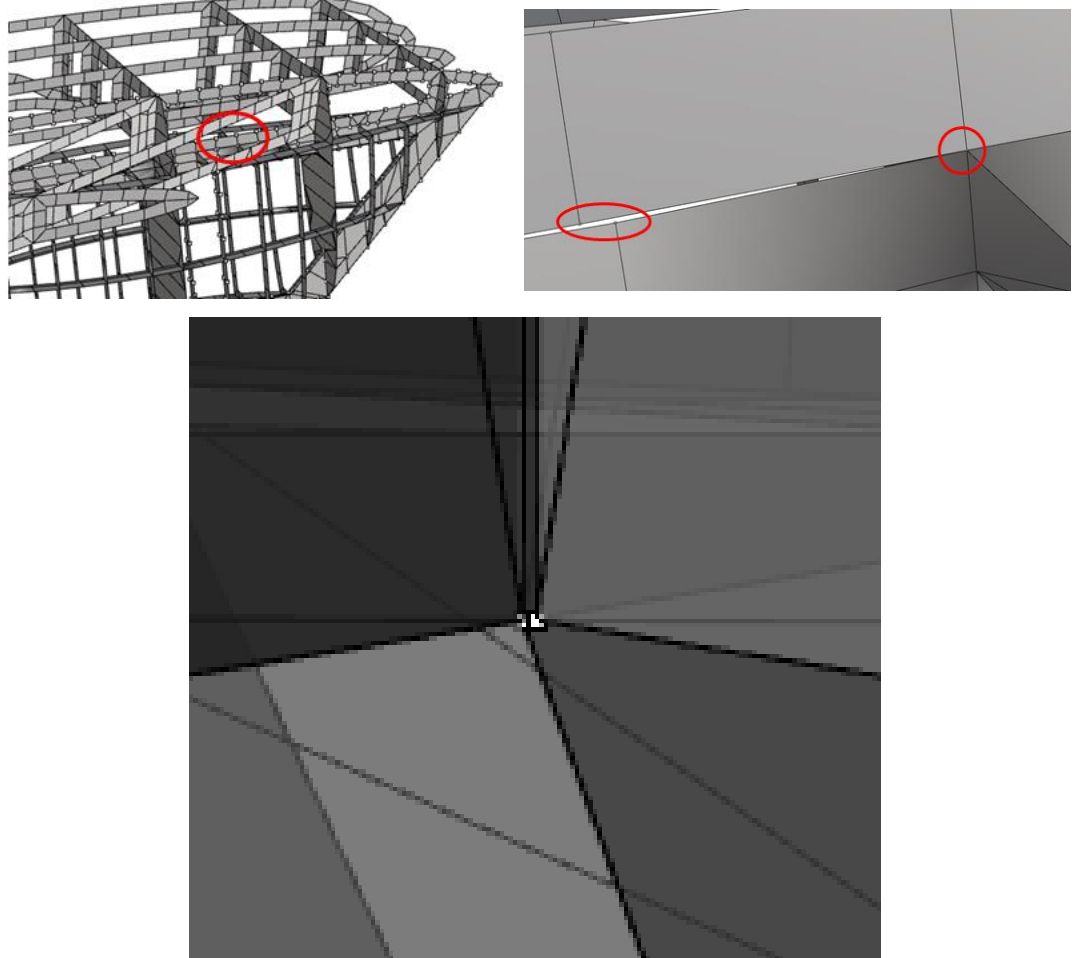


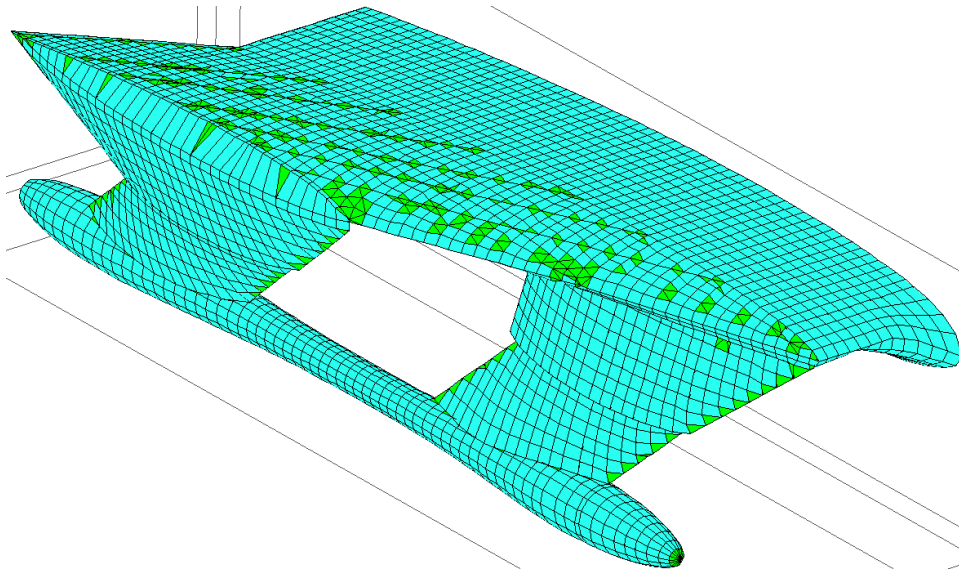
Figure 53: Node Discontinuities

10. Use the Rhino “Check” to check for free edges. Free edges where there should not be, e.g. structure intersections, need to be corrected or will result in errors when reviewing FEA results.
11. Export the mesh as a .ply file and import in to MAESTRO.
12. Use the MAESTRO dropdown menu Tools → Re-Number FeTag command. Then check for free edge in dropdown menu View Tools → Edges Tools → Free edges. Note where and modeling free edges errors occur and any visually inspect for free edges where they should not appear.

13. Additionally, use the Tools → Integrity Check → Overlapped Elements as well as Tools → Integrity Check → Warped Quad. Prior to making any Boundary Conditions, Load Cases, MAESTRO groups, etc.; it is recommended to correct errors found in steps 12 and 13 in Rhino and reimport in to MAESTRO. Rhino offers an “undo” feature in the event a mistake is made; MAESTRO does not.
14. If free edges or other mesh errors are found after setting up boundary conditions, loads, load cases; they can be corrected in MAESTRO. Selective use of “save” or “save as” will ensure a point to return to in the event the error is made worse, which can not be easily undone.

One of the requirements to create an acceptable mesh is to ensure that all end nodes of individual mesh ends are connected to one another, i.e. node-to-node connection. Node-to-node connection must occur between all major component interface including hull to struts to superstructure and all their interfacing internal structural components. The MAESTRO Marine website features several in-depth tutorials on preparing a mesh in Rhino and exporting to MAESTRO.

Once the vessel has been converted to a mesh, it can be exported from Rhino as a .ply file and imported in to MAESTRO. Figure 54 shows the vessel once it has been imported into MAESTRO. The teal color indicates the mesh is a four-sided (quad) element and the green indicates the mesh is three-sided (tri) element. When working in MAESTRO, quad elements should primarily be used as prescribed in the user manual. In total, the HY2-SWATH has been represented with over 12,000 quad and tri-elements.



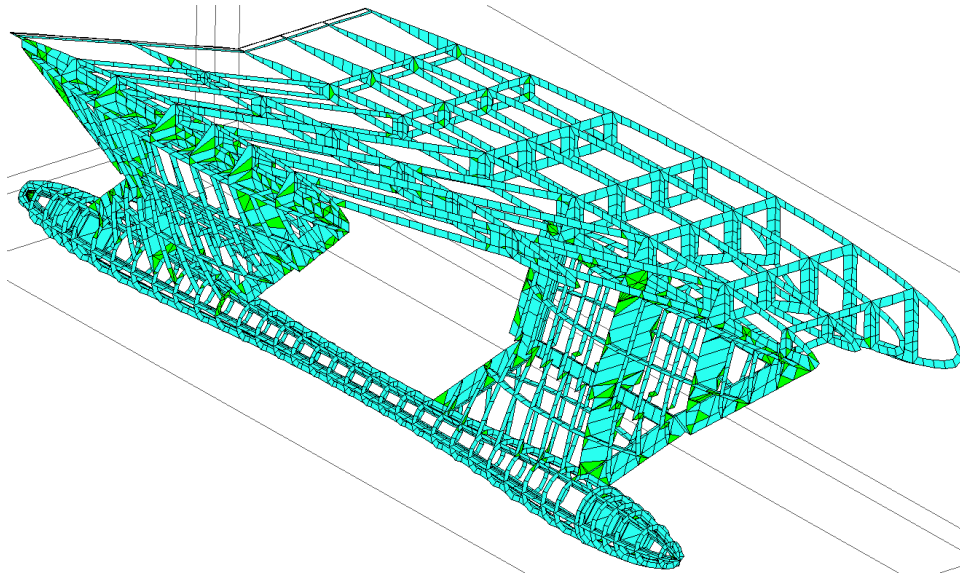


Figure 54: MAESTRO Model Mesh

Once the model was imported into MAESTRO, a free edge check command was run to verify the integrity of the model. A “good mesh” in the Rhino could still result in mesh errors in MAESTRO and vice versa. Figure 55 shows the intersection of the longitudinal stiffeners in the hull that show free edges, as indicated by the red outline on the mesh. This free edge should not exist and indicates the stiffeners are not correctly attached to each other. Figure 55 also shows the results of correctly attaching the stiffeners as the free edge integrity check no longer outlines the meshes, at their intersection, in red.

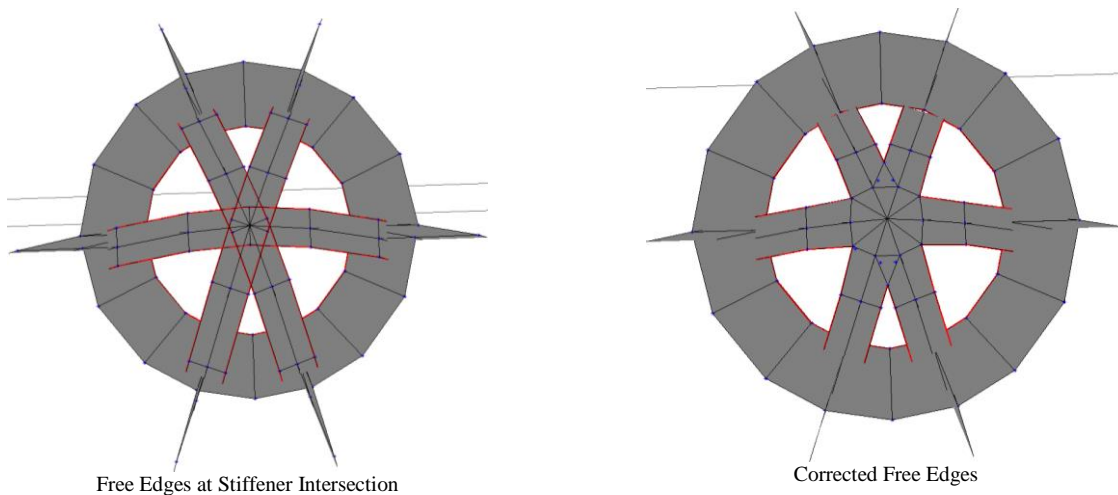


Figure 55: MAESTRO Free Edge Correction

Similarly, all concave quads, collapsed quad elements, and collapsed tri-elements were checked for and corrected. The next step is to apply the material properties, structural element thickness, loads and boundary conditions.

4.2 Material Properties, Loads and Boundary Conditions

In MAESTRO, materials definition is accomplished by entering the material properties in the materials dialog box. Aluminum 7075-T; 7075-T651 was the only material used in this model and is consistent with the material used in the reference vessel of the AMVS module. The properties are shown in Figure 56.

Material

Name	Al 7075-T6	ID	2	Type	Isotropic
Name	Value				
Young's Modulus Ex(N/m ²)	7.19e+10				
Poisson Ratio	0.33				
Density(kg/m ³)	2950.5				
Yield Stress(N/m ²)	5.03e+08				
Ultimate Tensile Strength(N/m ²)	5.72e+08				

Figure 56: Aluminum 7075 Material Properties

In AMVS module, a 5% allowance factor has been applied to the loads as described in Table 1. This factor is to account for some of the structure not represented in the models such as structural brackets. To apply an equivalent allowance factor to the structural weight, the material density was increased by 5%.

The loads were applied to the MAESTRO model in a fashion to most similarly replicate the loads applied in the AMVS module with the applied loads equivalent to those in Table 1. As stated previously, the applied loads due to structural weight have been applied as calculated in MAESTRO and are not exactly equal to the structural loads in Table 1. Concentrated forces used in AMVS module were applied as concentrated forces in the MAESTRO model and can be seen in Figure 57. Distributed forces used in AMVS module were applied as concentrated forces in the MAESTRO model and can be seen in Figure 58.

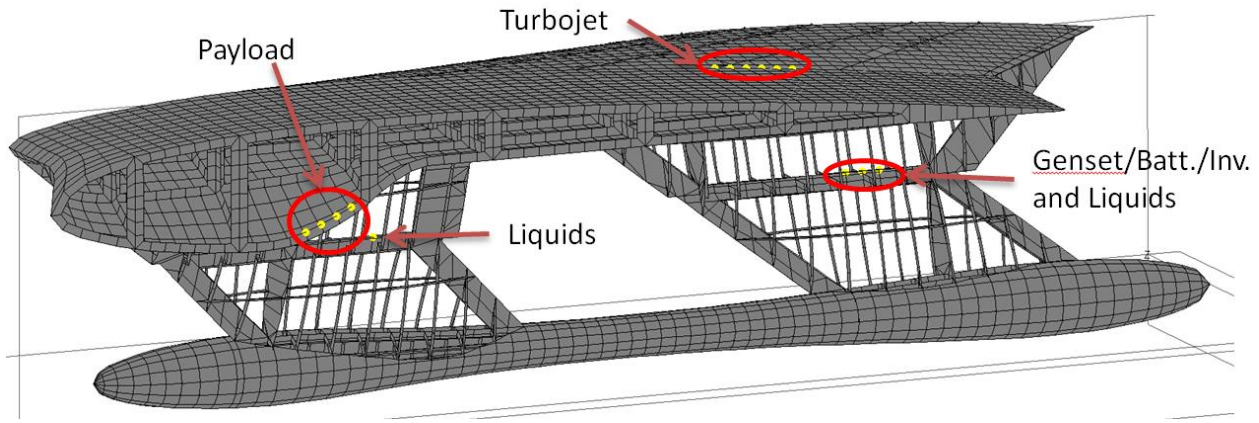
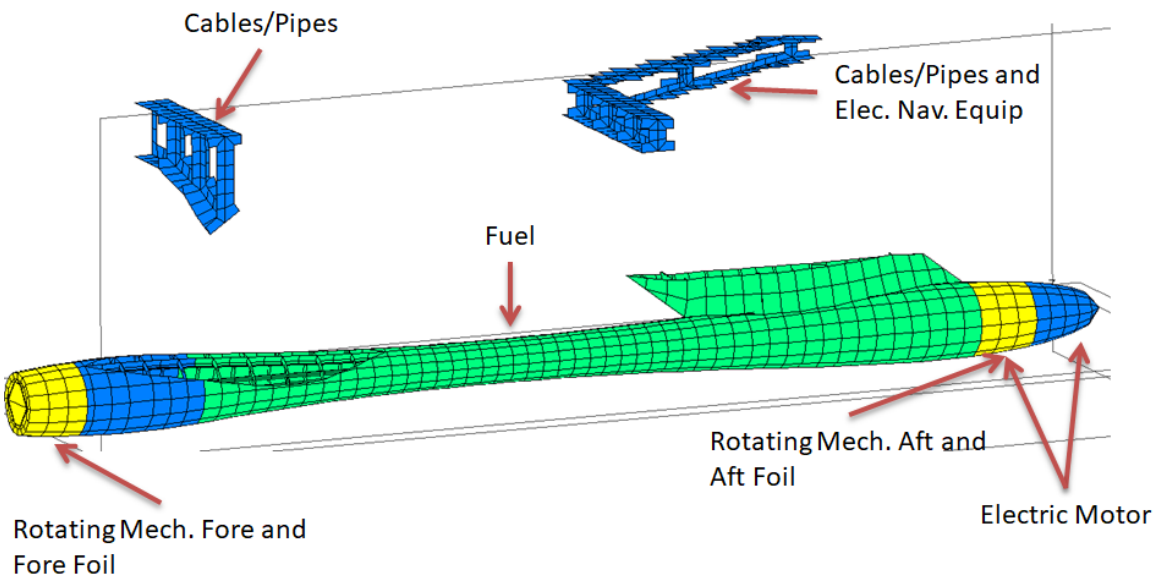
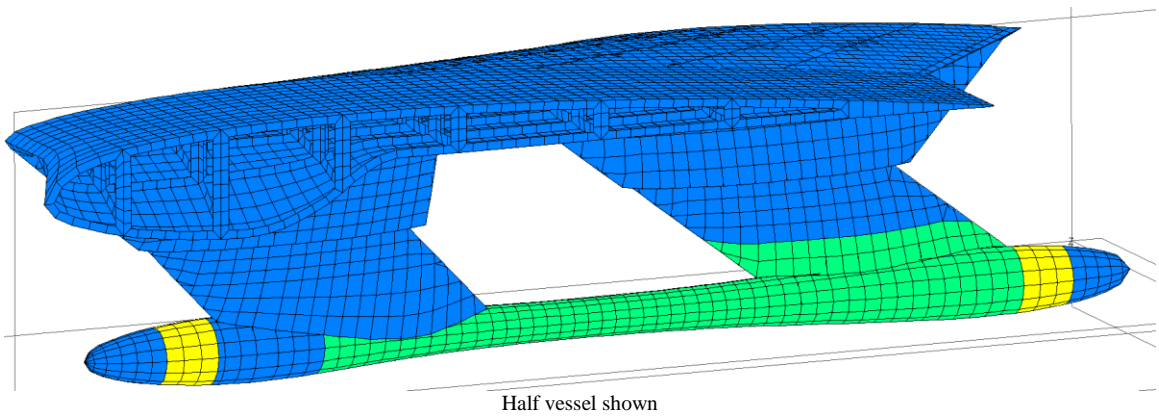


Figure 57: Concentrated Forces



Vessel divided for better visualization of loads

Figure 58: Distributed Forces

Once the loads have all been defined, load cases were created. A load case for buoyancy mode, flying mode, hogging condition, and sagging condition were created, again, as similarly as possible to the AMVS module reference vessel scenario.

In buoyancy mode, MAESTRO is able to trim and balance the vessel and no additional boundary condition restraints need to be applied. In flying mode, pins were placed on all of the hull mesh nodes where the hydrofoils are located. The aft hydrofoil pins restrict translation in the x-, y-, and z-directions. The forward pins restrict translation in the y-direction (heave direction). This is the same type of boundary condition applied in the AMVS module. Figure 59, shows the boundary condition restraints at the nodes where hydrofoils are located. They are shown in pink lines in the figure.

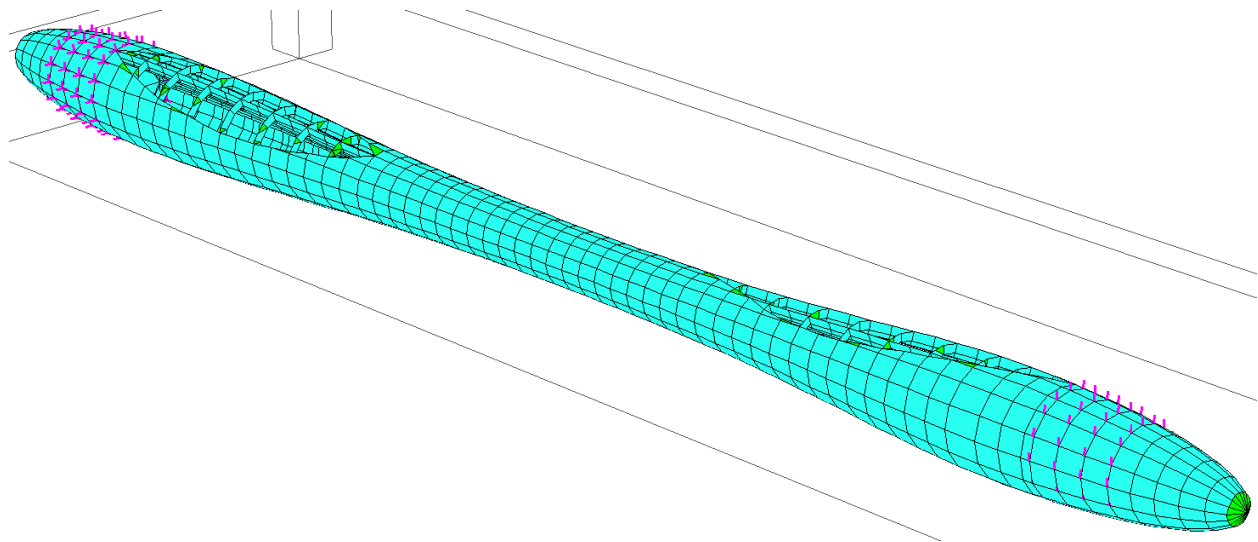


Figure 59: Flying Mode Restraints (Only Hull Shown)

In the hogging and sagging conditions, a series of x-y-z translation pins were placed over the length, as calculated by the AMVS module reference vessel hogging and sagging scenarios, and in accordance with DNVGL HSC rules. The pins were placed along the bottom half of the hull over the calculated hull. Figure 60 shows the hogging restraints and are colored in pink. Figure 61 shows the sagging restraints and are also colored pink.

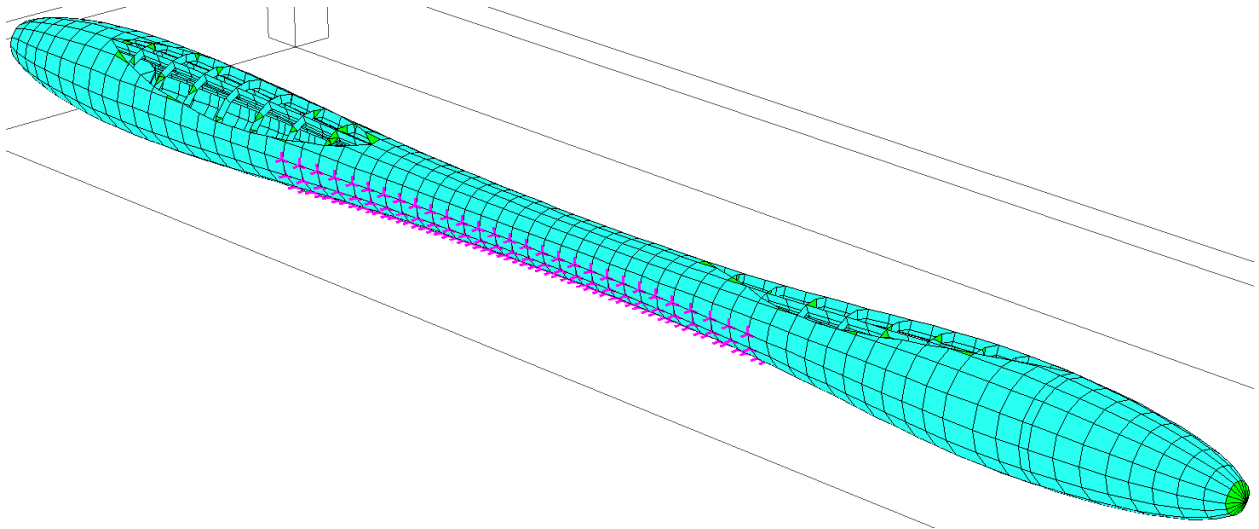


Figure 60: Hogging Condition Restraints (Only Hull Shown)

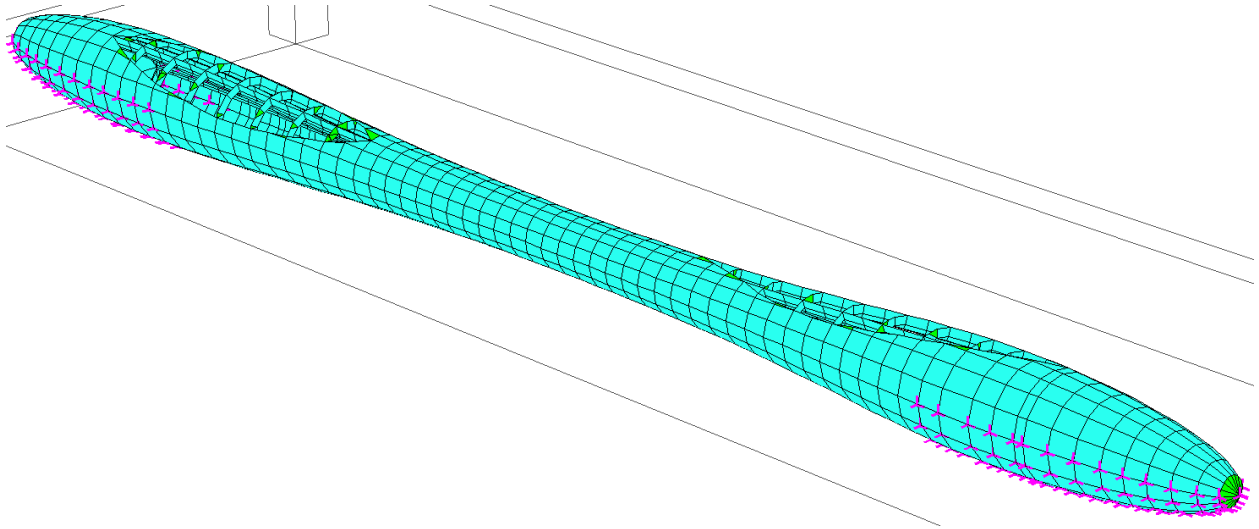


Figure 61: Sagging Condition Restraints (Only Hull Shown)

In addition, the hogging and sagging conditions were given and additional acceleration to gravity as delineated in the DNVGL HSC rules. The additional acceleration ($g + 28.92\text{m/s}^2$) was the same as that which was calculated by the AMVS module.

Once the load cases have been created, the model is “balanced” in the buoyancy mode and the FEA analysis was conducted for all load cases created. The weight summary report and balance output for the buoyancy mode has been provided in Figure 62 and Figure 63. Figure 62 shows the HY2-SWATH’s total displacement (after the vessel has mirrored) is 527,529 N or 53.8 MT. It also shows the trim angle is -0.375 deg. (by the stern). Figure 63 shows the weight break down by structural modules created in MAESTRO as well as the weight due to the applied concentrated and distributed loads.

```

***Information Only. No effect on FE-Analysis***
*Displacement= 527529 N, Volume=52.4349 m^3
*The following parameters are in the Ship Coordinate system:
*Center of Buoyancy: xCB= 10411.5 mm, yCB=644.096 mm, zCB=0 mm
*Center of Gravity: xCG= 10391 mm, yCG=1827.82 mm, zCG=0 mm
*Center of Flotation: xCF= 11748.1 mm, yCF=2252.13 mm, zCF=0 mm
*Trim Angle(Deg)=-0.375233
*Fore Draft Point (mm)=(19537.011, 2303.141, 3660.728)
*Aft Draft Point (mm)=( 3764.859, 2199.847, 5299.683)
*Fore Draft Point at z=0 (mm)=(19537.011, 2303.141, 0)
*Aft Draft Point at z=0 (mm)=( 3764.859, 2199.847, 0)
*Distance to origin =-2175.143 mm
*BMT= 7885.98 mm
*BML= 10048 mm
*It=4.13501e+14 mm^4
*I1=5.26866e+14 mm^4
*GMT=6702.14 mm
*GML=8864.16 mm

Balance Completed

```

Figure 62: Buoyancy Mode Load Balancing Outputs

```

-----Summary of Module Self Weight-----
MASS(kg)      XCG(mm)      YCG(mm)      ZCG(mm)      Module Name
977.943       13214.7      4464.36      2748.63      /top/superstructure stiffeners
1226.17       9976.71     -52.7278    4503.16      /top/hull shell
2027.65       11106.5     2581.24     4637.34      /top/strut shell
3400.03       12103      4438.35     2733.41      /top/superstructure shell
686.017       10032.6     0.0736272   4500         /top/hull stiffeners
1154.2        11427.3     2853.2      4576.74      /top/strut stiffeners

18944         11496.9     2947.51     0            ==>Total Module Weight(Full Ship, Exclude Tank Weight)
18944         11496.9     2947.51     0            ==>Total Force due to Weight(Full Ship)= 185777N
*****Summary of Module Gross Weight(Exclude Volume and Bay Set Weight)*****
Load case #1 "Buoyancy"
-----Summary of Nodal Group Weight-----
MASS(kg)      XCG(mm)      YCG(mm)      ZCG(mm)      Nodal Group Name
1575          8807.42     4658.13     2976.5       node/turbojet
150           10604.8     2239.12     4499         node/liquids
787.5         5876.6     2239.12     5313.97      node/genset_batt_inv
2500          17687.6     3432.85     -0.000150055 node/payload
5012.5        12829.8     3594.58     1904.76      ==>Total Weight of Nodal Group Mass

-----Summary of Plate Group Weight-----
MASS(kg)      XCG(mm)      YCG(mm)      ZCG(mm)      Plate Group Name
236.25        1366.44     0.0165616   4500.02      plate/electric motor
1611.75       18125.3     0.000306623 4500         plate/forefoil
1648.5        1809.76     0.0277887   4500.03      plate/aftfoil
131.25        1809.76     0.0277887   4500.03      plate/rotating mech aft
131.25        18125.3     0.000306623 4500         plate/rotating mech fore
170.625       16950.7     4521.51     1360.51      plate/cables and pipes_fwd
170.625       8100.4     4427.49     3183.27      plate/cables and pipes_aft
262.5         8100.4     4427.49     3183.27      plate/elec_nav_equip
8030.89       8037.22     62.5711     4538.84      plate/fuel_rev1
12393.6       8559.46     257.527     4435.93      ==>Total Weight of Plate Group Mass

*****Combined Weight Summary (include weight on coincide nodes)*****
MASS(kg)      XCG(mm)      YCG(mm)      ZCG(mm)      Module Name
4813.94       14819.2     3949.05     1299.91      /top/superstructure stiffeners
8627.01       8884.61     -41.5252    4501.46      /top/hull shell
1265          9645.76     2221.62     4699.34      /top/strut shell
4251.13       11126.3     4489.65     2843.43      /top/superstructure shell
4117.32       9038.76     12.8209     4500.98      /top/hull stiffeners
3803.75       9093.06     2241.7      4770.16      /top/strut stiffeners

53756.3      10391       1827.82     0            ==>Total Module Weight(Full Ship, Exclude Tank Weight)
( 18944)      -->Total Self Weight(Included in Total Module Weight)
( 10025)      -->Total Nodal Group Weight(Included in Total Module Weight)
( 24787.3)    -->Total Plate Group Weight(Included in Total Module Weight)
53756.3      10391       1827.82     0            ==>Total Force due to Weight(Full Ship)= 527169N

```

Figure 63: Buoyancy Weight Summary

Figure 64 shows a profile view of the HY2-SWATH after it has been balanced. After it has been balanced, the waterline can be toggled on and off. The figure shows that waterline is just above the lower strut's top edge. As stated previously, the trim angle is -0.375 deg. (by the stern). In Maestro, the negative sign on the trim angle indicates the stern is lower than the bow. In the AMVS module, a negative sign on the trim angle indicates the bow is lower than the stern.

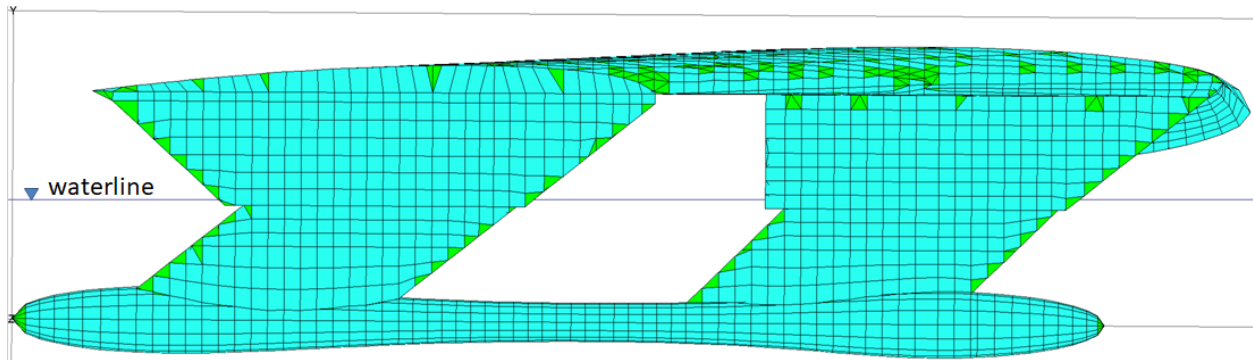
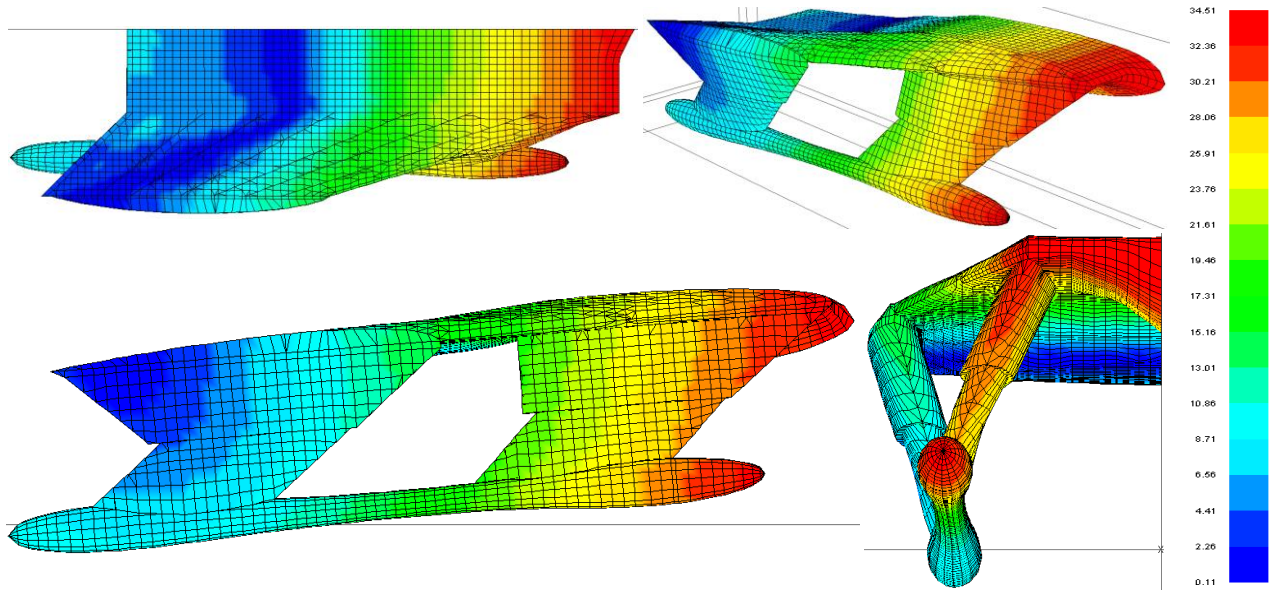


Figure 64: Profile View Showing Waterline

After running the FEA analysis, the results for each load case scenario created can be viewed. Sections 4.3 - 4.6 show the FEA results. The deflections figures show the profile, body, plan, and perspective views of the HY2-SWATH. Similar to the AMVS module, the deflection results have been exaggerated or magnified by 42 to allow the deflections to be seen more easily. The origin is at the vessel center line, stern and keel of the vessel. The positive y-direction is up, x-direction forward towards the bow, and z-direction towards starboard.

4.3 Buoyancy Mode Results

Figure 65 shows the HY2-SWATH displacement for buoyancy mode. As stated previously, the displacement results have been magnified by 42 for better visualization. The maximum y-displacement observed in the buoyancy mode condition was 34.50 mm, located at the centerline-leading edge of the wing-shaped superstructure. The maximum displacement represents the total translation of a node or element. It does not necessarily mean that a specific node/element has solely displaced that distance, but that several nodes and elements, together, have gradually translated to a final position. That final sum of gradual displacements is the total displacement.



Deflection Magnified by 42x factor – Displacement in mm

Figure 65: MAESTRO Reference Model Displacement Results (Buoyancy Mode)

Figure 66 shows the front view and highlights the node location with the max y-direction displacement. The figure also shows the displacements in the x- and z- directions, as well as the rotations in all three directions at that node.

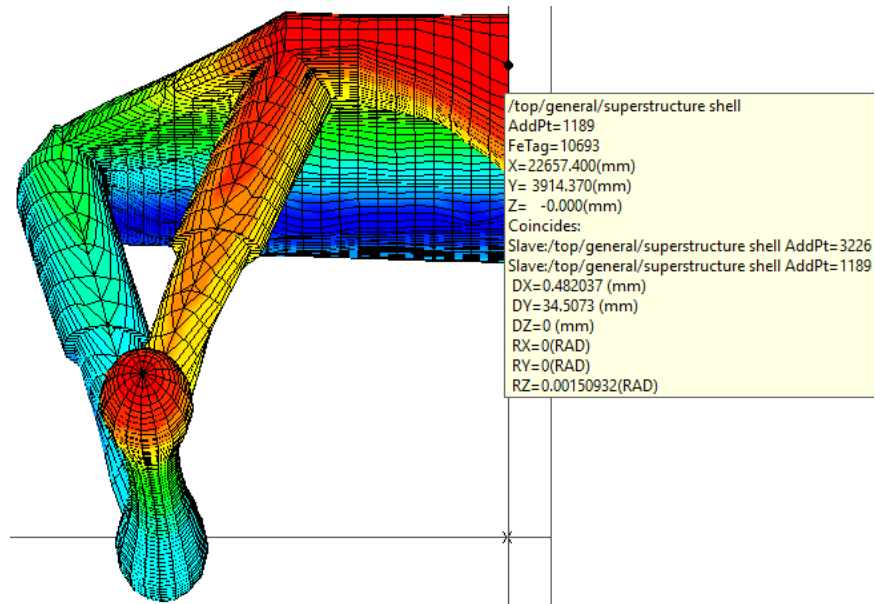
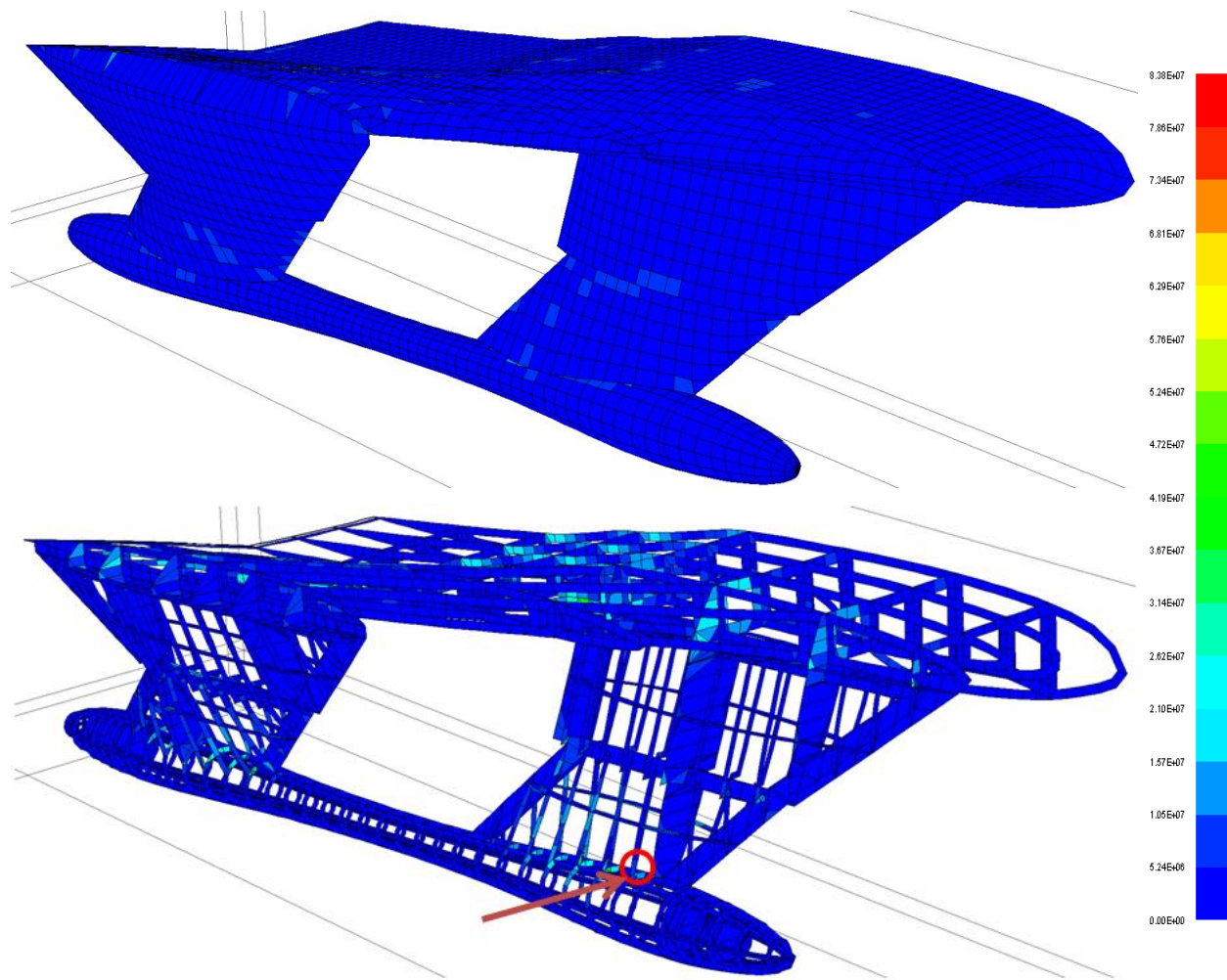


Figure 66 : Max Displacement Node Location (Buoyancy)

Figure 67 shows the HY2-SWATH Von Mises stresses. Von Mises stress is a scalar stress value obtained using the principle stresses shown in Equation 21.

$$\begin{aligned}\sigma_{VM} &= \sqrt{\frac{(\sigma_{11} - \sigma_{22})^2 + (\sigma_{22} - \sigma_{33})^2 + (\sigma_{33} - \sigma_{11})^2 + 6(\sigma_{12}^2 + \sigma_{23}^2 + \sigma_{31}^2)}{2}} \\ &= \sqrt{\frac{(\sigma_1 - \sigma_2)^2 + (\sigma_2 - \sigma_3)^2 + (\sigma_3 - \sigma_1)^2}{2}}\end{aligned}\tag{Equation 21}$$

When the Von Mises stress is higher than the material yield strength, then the material yields. The color gradient scale on the right side of the figure has been modified to show elements in red if they subject to failure using a safety factor of 6. In other words, the elements will display in red if they are 1/6 of the yield stress or greater. This color gradient scaling has been used for all the loading conditions in Sections 4.4 - 4.6. The top image of the figure shows the stress on the shell plating of the vessel and the bottom image of the figure shows the stress on the internal structure with the shell plating hidden.



Displacement Magnified by 42x factor – Stress in N/m^2

Figure 67: Von Mises Stress on Shell Plating and Internal Structure (Buoyancy)

The higher stresses are seen where the struts meet the hull/superstructure and at the midship section of the superstructure, in between the turbojets and where there is less support from the struts. The highest stress is 5.36×10^7 Pa and provides a SF of 9.38 over the yield stress (5.03×10^8 Pa). The highest stress is seen in the forward strut stiffeners where the stiffener meets the hull and is circled in red in Figure 67. Figure 68 provides a zoomed-in image of the red circle in Figure 67 and highlights the element with the highest Von Mises stress.

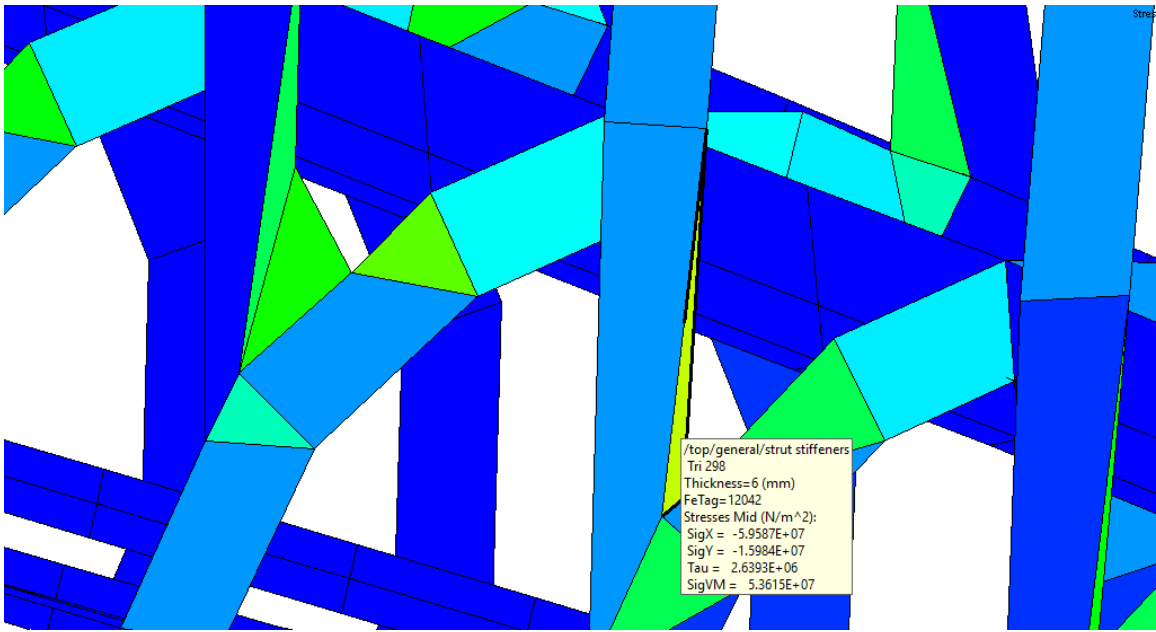
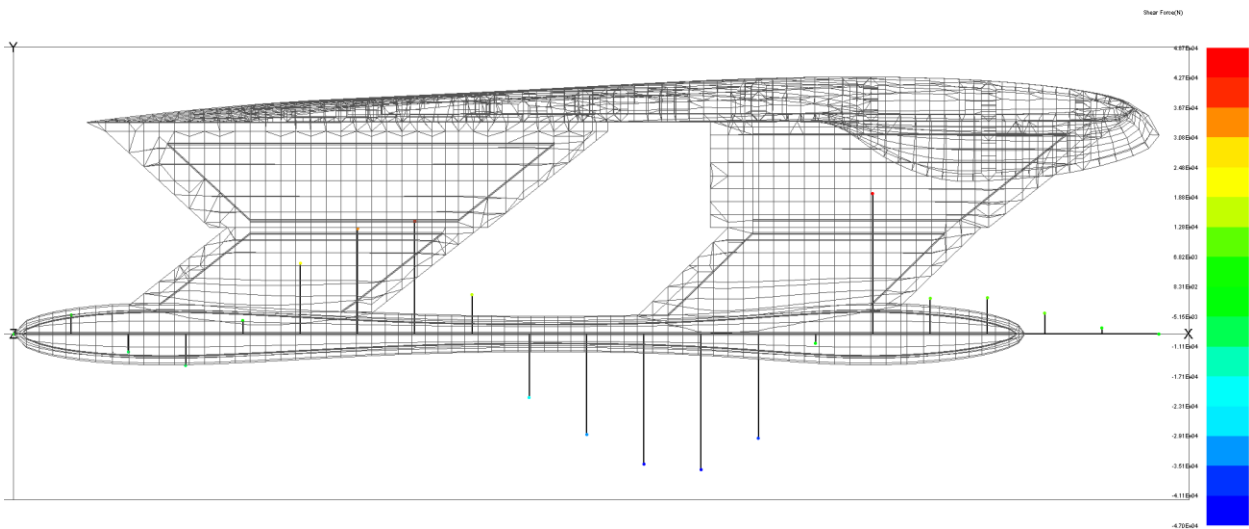


Figure 68: Zoomed Highest Stress Element (Buoyancy)

Figure 69 - Figure 70 show the longitudinal/transverse shear and bending moments for buoyancy mode. The shear and bending moment are provided as if the vessel has been projected on to the line at the base of the HY2-SWATH. The value of the shear/bending moment has been color coded in accordance with the color bar values on the right side of the image. The color bar is scaled from the lowest and highest values of shear or bending moment seen in the respective longitudinal or transverse view. The results have been summarized in Table 22.



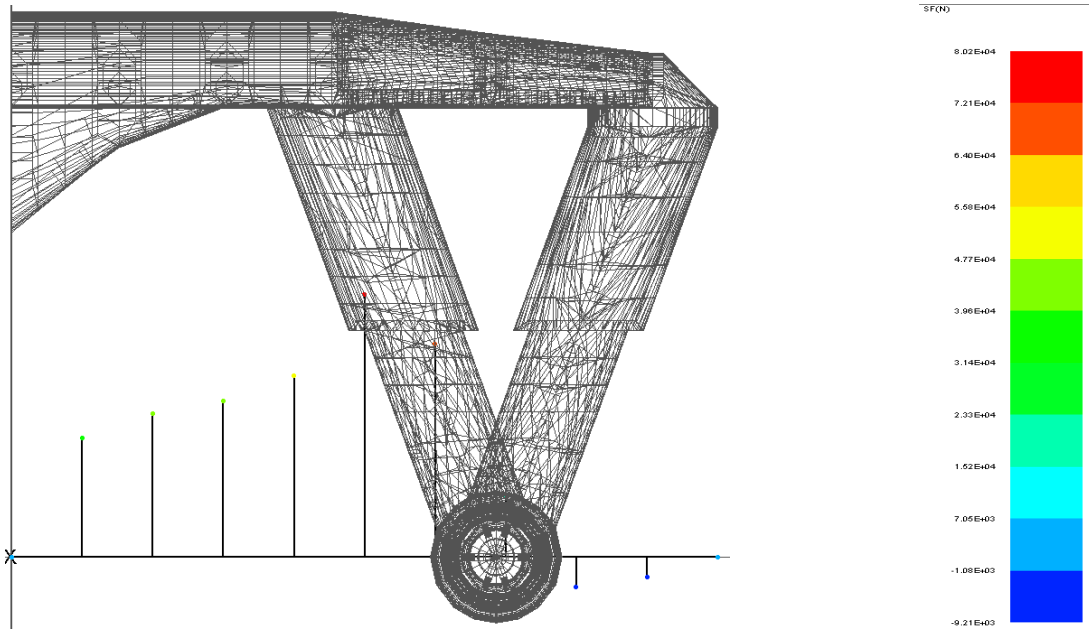
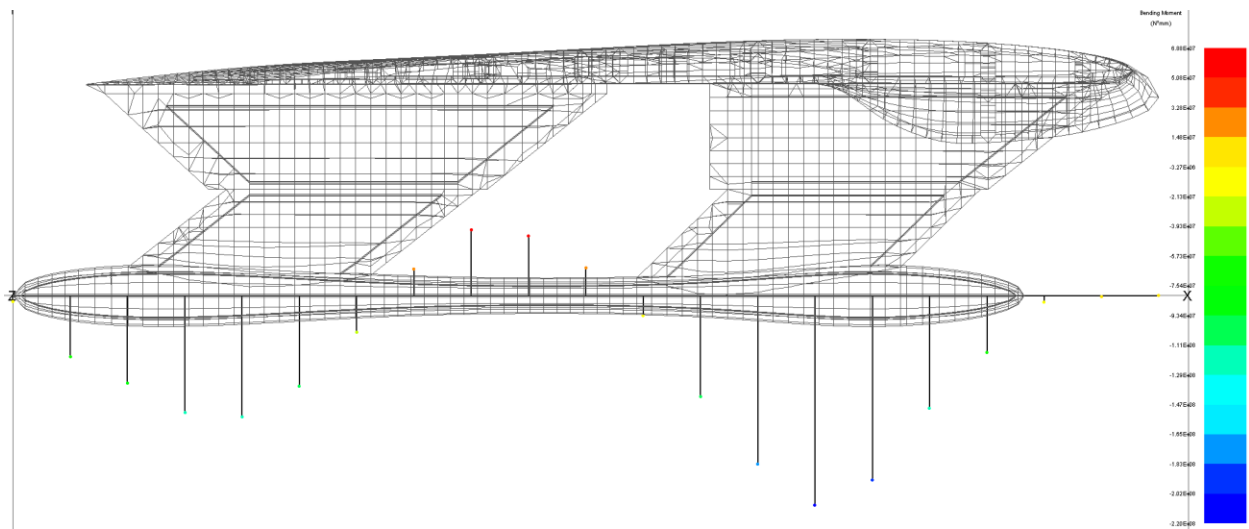


Figure 69: Longitudinal and Transverse Shear (Buoyancy Mode)



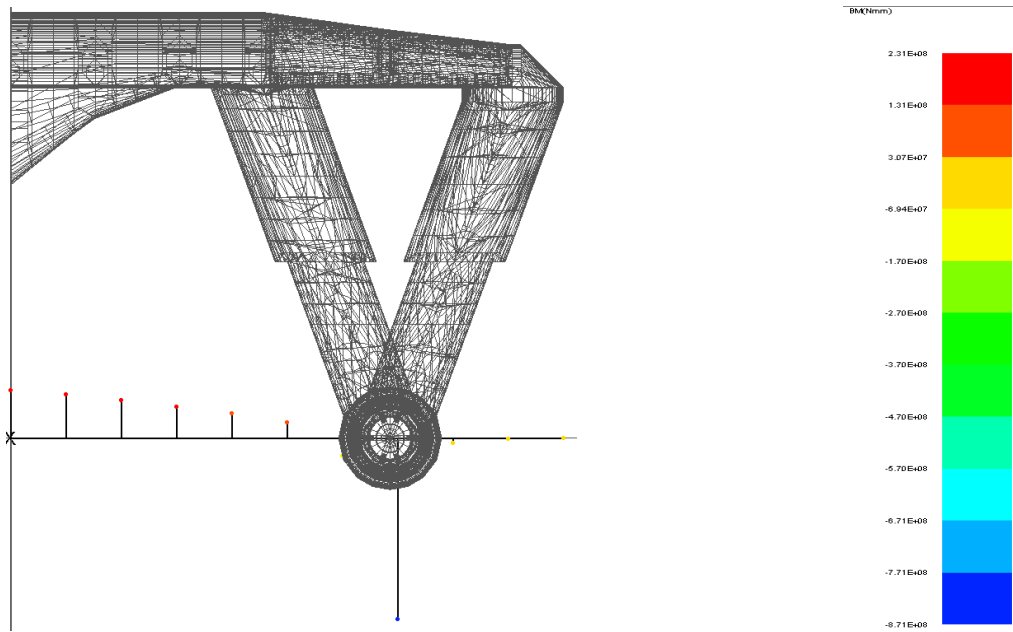
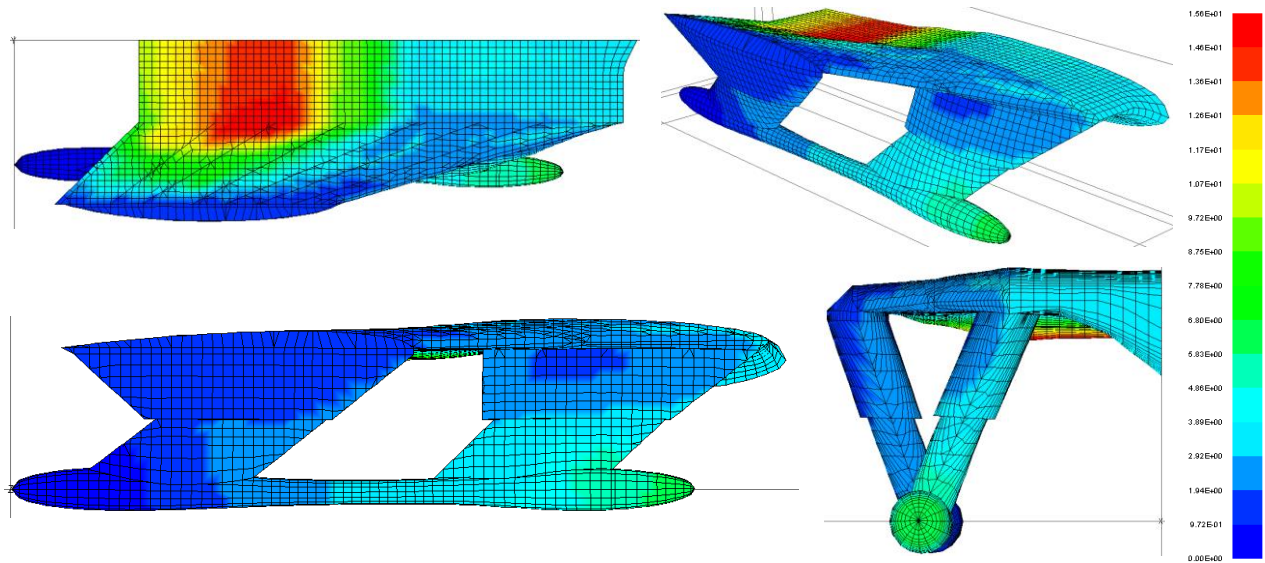


Figure 70: Longitudinal and Transverse Bending Moment (Buoyancy Mode)

Table 22 : Shear and Bending Moment Summary Results (Buoyancy Mode)				
	Shear (N)		Bending Moment (N*mm)	
	Min	Max	Min	Max
Longitudinal View	-4.70×10^4	4.87×10^4	-2.20×10^8	6.88×10^7
Transverse View	-9.21×10^4	8.02×10^4	-8.71×10^8	2.31×10^8

4.4 Flying Mode Results

Figure 71 shows the HY2-SWATH displacement for flying mode. Again, the displacement results have been magnified by 42 for better visualization. The max y-deflection observed in the flying mode condition was -15.49 mm located towards the aft-center of the superstructure where the turbojet is located.



Deflection Magnified by 42 – Displacement in mm

Figure 71: MAESTRO Reference Model Displacement Results (Flying Mode)

Figure 72 shows the top-down view of the HY2-SWATH and highlights the node location with the max y-direction displacement. The figure also shows the displacements in the x- and z- directions, as well as the rotations in all three directions at that node.

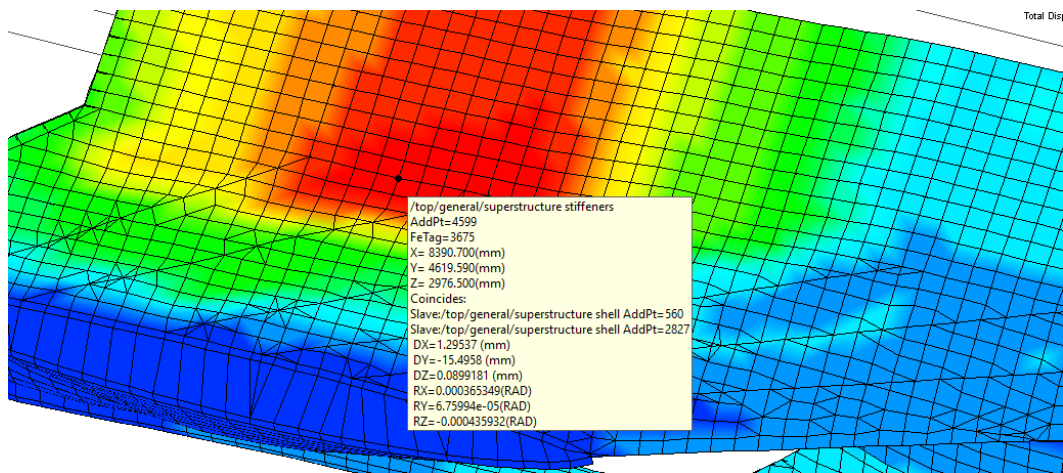
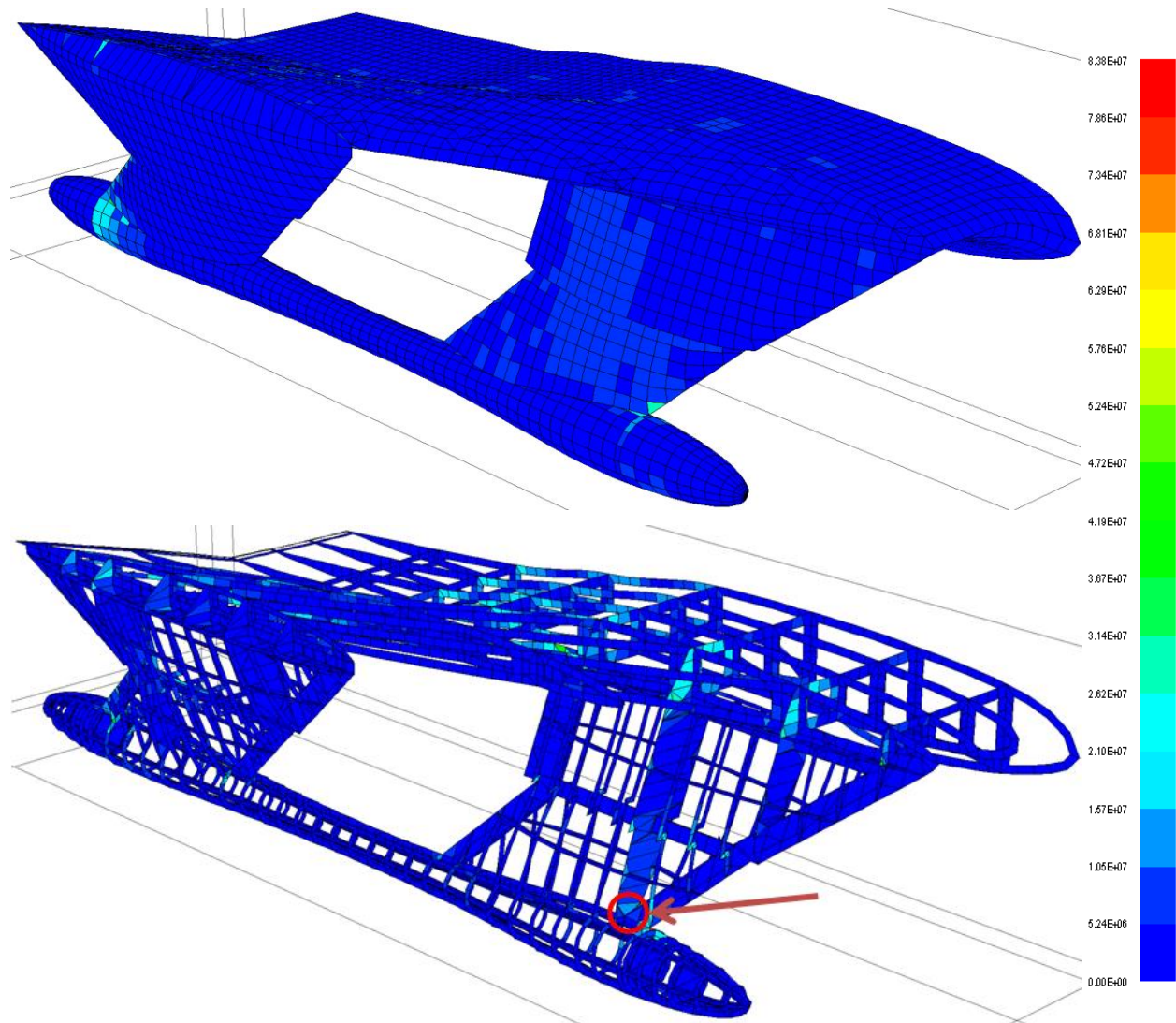


Figure 72 : Max Displacement Node Location (Flying)

Figure 73 shows the HY2-SWATH Von Mises stress. The top image of the figure shows the shell plating of the vessel and the bottom image of the figure shows the internal structure with the shell plating peeled away.



Displacement Magnified by 42x factor – Stress in N/m²

Figure 73: Von Mises Stress on Shell Plating and Internal Structure (Flying)

The higher stresses are seen again where the struts meet the hull/superstructure and at the midship section of the superstructure, where there is less support from the struts. The highest stress is 1.20×10^8 Pa and provides a SF of 4.19 over the yield stress (5.03×10^8 Pa). The highest stress is seen in the hull stiffeners where it meets with the forward strut stiffeners and is circled in red in Figure 73. Figure 74 provides a zoomed in image of the red circle in Figure 73 and highlights the element with the highest Von Mises stress. This figure also shows a heavily stressed element just forward where the forward hydrofoil ends and the hull interfaces with the forward structural girder of the strut.

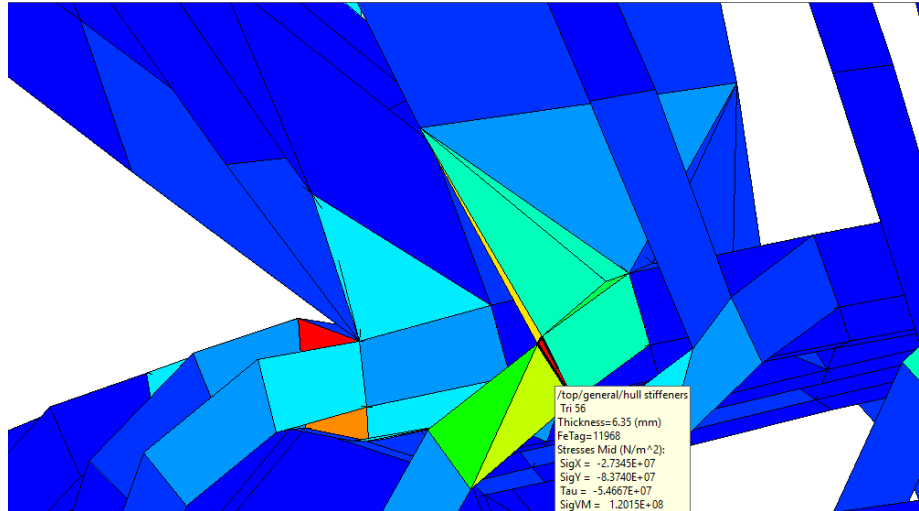
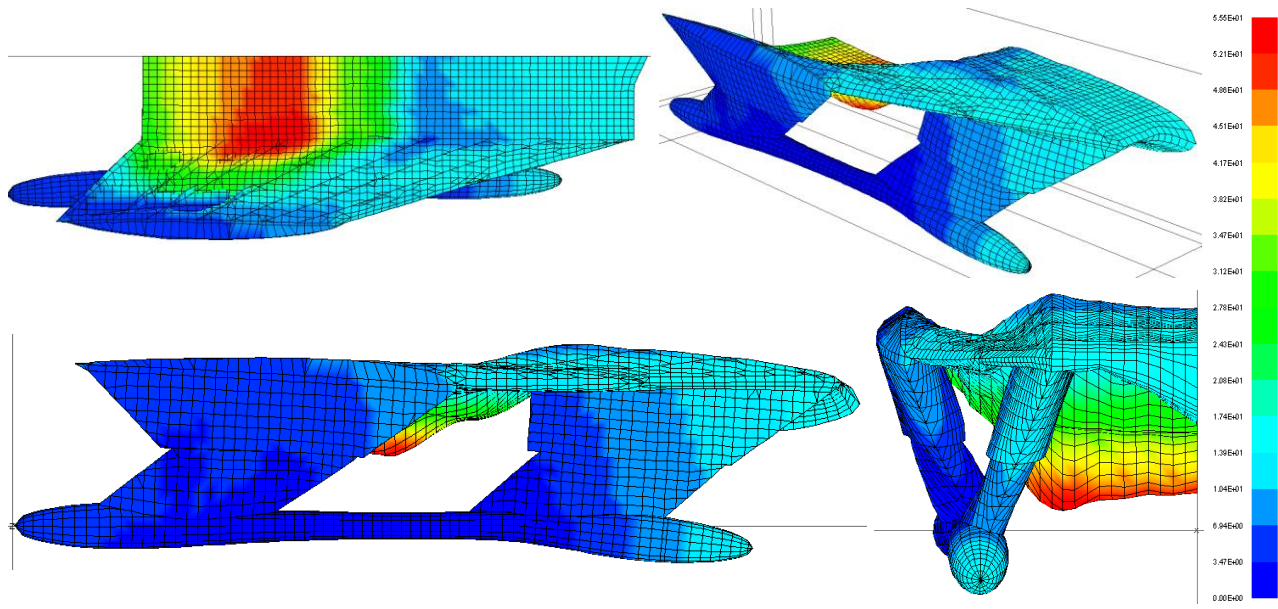


Figure 74: Zoomed Highest Stress Element (Flying)

4.5 Hogging Condition Results

Figure 75 shows the HY2-SWATH displacement the hogging condition. Again, the displacement results have been magnified by 42 for better visualization. The max displacement observed in hogging condition was -54.81 mm located towards the aft-center of the superstructure where the turbojet is located. This is the same node of the max displacement seen in flying mode.



Deflection Magnified by 42x factor – Displacement in mm

Figure 75: MAESTRO Reference Model Displacement Results (Hogging Condition)

Figure 76 shows the top-down view of the HY2-SWATH and highlights the node location with the max y-direction displacement. The figure also shows the displacements in the x- and z- directions, as well as the rotations in all three directions at that node.

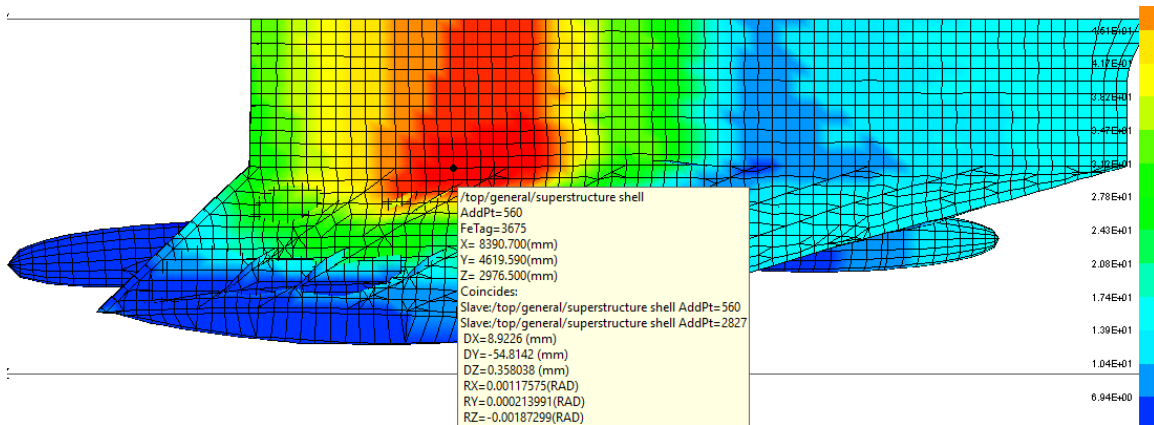
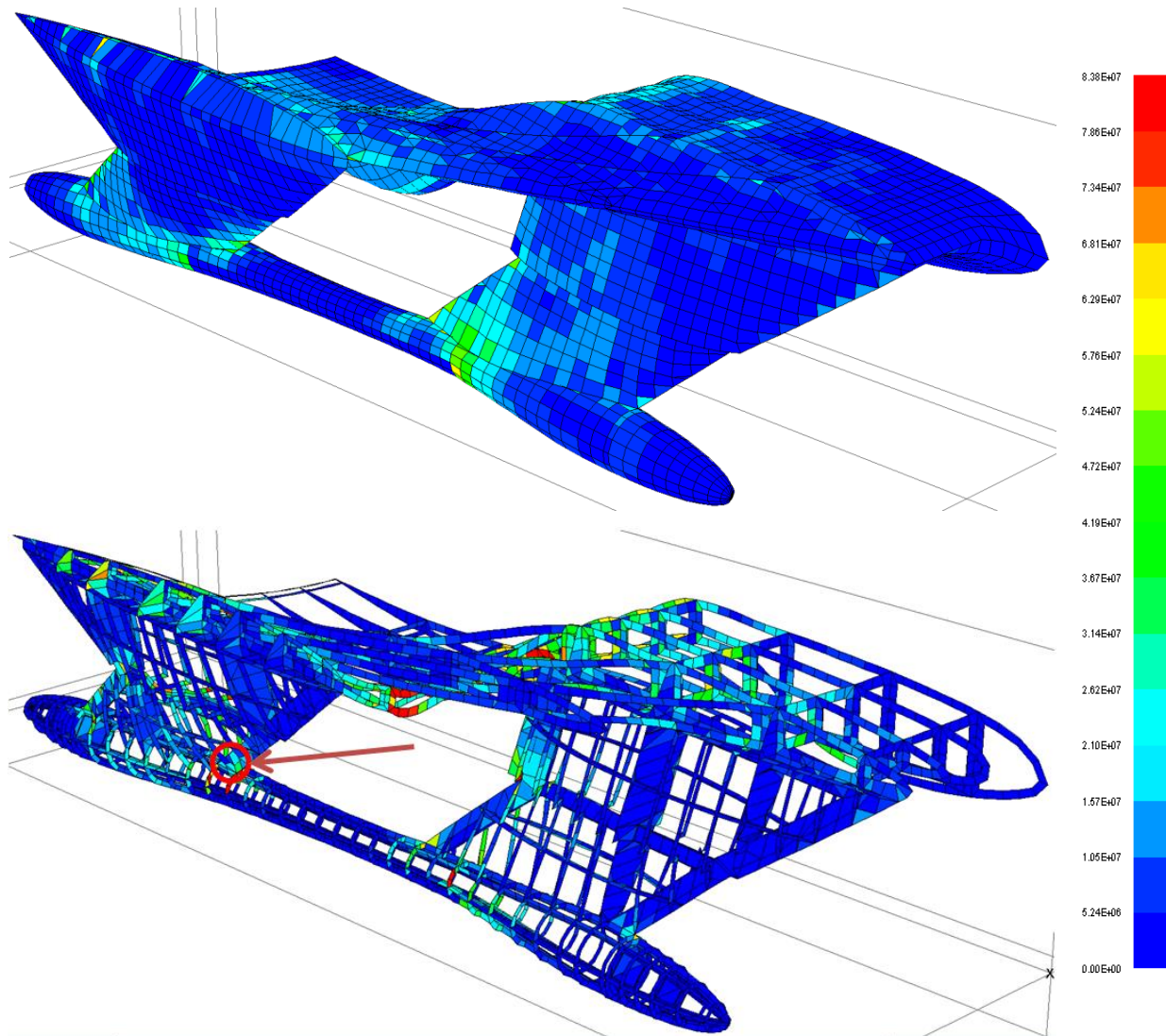


Figure 76: Max Displacement Node Location (Hogging)

Figure 77 shows the HY2-SWATH Von Mises stress. The top image of the figure shows the shell plating of the vessel and the bottom image of the figure shows the internal structure with the shell plating peeled away.



Displacement Magnified by 42x factor - Stress in N/m²

Figure 77: Von Mises Stress on Shell Plating and Internal Structure (Hogging)

The higher stresses are seen in the where the struts meet the hull/superstructure and at the midship section of the superstructure, where there is less support from the struts. The highest stress is 2.58×10^8 Pa and provides a SF of 1.95 over the yield stress (5.03×10^8 Pa). The highest stress is seen in the hull stiffeners where the stiffener meets the aft stiffener and is circled in red in Figure 77. Figure 78 provides a zoomed in image of the red circle in Figure 77 and highlights the element with the highest Von Mises stress.

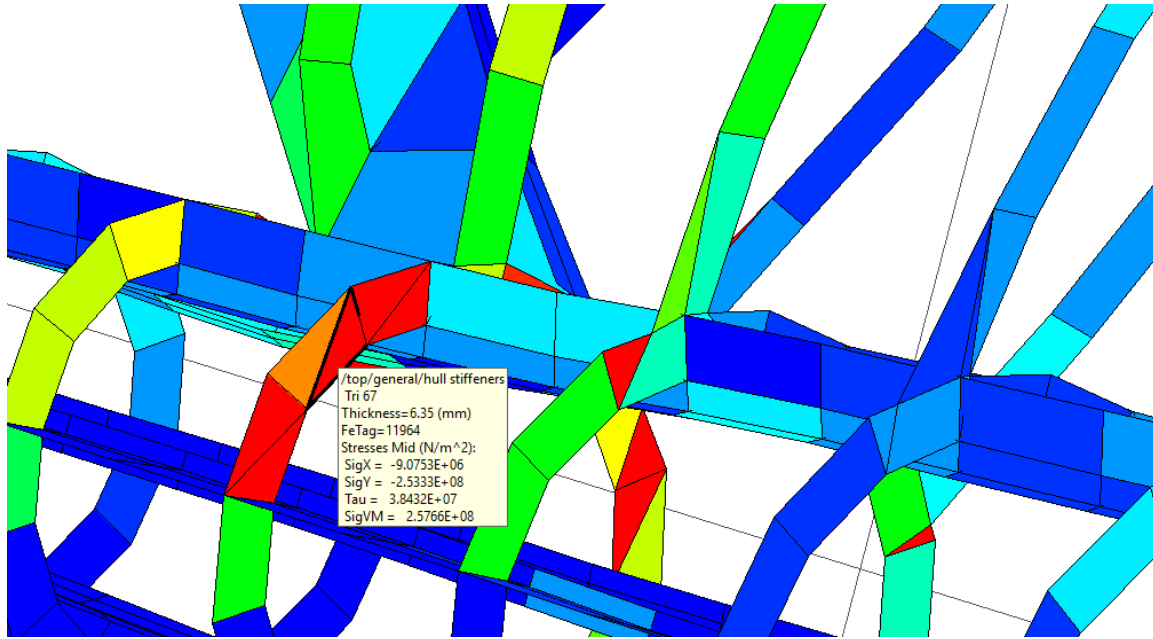
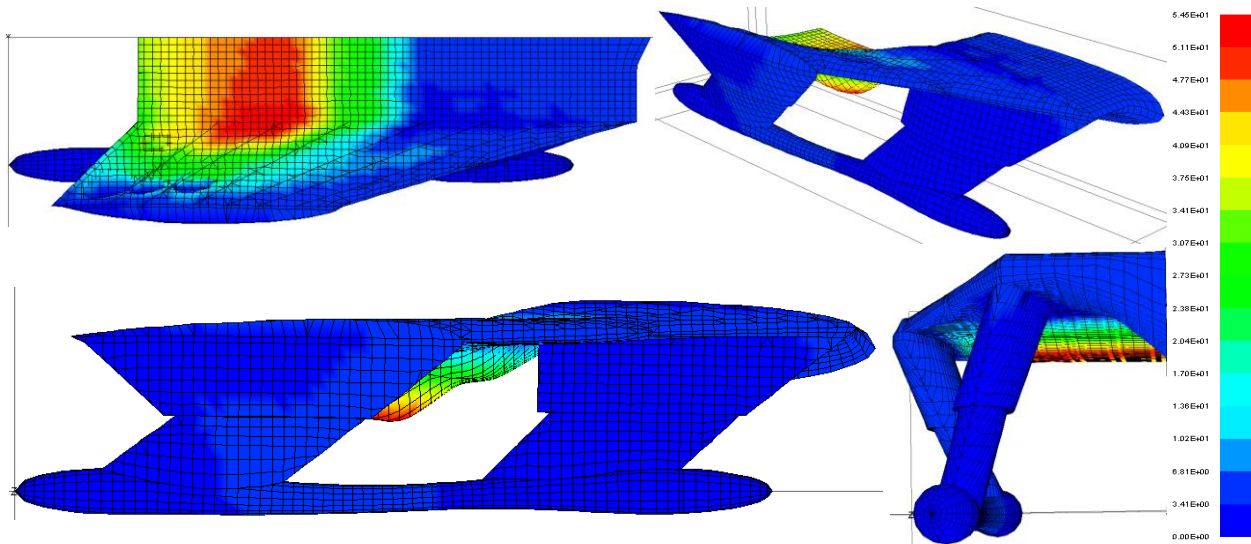


Figure 78: Zoomed Highest Stress Element (Hogging)

4.6 Sagging Condition Results

Figure 79 shows the HY2-SWATH displacement for the sagging load case scenario. To maintain consistency, the displacement results have been magnified by 42 for better visualization. The max displacement observed in the sagging load case scenario was -54.34 mm located towards the aft-center of the superstructure, where the turbojet is located. This is the same exact place as the max displacement seen in flying mode and hogging load cases.



Deflection Magnified by 42x factor – Displacement in mm

Figure 79: MAESTRO Reference Model Structural Displacement Results (Sagging Condition)

Figure 80 shows the top-down view of the HY2-SWATH and highlights the node location with the max y-direction displacement. The figure also shows the displacements in the x- and z- directions, as well as the rotations in all three directions at that node.

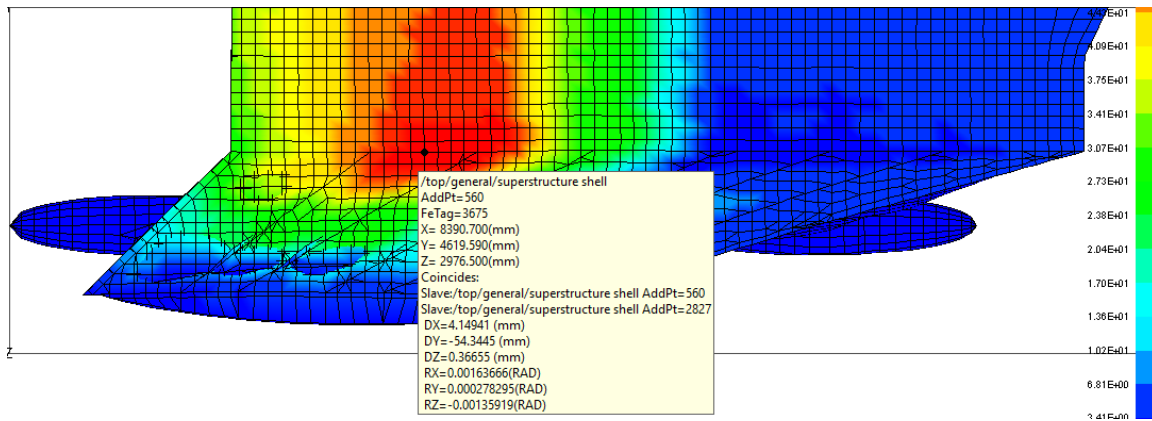
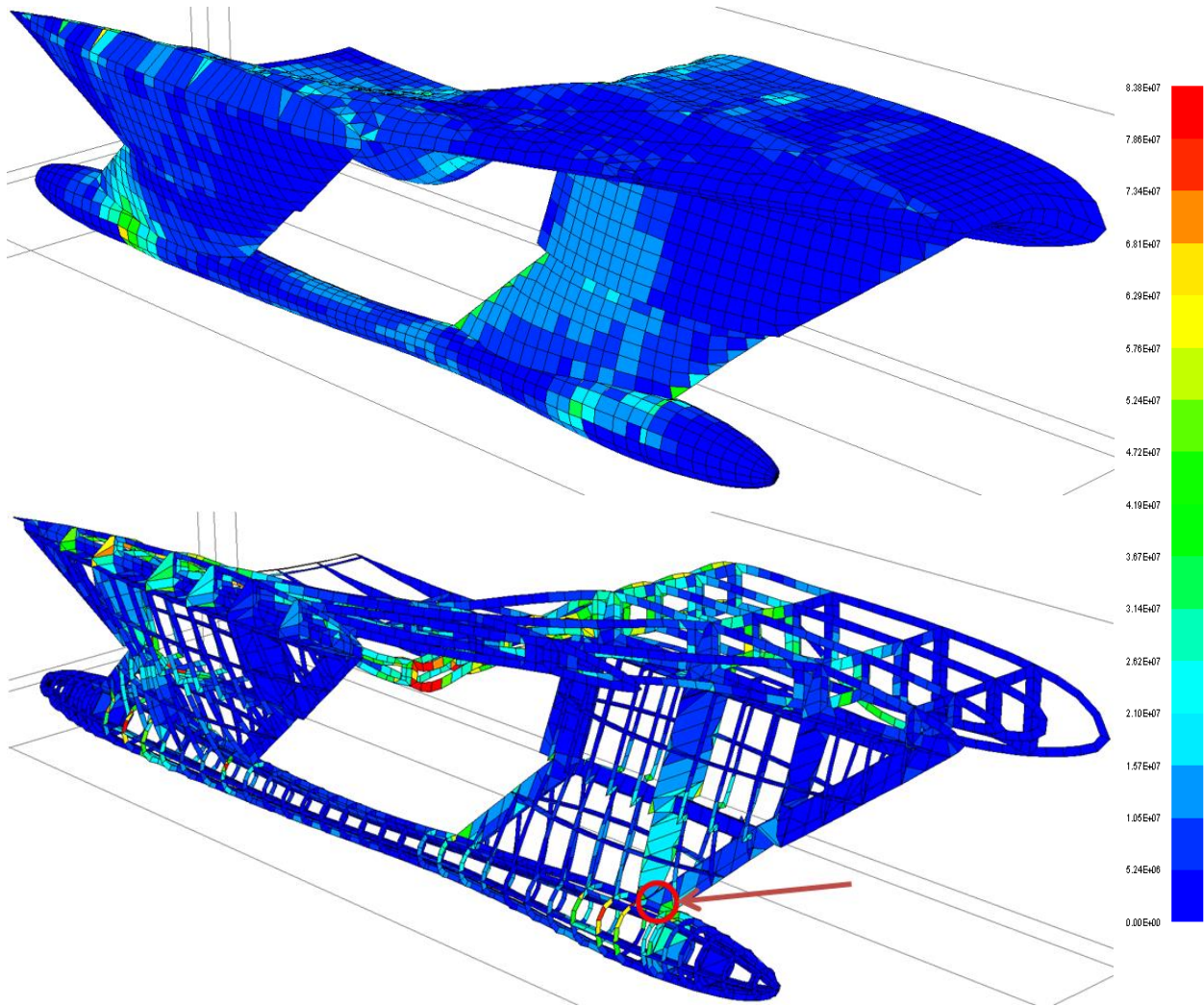


Figure 80: Max Displacement Node Location (Sagging)

Figure 81 shows the HY2-SWATH Von Mises stress. The top image of the figure shows the shell plating of the vessel and the bottom image of the figure shows the internal structure with the shell plating peeled away.



Displacement Magnified by 42x factor – Stress in N/m²

Figure 81: Von Mises Stress on Shell Plating and Internal Structure (Sagging)

The higher stresses are seen in the where the struts meet the hull/superstructure and at the midship section of the superstructure, where there is less support from the struts. The highest stress is 1.94×10^8 Pa and provides a SF of 2.59 over the yield stress (5.03×10^8 Pa). The highest stress is seen in the hull stiffeners where the stiffener meets the aft stiffener and is circled in red in Figure 81. Figure 82 provides a zoomed in image of the red circle in Figure 81 and highlights the element with the highest Von Mises stress.

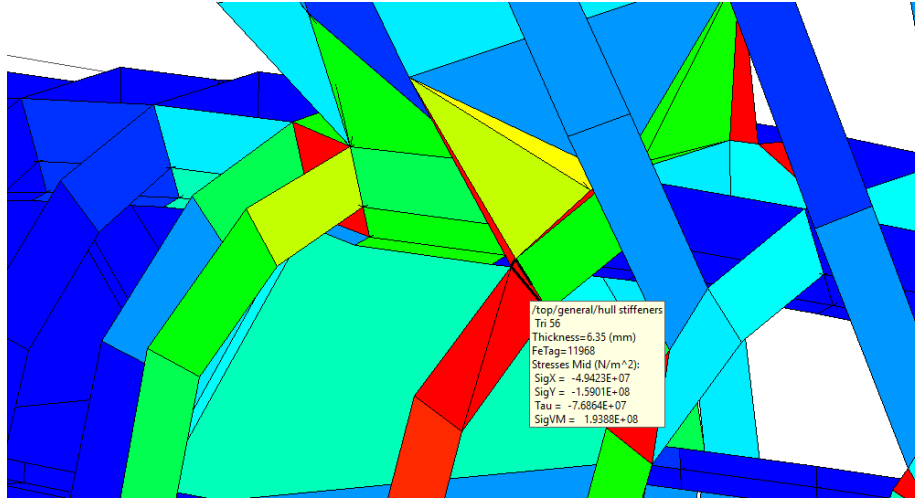


Figure 82: Zoomed Highest Stress Element (Sagging)

5. HY2-SWATH Multi-Fidelity Model Analysis and Future Work

The multi-fidelity analysis method provides way to quickly explore the design space by generating numerous variations of the HY2-SWATH quickly, using the AMVS module and comparison analysis method to increase the accuracy using a high-fidelity analysis module. Once the two fidelity methods have been created and run, they can be scrutinized and refined to further increase their accuracy. Additionally, structural modifications can be made to the vessel in areas of high stress and displacement to strengthen weak areas. Thus, it is important to note how the HY2-SWATH modeled in MAESTRO differs from HY2-SWATH modeled in the AMVS module.

5.1 Multi-Fidelity Model Analysis

Table 23 shows the AMVS module displacement results for the reference HY2-SWATH and the location of the displacements within each frame analyzed and for each load case. These displacements are in the AMVS w-direction or equivalently in MAESTRO's y-direction.

Table 23: AMVS Max Displacement Results Summary						
Load Case	Forward Frame Location	Forward Frame Displacement (mm)	Aft Frame Location	Aft Frame Displacement (mm)	Hull Frame Location	Hull Frame Displacement (mm)
Buoyancy Mode	Node 7	-5.33	Node 6	-4.50	Node 10	0.752
Flying Mode	Node 7	-5.33	Node 6	-4.50	Node 11	-65.1
Hogging	Node 7	-21.0	Node 6	-17.78	Node 21	-43.0
Sagging	Node 7	-21.0	Node 6	-17.78	Node 11	-14.9

Table 24 shows the AMVS module principle stress results for the reference HY2-SWATH. It shows the max stress and the location where the stress is found in each frame and for each load case.

Load Case	Forward Frame Location	Forward Frame Stress, σ_1 (Pa)	Forward Frame Stress, σ_2 (Pa)	Aft Frame Location	Aft Frame Stress, σ_1 (Pa)	Aft Frame Stress, σ_2 (Pa)	Hull Frame Location	Hull Frame Stress, σ_1 (Pa)	Hull Frame Stress, σ_2 (Pa)
Buoyancy Mode	Element 6	3.931×10^6	-9.246×10^3	Element 5	2.653×10^6	-1.967×10^4	Element 10	1.037×10^6	0
Flying Mode	Element 6	3.931×10^6	-9.246×10^3	Element 5	2.653×10^6	-1.967×10^4	Element 11	7.614×10^7	0
Hogging	Element 6	1.553×10^7	-3.651×10^4	Element 5	1.047×10^7	-7.769×10^4	Element 7	6.933×10^7	0
Sagging	Element 6	1.553×10^7	-3.651×10^4	Element 5	1.047×10^7	-7.769×10^4	Element 6	4.020×10^7	0

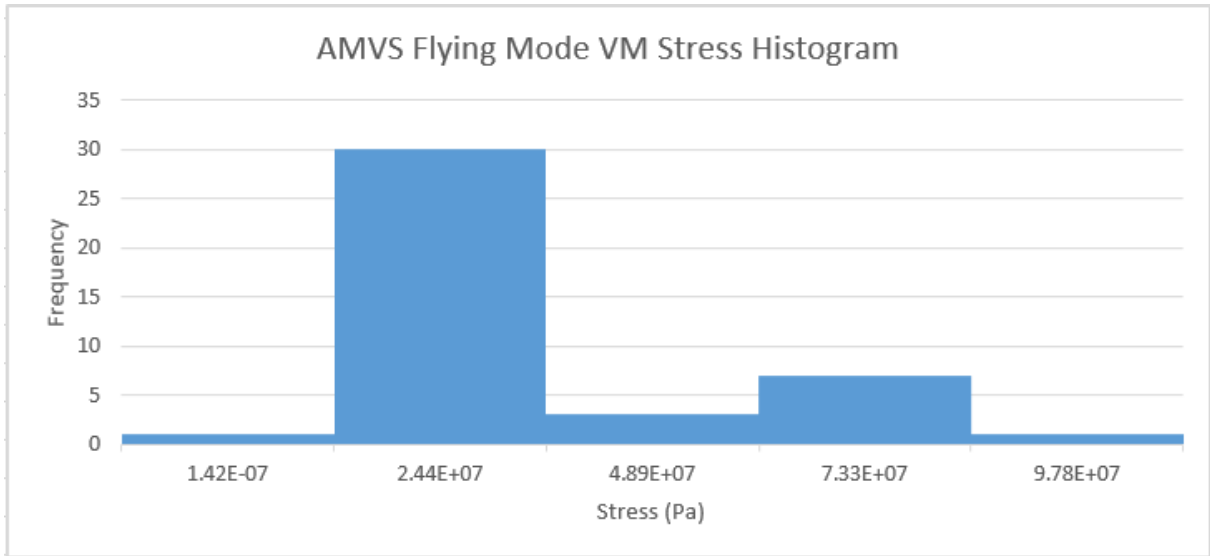
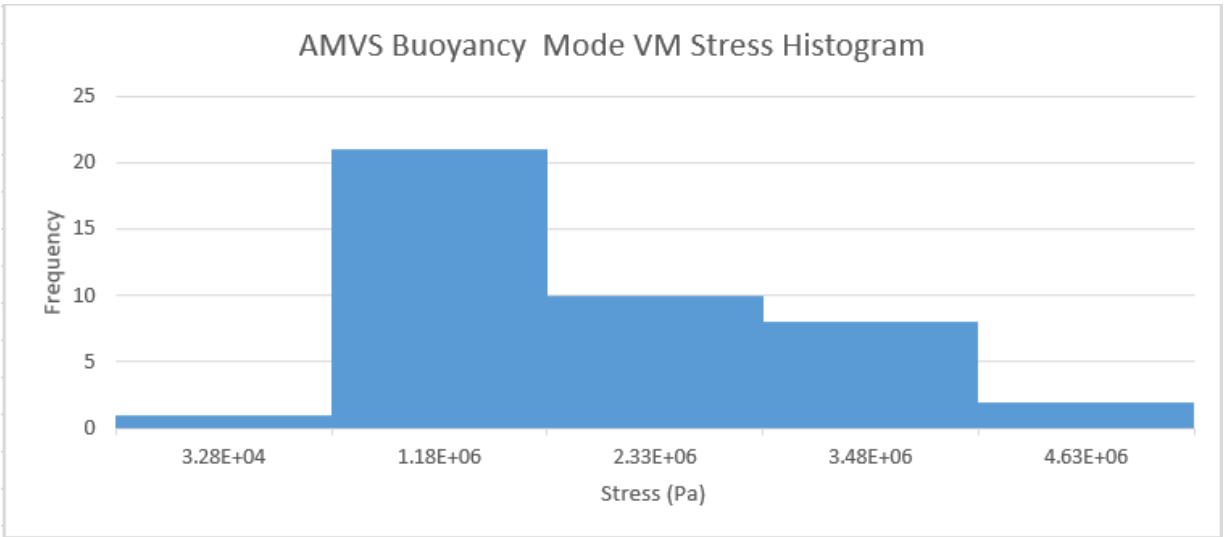
Using Equation 21, the AMVS module principal stresses were used to calculate the Von Mises stress and are summarized in Table 25. Since σ_1 has a much greater value than σ_2 , it appears that the Von Mises Stress, σ_{VM} , is equivalent to σ_1 with the number of significant figures displayed.

Load Case	Forward Frame Location	Forward Frame Stress, σ_{VM} (Pa)	Aft Frame Location	Aft Frame Stress, σ_{VM} (Pa)	Hull Frame Location	Hull Frame Stress, σ_{VM} (Pa)
Buoyancy Mode	Element 6	3.931×10^6	Element 5	2.653×10^6	Element 10	1.037×10^6
Flying Mode	Element 6	3.931×10^6	Element 5	2.653×10^6	Element 11	7.614×10^7
Hogging	Element 6	1.553×10^7	Element 5	1.047×10^7	Element 7	6.933×10^7
Sagging	Element 6	1.553×10^7	Element 5	1.047×10^7	Element 6	4.02×10^7

To further improve understanding of the stresses on the reference HY2-SWATH, as a whole, statistical information was calculated on all the stresses for each load case. The Von Mises stress was calculated for each element for the three frames of analysis and the range, average, standard deviation, and the number of standard deviations from the average for the max stress. The values are reported in Table 26.

Load Case	Stress Range, Max-Min (Pa)	Average, μ (Pa)	Standard Deviation, σ (Pa)	Max Stress Std. Dev. From Avg. ($\mu \pm \sigma$)
Buoyancy Mode	3.903×10^6	1.332×10^6	1.149×10^6	2.27
Flying Mode	7.615×10^7	1.622×10^7	2.445×10^7	2.45
Hogging	6.933×10^7	1.236×10^7	1.562×10^7	3.65
Sagging	4.020×10^7	1.371×10^7	1.199×10^7	2.21

Additionally, histograms (Figure 83) were created to help visualize the stress data distribution.



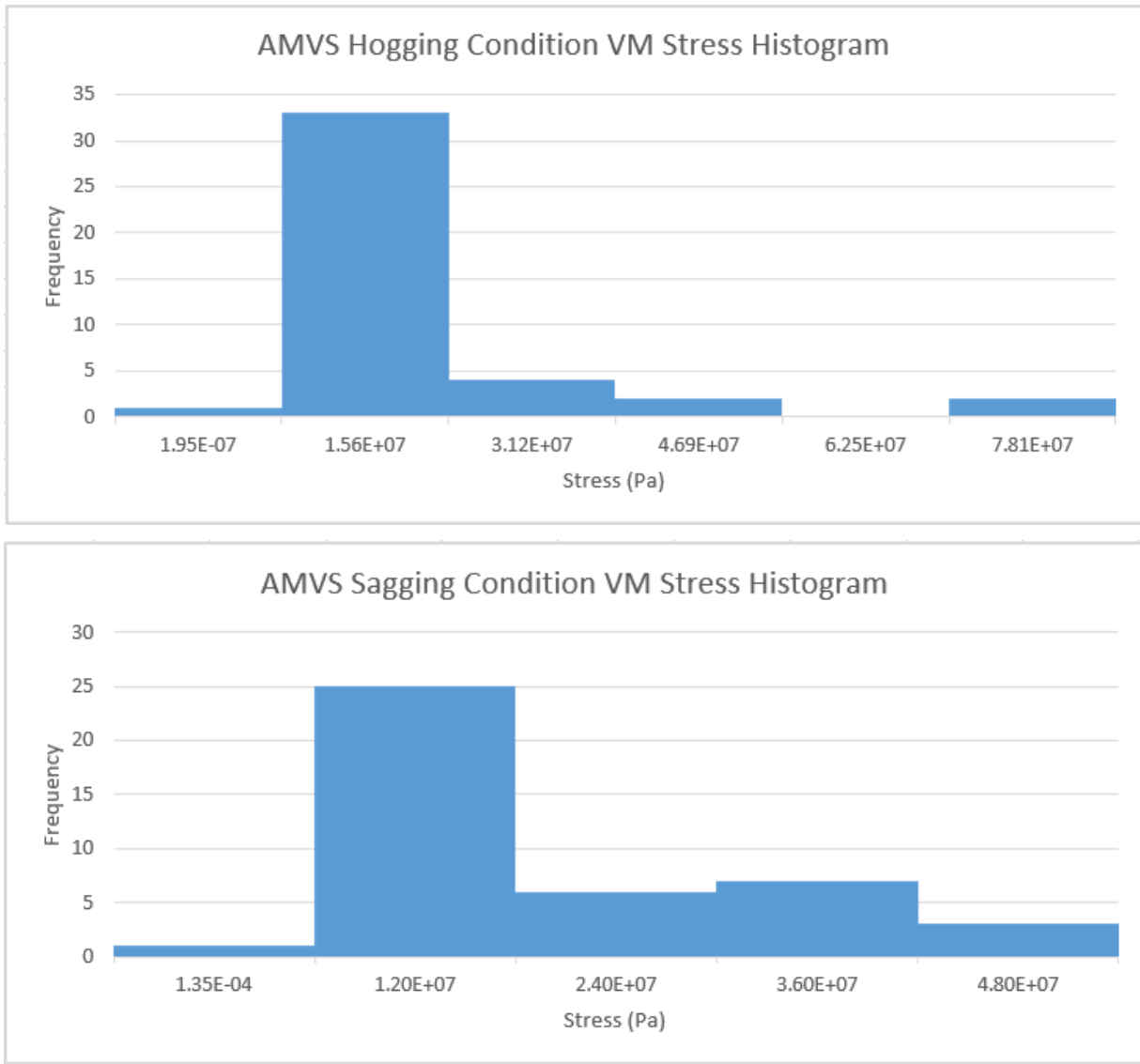


Figure 83: AMVS Von Mises Stress Histograms

Table 27 summarizes the location and max displacements found in the MAESTRO model for the different load case scenarios. The max displacements all occurred in the MAESTRO's y-direction.

Table 27: MAESTRO Max Displacement Results Summary		
Load Case	Displacement Location	Displacement (mm)
Buoyancy Mode	FeTag 10693	34.50
Flying Mode	FeTag 3675	-15.49
Hogging	FeTag 3675	-54.81
Sagging	FeTag 3675	-54.34

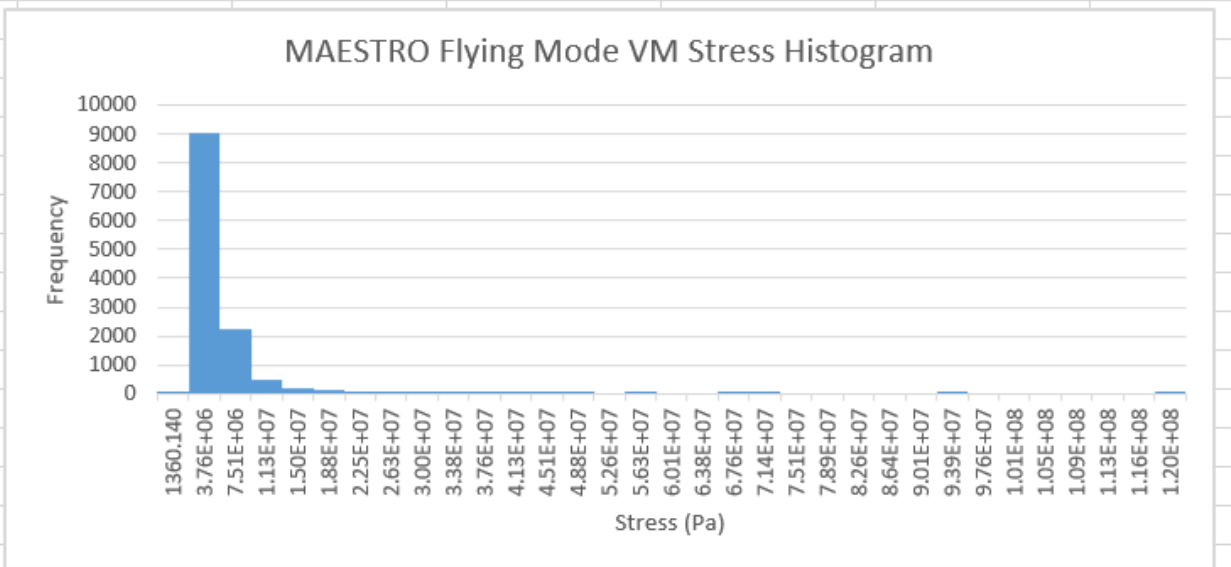
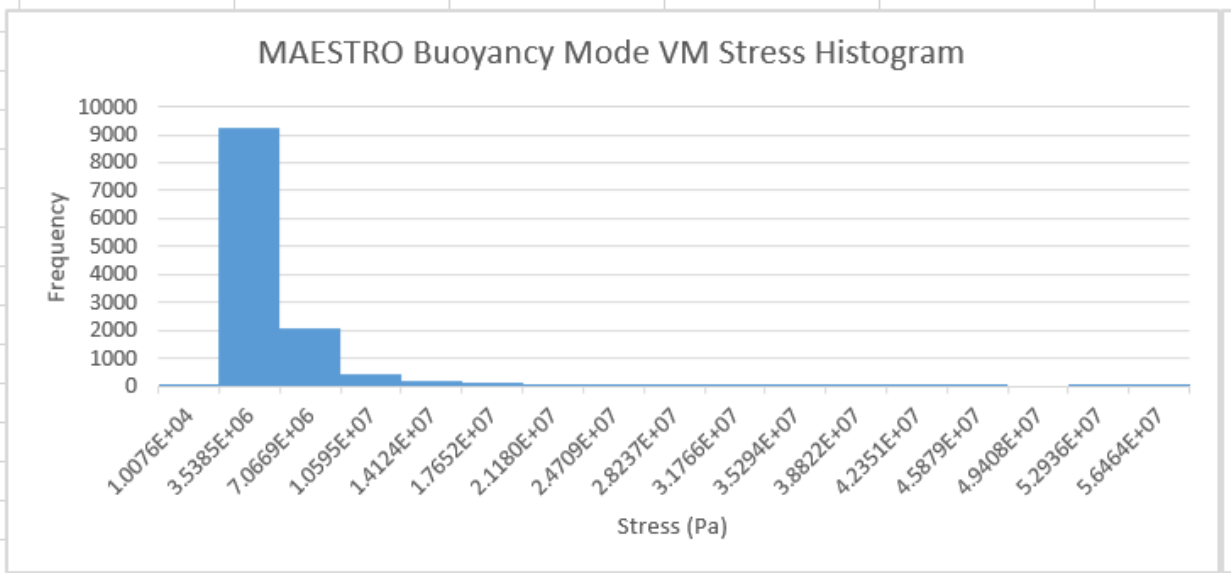
Table 28 summarizes the location and max stresses found in the MAESTRO model for the different load case scenarios.

Load Case	Stress Location	Max Stress (Pa)	Safety Factor
Buoyancy Mode	Strut Stiffener Tri 298 FeTag 12042	5.36×10^7	9.38
Flying Mode	Hull Stiffener Tri 56 FeTag 11968	1.20×10^8	4.19
Hogging	Hull Stiffener Tri 67 FeTag 11964	2.58×10^8	1.95
Sagging	Hull Stiffener Tri 56 FeTag 11968	1.94×10^8	2.59

MAESTRO's results for displacement are similar in magnitude to the AMVS module's calculation of the displacement. The max stress in the MAESTRO was about an order of magnitude greater than those calculated in the AMVS module. Due to the MAESTRO's highest element stresses existing in solely in tri-elements, the difference between the calculated low-fidelity/high-fidelity stress, and the highest stress existing in the same element in flying mode an sagging mode; further investigation and generation of statistical data to determine if the max stresses are outliers has been done. The statistical results are summarized in Table 29.

Load Case	Stress Range, Max-Min (Pa)	Average, μ (Pa)	Standard Deviation, σ (Pa)	Max Stress Std. Dev. From Avg. ($\mu \pm \sigma$)
Buoyancy Mode	5.361×10^7	2.858×10^6	3.528×10^6	14.39
Flying Mode	1.201×10^8	3.106×10^6	3.755×10^6	31.13
Hogging	2.577×10^8	1.038×10^7	1.359×10^7	18.22
Sagging	1.939×10^8	9.412×10^6	1.173×10^7	15.74

Figure 84 shows histograms to visualize the frequency of stress occurrences. The bin sizes used was the standard deviation to help determine if the max stresses were truly outliers.



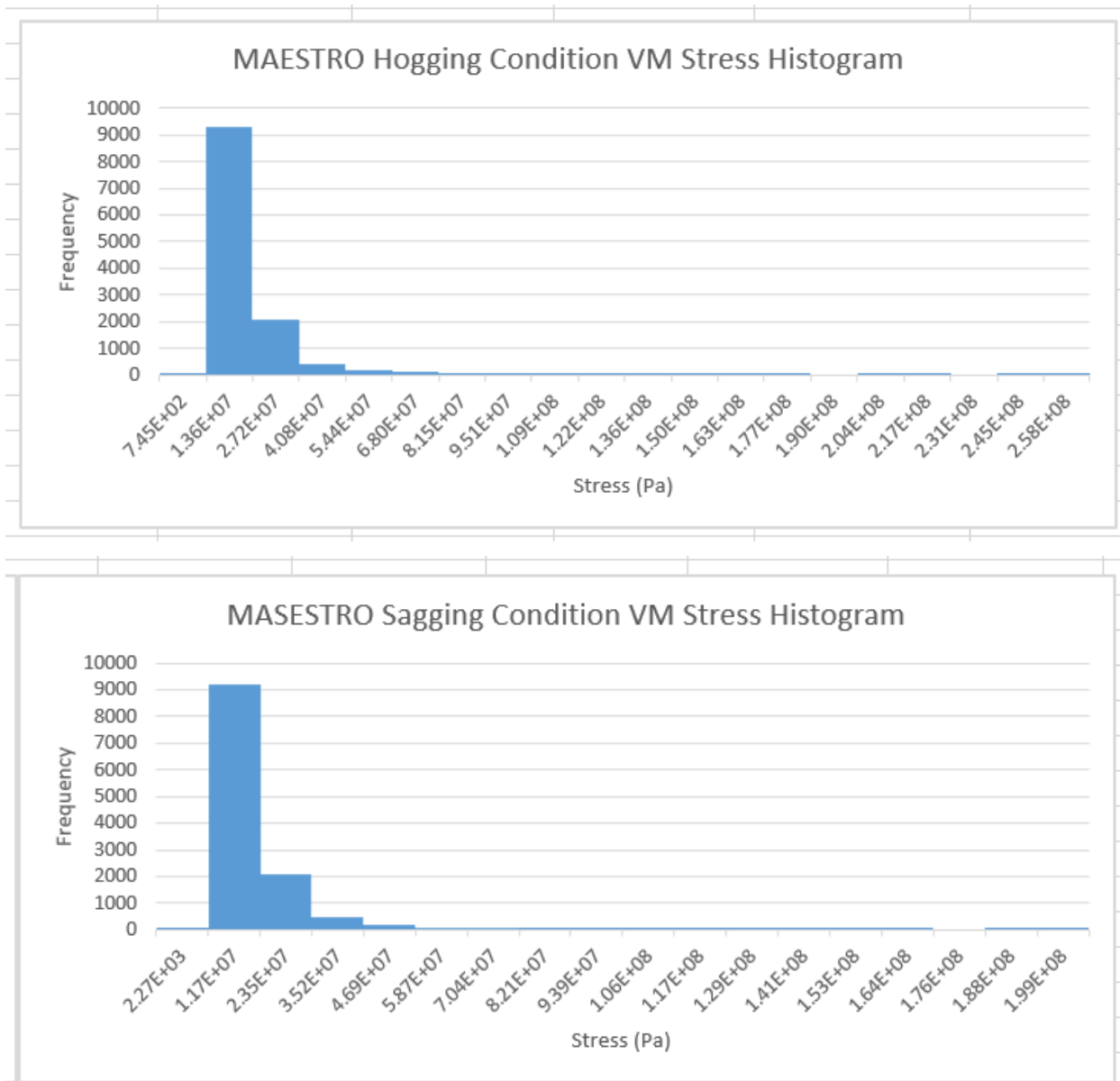


Figure 84: MAESTRO Von Mises Stress Histograms

While the histograms alone do not identify if the stress is truly an outlier, the existence of stress occurrence frequency less than 5 in a bin, strongly suggests the stress is an outlier. Before drawing final conclusions, investigation of the stresses in the elements directly adjacent to the element showing the max stress was gathered in Table 30.

Load Case	Max Stress (Pa)	Adjacent Left Element	Adjacent Top Element	Adjacent Right Element	Adjacent Bottom Element
Buoyancy Mode	5.36×10^7	1.11×10^7	N/A	N/A	1.21×10^7
Flying Mode	1.20×10^8	5.28×10^7	6.48×10^7	2.58×10^7	N/A
Hogging	2.58×10^8	1.66×10^8	6.83×10^7	1.25×10^8	N/A
Sagging	1.94×10^8	8.66×10^7	1.16×10^8	4.01×10^7	N/A

While the statistical data suggests the highest stresses found are outliers the investigation in to the adjacent element stresses suggests that there are high stresses in the regions surrounding the max stress elements. All of the high stressed elements are at the intersection of the hull’s internal structure with the strut’s internal structure. The element mesh in these areas should be refined and additional structure added for a higher fidelity analysis as well as structural strengthening. Other sources contributing to the difference in stresses seen between the AMVS module and MAESTRO module will be investigated.

One potential source contributing to the stress differences can partially be attributed to additional structure (and its weight) being included in the MAESTRO model. This is discussed further in Section 5.2. The AMVS module shows that the greatest displacement magnitudes:

1. Flying mode – hull midship
2. Hogging condition – hull leading edge
3. Hogging/Sagging condition – aft frame center of superstructure

The largest displacements found in the MAESTRO model was in the center of wing-shaped superstructure which correlates most to item 3 in the list above.

One significant difference in vessel element displacements was the MAESTRO model, in the buoyancy load case, indicates the leading edge of the superstructure (center region of superstructure) displaces in the positive y-direction (up). The AMVS module indicates the same section would displace down. This is partially due to MAESTRO’s displacements include the displacement due to trim while the AMVS module strictly considers the displacement of the structure only.

The max stress calculated by the AMVS module was in the hull in flying mode, followed closely by the hull in hogging condition. When considering the stress on the whole vessel, the hogging condition yields the greatest average stress. The MAESTRO model indicates the greatest stress is in the hull in hogging condition.

It is important to emphasize that neither model indicates the vessel structure will truly fail. To achieve the desirable safety factor of 6 for any load case, the structure can be modified, in both the AMVS module and the MAESTRO model, to strengthen the identified weak areas.

5.2 Future Work

It wasn't until the low-fidelity and high-fidelity model results were compared side-by-side that the differences became apparent and the impact the differences had on the results. The lessons-learned is an advantage of the multi-fidelity approach as the models can be refined in future versions of the modules.

After completing this process, there are several proposed steps to incorporate in to the structural module for future improvement. The first enhancements proposed are in the MAESTRO model. Areas of high stress and displacement need to be structurally reinforced to reduce the displacement/stress and increase the safety factor. Figure 85, shows an initial example of a high stress area that has been reinforced to reduce the stress.

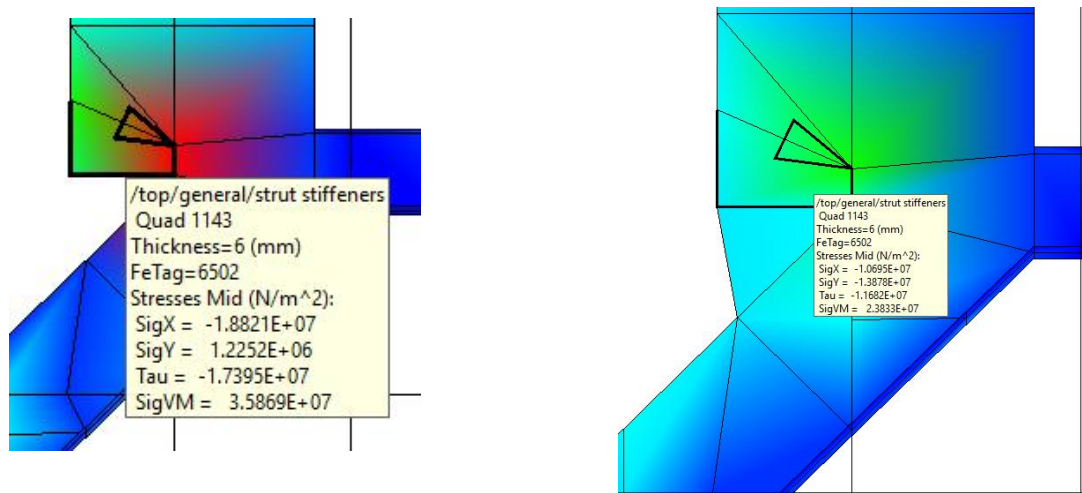


Figure 85: MAESTRO Structural Reinforcement Example

Additionally Section 20 provides an additional example of how to proceed with structural reinforcement in order to reduce the amount of deflection seen at the location of the turbojets. The girder supporting the turbojets has been modified to be a solid bulkhead. This simple change reduced the max deflection in all load cases. In the hogging condition load case (most stress/deflection load case), the max deflection was reduced from -54.81 mm to -16.9 mm. Additionally, the some of the ring stiffeners in the hull have been modified to include flanges to reduce the stress in high stress areas. However, as seen in Sections 4.3 - 4.6 and in Section 20 there are still areas of concern that require more strategy to effectively accomplish increasing the strength without adding a significant amount of weight.

In addition to strengthening weak areas, some of MAESTRO's other floating vessel analysis features have not been used. To create a one-to-one comparison between the AMVS module and the MAESTRO model, boundary conditions were used to simulate hogging and sagging wave conditions as delineated by the DNVGL High Speed Craft rules. MAESTRO features the ability to input wave characteristics and create load conditions using different waves. An interesting comparison would be the

results seen between the DNVGL hogging/sagging wave conditions and the simulated loads as applied by a wave.

The MAESTRO model is currently only set up to analyze the reference HY2-SWATH structural configuration. A more challenging goal is to automate structural variations through modification of input variables, like the AMVS module has been done. MAESTRO does not currently feature a programming language through which this could be accomplished and thus would require programming in Rhino to generate a MAESTRO acceptable mesh, distributed/concentrated load(s), loading case(s) and boundary condition(s). Once the MAESTRO model is parametrically modifiable, it too can be incorporated in to a global network software manager to automatically generate structural variations of the vessel and used for design space exploration required in the SBD method.

The modifications to the AMVS module primarily include changes to increase the model fidelity. The differences found in the calculated results can primarily be attributed to the differences in the geometry. Several structural elements have not been incorporated into the AMVS module, at this time, but can be included in future versions of the AMVS module. They include:

- watertight bulkheads in the struts
- bulbous section of the superstructure where the payload is positioned

In addition to including additional structure in the AMVS module, the cross-section of the forward and aft frame superstructure cross-sections should be modified. Instead of using the whole superstructure cross-section, the cross-section should be split forward and aft. The aft frame superstructure receives too much strength from the forward/leading edge section of the superstructure preventing the deflection seen in the high-fidelity MAESTRO model. Splitting the superstructure cross-section forward and aft could provide a more accurate representation of the large deflections seen in the near the turbojet location in the 3D MAESTRO model. Alternatively, a fourth frame could be created to analyze the superstructure in the longitudinal direction which can also be coupled with the other frames.

The AMVS module should be run to generate more designs. The module should be integrated in to software manager like ModelCenter to take advantage of some of the intrinsic algorithms. These algorithms can conduct a larger design space exploration, using a larger number of input variables, in a time efficient manner and in which the AMVS module is already capable of doing. Additionally, using ModelCenter would allow the AMVS module to be coupled with some of the other HY2-SWATH modules to explore the design space in multiple ship design disciplines.

6. Conclusions

The fundamental focus for this thesis was on the development of a parametrically modifiable AMVS module using a low-fidelity structural analysis method implemented using a numerical 2D Finite Element Analysis (FEA) applied to the HY2-SWATH. The AMVS module's accuracy was compared with using a side-by-side comparison of the reference HY2-SWATH as calculated by the AMVS module and MAESTRO. AMVS module is used to analyze an advanced marine vessel in displacement and foil-borne modes as well hogging and sagging extreme wave conditions that the vessel may encounter during its operation. AMVS demonstrates the capability to explore the HY2-SWATH design space and evaluate the structural feasibility of the advance marine vehicle designs through consideration of the material, stiffener/girder dimensions, stiffener/girder arrangement, and machinery/equipment weights onboard.

An initial variable sweep of five different materials (Table 17), stiffener count (Table 18), and vessel shell plating from 4 mm to 7 mm, was run in the AMVS module to explore the design space. The different combination of the variables yields 60 different structural variations to the HY2-SWATH. All 60 variations were analyzed for the four load case scenarios. The results of the design space exploration have been provided in the appendices and include the raw data collected as well as histograms and variable sensitivity plots to analyze the data visually. From the 60 structural HY2-SWATH variations, there are four feasible HY2-SWATH solutions that support the equipment, machinery, tanks, and payload as required by the vessel operations and stakeholder requirements. From the histograms, it is apparent the feasible solutions are most limited by the buoyancy provided by the hull, material used, and the hydrofoils' designed lift. As the structure of the HY2-SWATH has not previously been investigated, it is significant to find there are feasible solutions, even in the small sample size run. The inclusion of more structural variations will result in more feasible solutions.

The reference vessel displacement outputs from the AMVS module and high-fidelity MAESTRO model have a general correlation to one another. The models deflected similarly at the same locations; however, the magnitude of the deflections slightly differed. Both models indicate the largest displacements, in the wing-shaped superstructure, occurred at the location of the turbojets loads. In the high-fidelity model the location of turbojets caused the largest displacement overall in the flying mode, hogging, and sagging load case scenarios. In general, the hull displacements calculated by the high-fidelity model, for all loading conditions, were smaller than the displacements calculated by the AMVS module. The AMVS module analyzed the hull in a slightly more severe configuration due to the analysis of the hull frame in the absence of the structural support provided by the strut-superstructure, yet loaded as if they (and all internal machinery) were present. This resulted in greater magnitude displacements observed in the AMVS module. Based on these results, it would be useful to consider a closed longitudinal frame to include the hull, struts and superstructure.

The stress outputs from the AMVS module and the high-fidelity MAESTRO model have a general correlation to one another, as well. Table 26 and Table 29 help to compare the stress values between the two models for the different load cases. While the MAESTRO model calculates a much larger range of stresses and an order of magnitude greater max stress, the average and the standard deviation are more similar between the two models. The exception is the flying mode load case in which the average and standard deviation is an order of magnitude larger as calculated by the AMVS module. As previously discussed, the greater stresses calculated, for flying mode, in the AMVS module could be attributed to analyzing the hull in a slightly more severe configuration than the MAESTRO module. The differences found between the stresses and displacements calculated in the two models can be accounted for by imposing a higher safety factor in the more approximate AMVS module and a reduced safety factor in the more precise MAESTRO model.

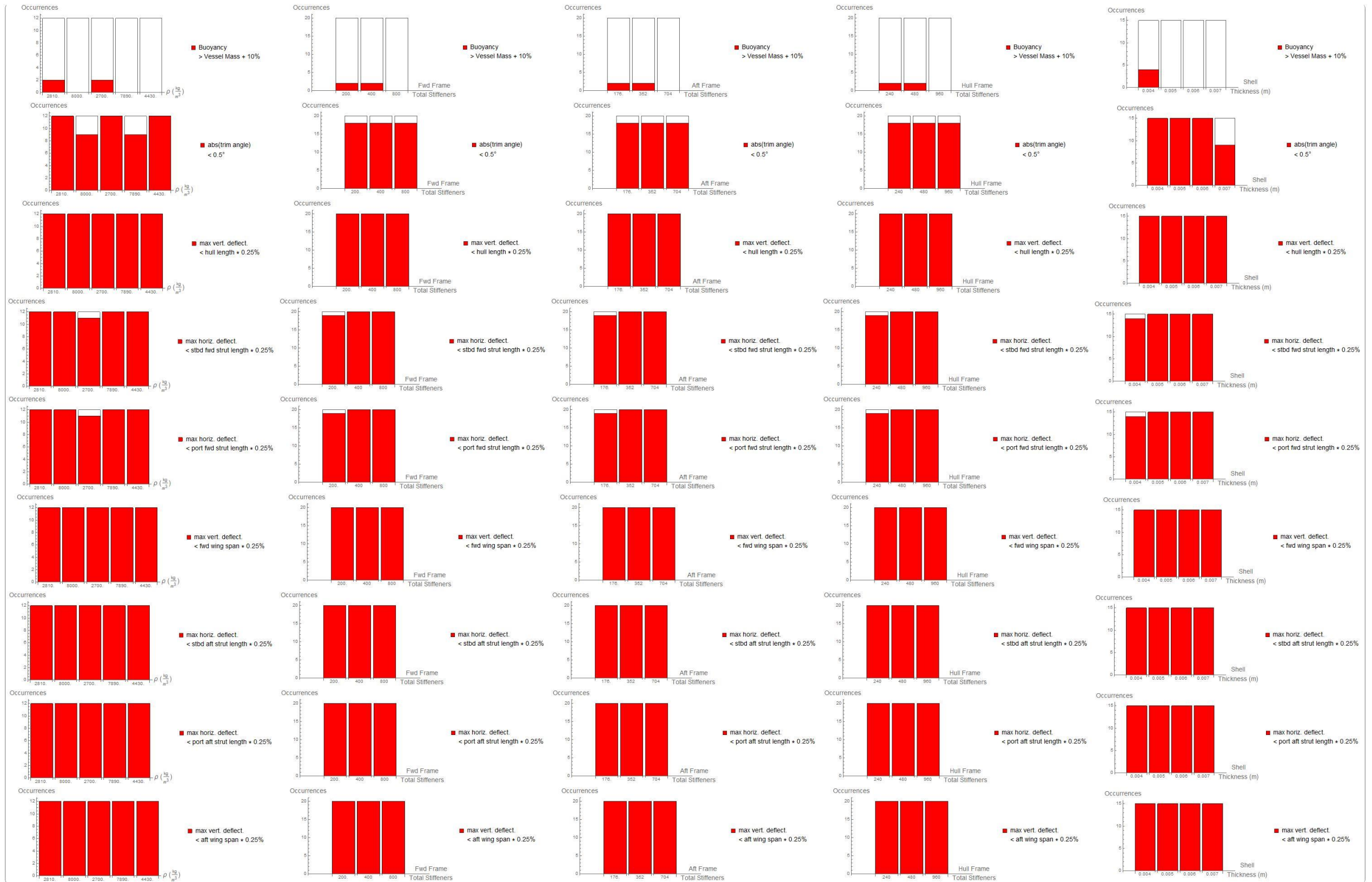
The MAESTRO high-fidelity model has helped to pinpoint some structurally weak areas in the vessel, as well as has helped identify how the low-fidelity AMVS module can be improved to increase its fidelity while still retaining its quick computational speed.

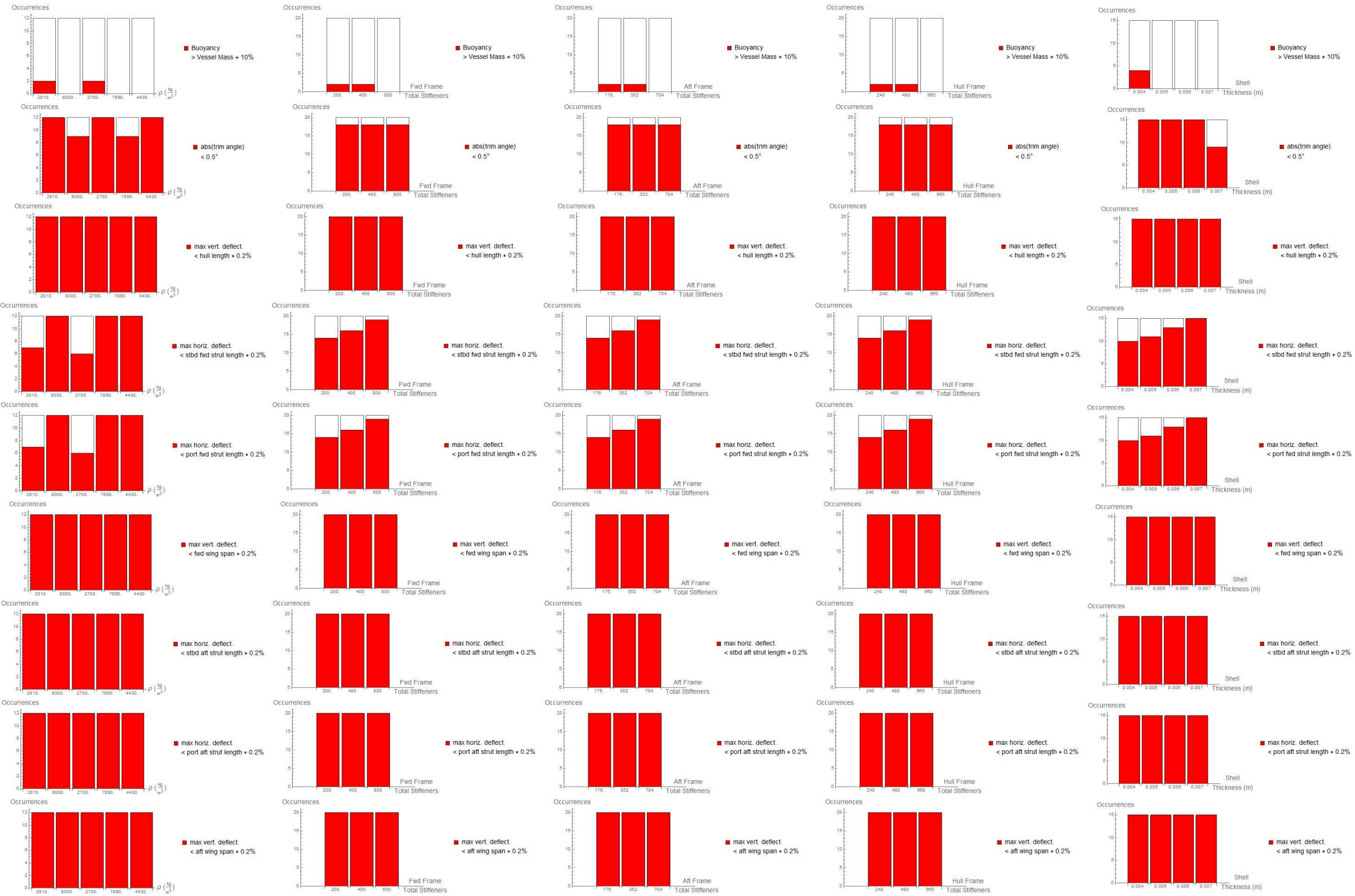
7. References

- [1] Genta, John (John Anthony). “Using the Principles of Set-Based Design to Realize Ship Design Process Improvement.” DSpace@MIT, Massachusetts Institute of Technology, 1 Jan. 1970, hdl.handle.net/1721.1/104387.
- [2] Singer, David J., et al. What Is Set-Based Design? 4 Feb. 2008, www.doerry.org/norbert/papers/SBDFinal.pdf.
- [3] Global Shipbuilding Industrial Base Benchmarking Study Part I: Major Shipyards. Office of the Deputy under Secretary of Defense (Industrial Policy), May 2005, www.nsrp.org/wp-content/uploads/2015/08/FMI-Global_Industrial_Benchmarking-major_yards-Navy-rpt.pdf.
- [4] Pruner, Sara. “Design of a Supercavitating Hydrofoil for Ultra-High Speed Vessel with Numerical Methods.” MS Thesis, Naval Architecture Department, University of Genoa, 2011.
- [5] “High Speed, Light Craft and Naval Surface Craft.” IMO High Speed Craft Code, Det Norske Veritas, 2011.
- [6] Faltinsen, O. M. Hydrodynamics of High-Speed Marine Vehicles. Cambridge University Press, 2010.
- [7] Brizzolara S. (2004). Parametric Optimization of SWAT-Hull Forms by a Viscous-Inviscid Free Surface Method Driven by a Differential Evolution Algorithm. In: 25th Symposium on Naval Hydrodynamics. Saint John's (CA), August 2004, National Academies Press, vol. 5, p. 1-18.
- [8] Grannemann, Fritz. “SWATH- A New Concept for the Safety and Security at Sea.” Ciencia y Tecnología De Buques, www.shipjournal.co/index.php/sst/article/view/120/370. 8.17 (2015): 47-56. Web. 17 Nov. 2017
- [9] Buede, Dennis M. The Engineering Design of Systems: Models and Methods. 2nd ed., John Wiley & Sons, 2009.
- [10] Reddy, J. N. Introduction to the Finite Element Method. 3rd ed., McGraw-Hill Education, 2006.
- [11] Hughes, Owen F., et al. Ship Structural Analysis and Design. Society of Naval Architects and Marine Engineers, 2010.
- [12] Shames, Irving Herman, and Clive L. Dym. Energy and Finite Element Methods in Structural Mechanics. Taylor & Francis, 1985.
- [13] Brown, Alan, et al. “Set-Based Design Framework for Naval Ship Concept Exploration with Tight Integration of High-Fidelity Physics-Based Simulations.” American Society of Naval Engineers.
- [14] “DNV GL Rules for Classification: High Speed and Light Craft (RU-HSLC).” Rules and Standards - DNV GL, Det Norske Veritas (Norway) and Germanischer Lloyd, [rules.dnvgl.com/ServiceDocuments/dnvgl/#!/industry/1/Maritime/2/DNV%20GL%20rules%20for%20classification:%20High%20speed%20and%20light%20craft%20\(RU-HSLC\)](http://rules.dnvgl.com/ServiceDocuments/dnvgl/#!/industry/1/Maritime/2/DNV%20GL%20rules%20for%20classification:%20High%20speed%20and%20light%20craft%20(RU-HSLC)).

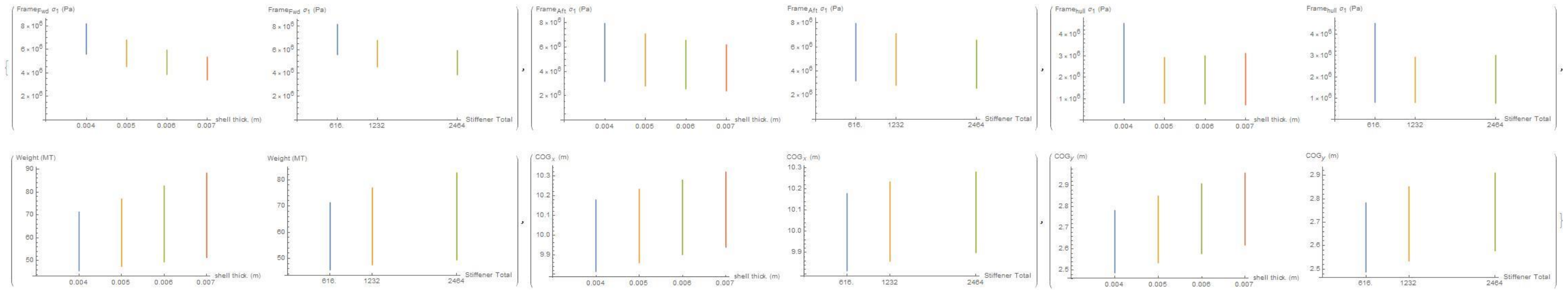
- [15] Bernstein, Joshua. "Design Methods in the Aerospace Industry: Looking for Evidence of Set-Based Practices." DSpace@MIT, Massachusetts Institute of Technology, 1 Jan. 1998, dspace.mit.edu/handle/1721.1/82675.
- [16] "MAESTRO." Maestro Marine, maestromarine.com/
- [17] Ragab, Saad. "Frames.m" Virginia Tech, 2002.
- [18] Williams S., Brizzolara S. (2017). Dynamic Stability of Foilborne Hydrofoil/SWATH with Anhedral Foil Configuration. *Transactions RINA*, Vol 159, Part B2, *Intl J Small Craft Technology*, pp.65-80, July-Dec. 2017.

9. APPENDIX B: Buoyancy Mode Histogram Plots

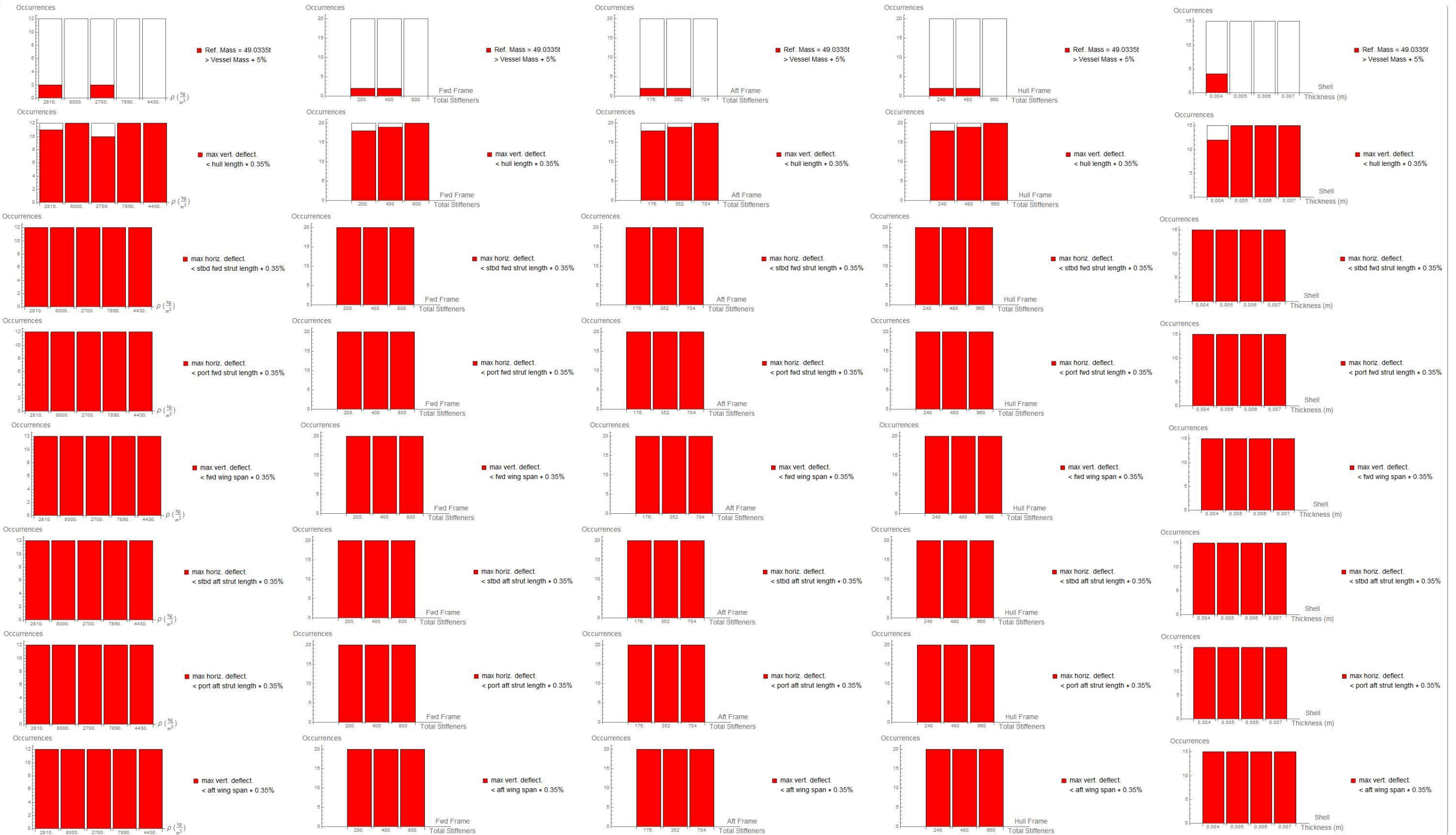


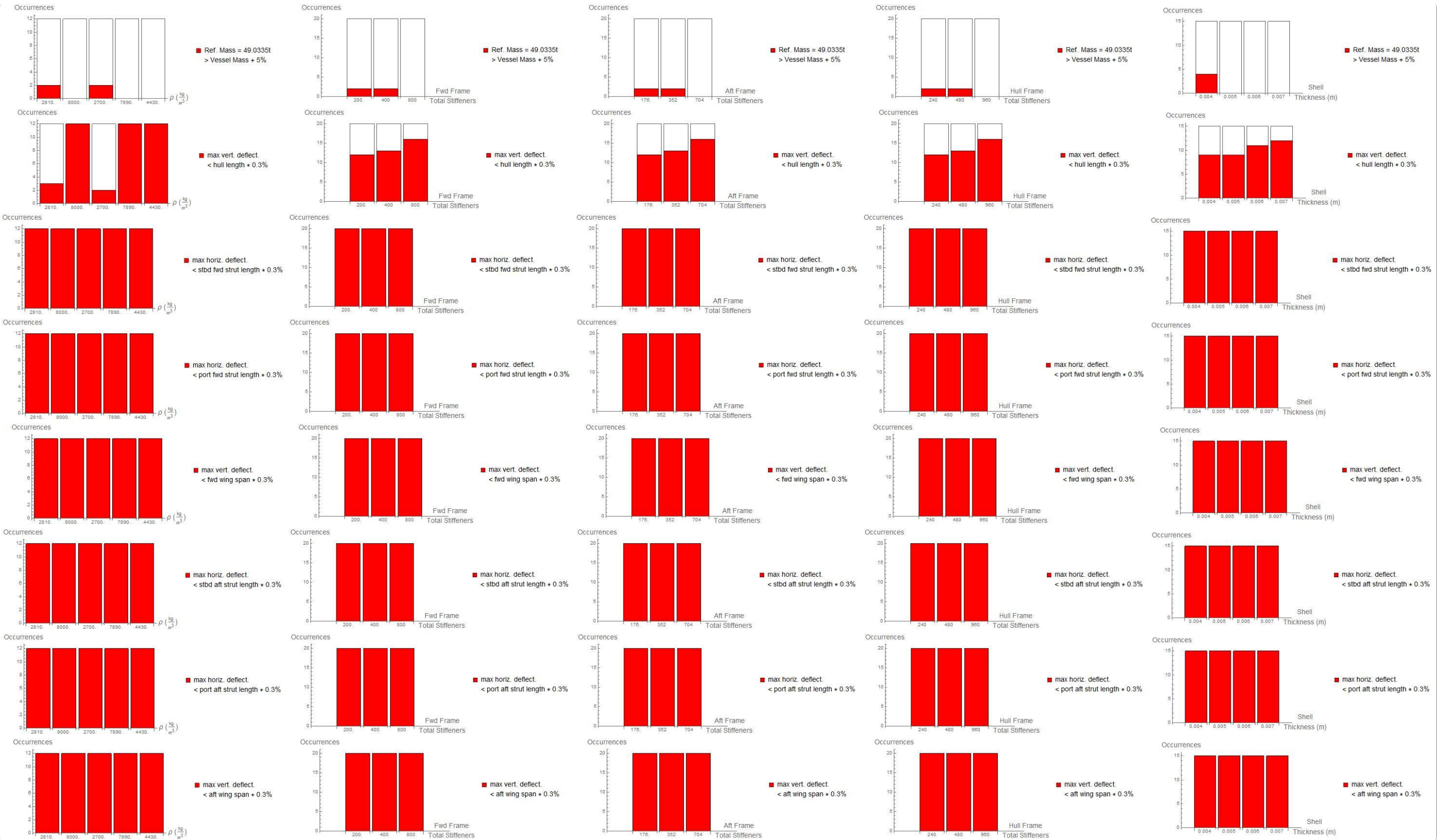


10.APPENDIX C: Buoyancy Mode Variable Sensitivity Plots

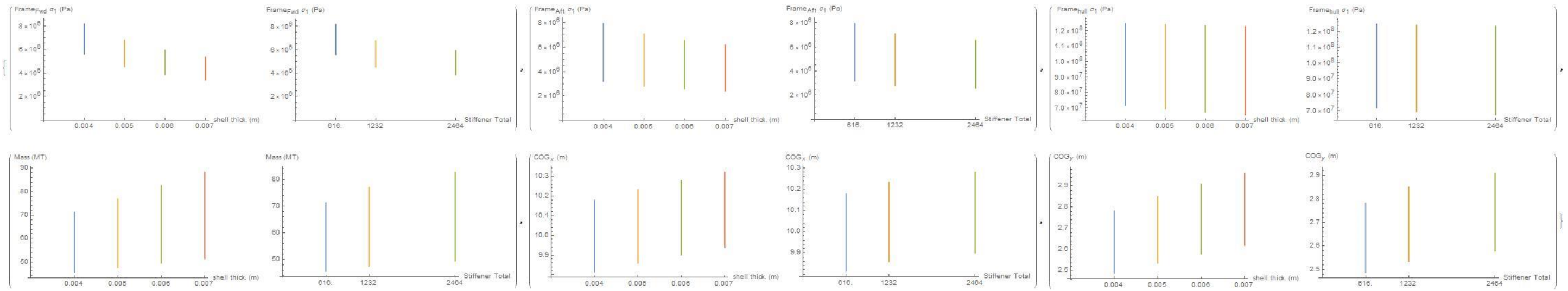


12.APPENDIX E: Flying Mode Histogram Plots

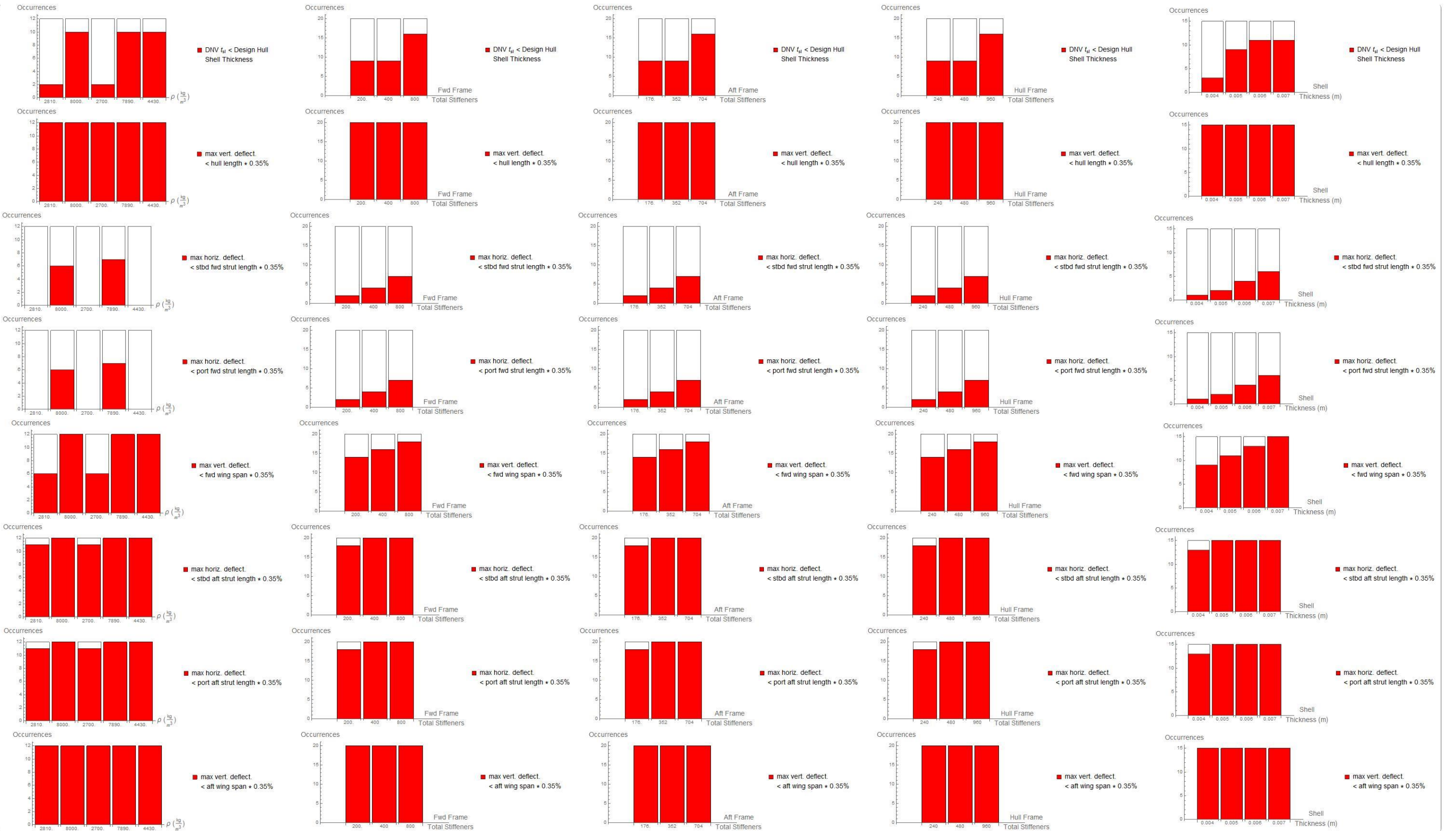


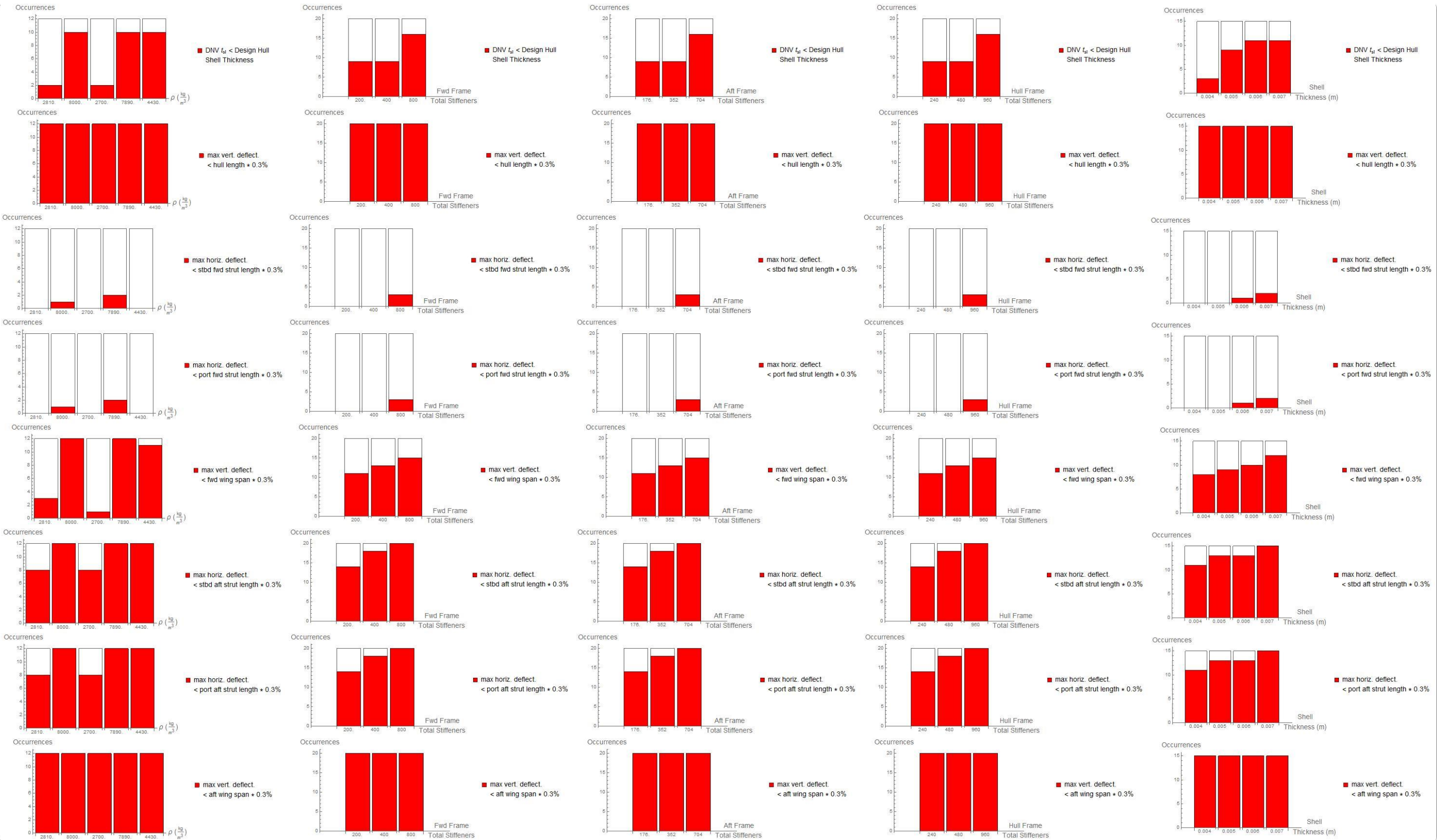


13.APPENDIX F: Flying Mode Variable Sensitivity Plots

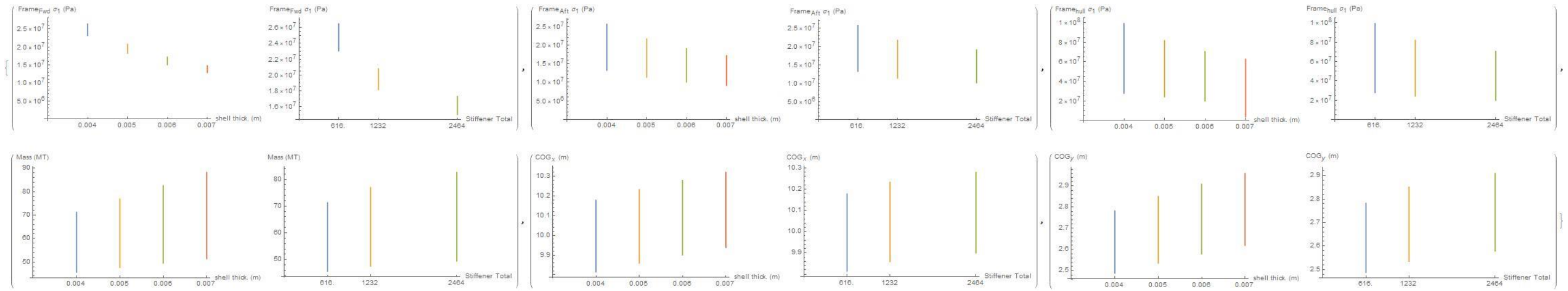


15.APPENDIX H: Hogging Condition Histogram Plots

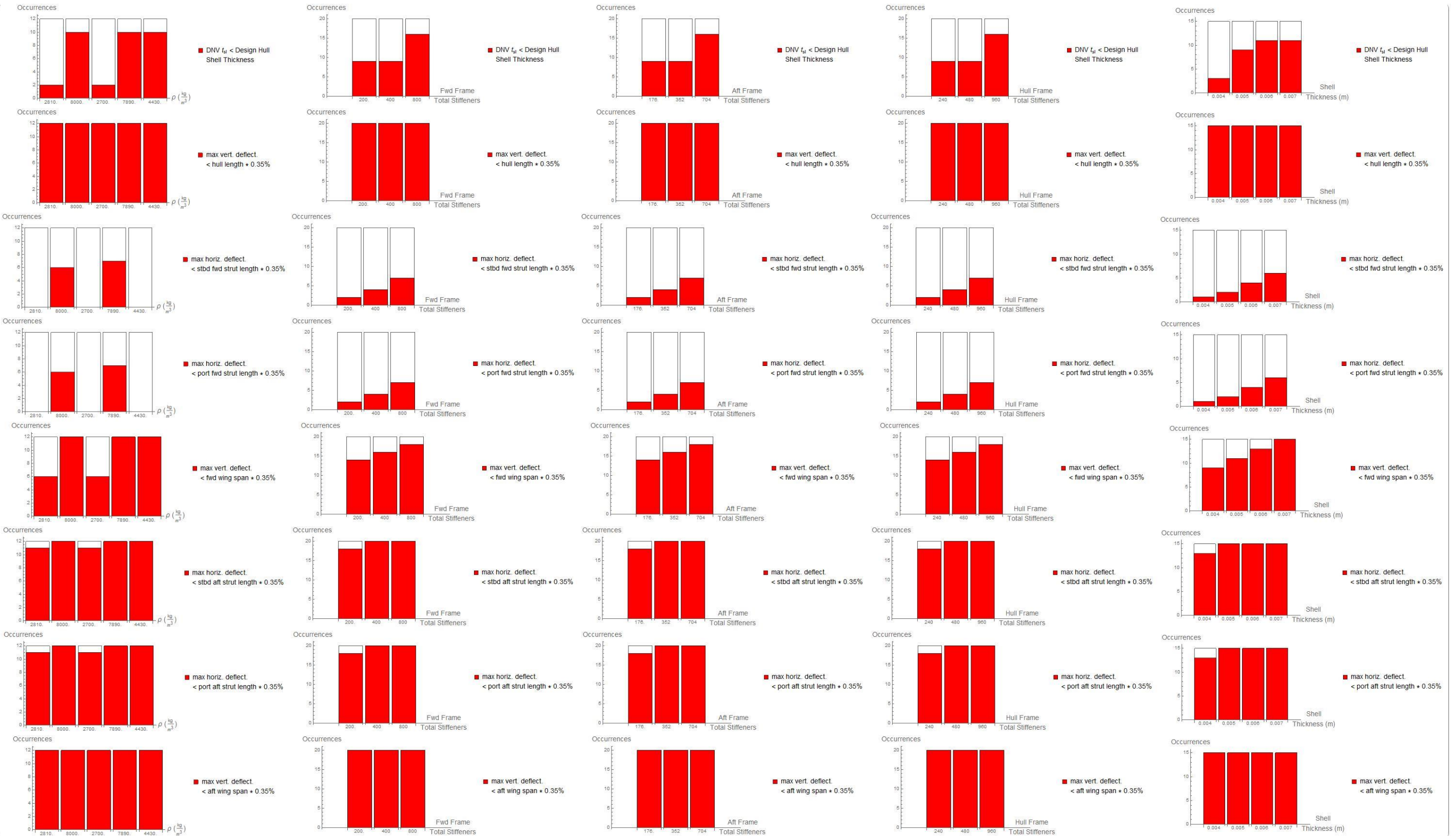


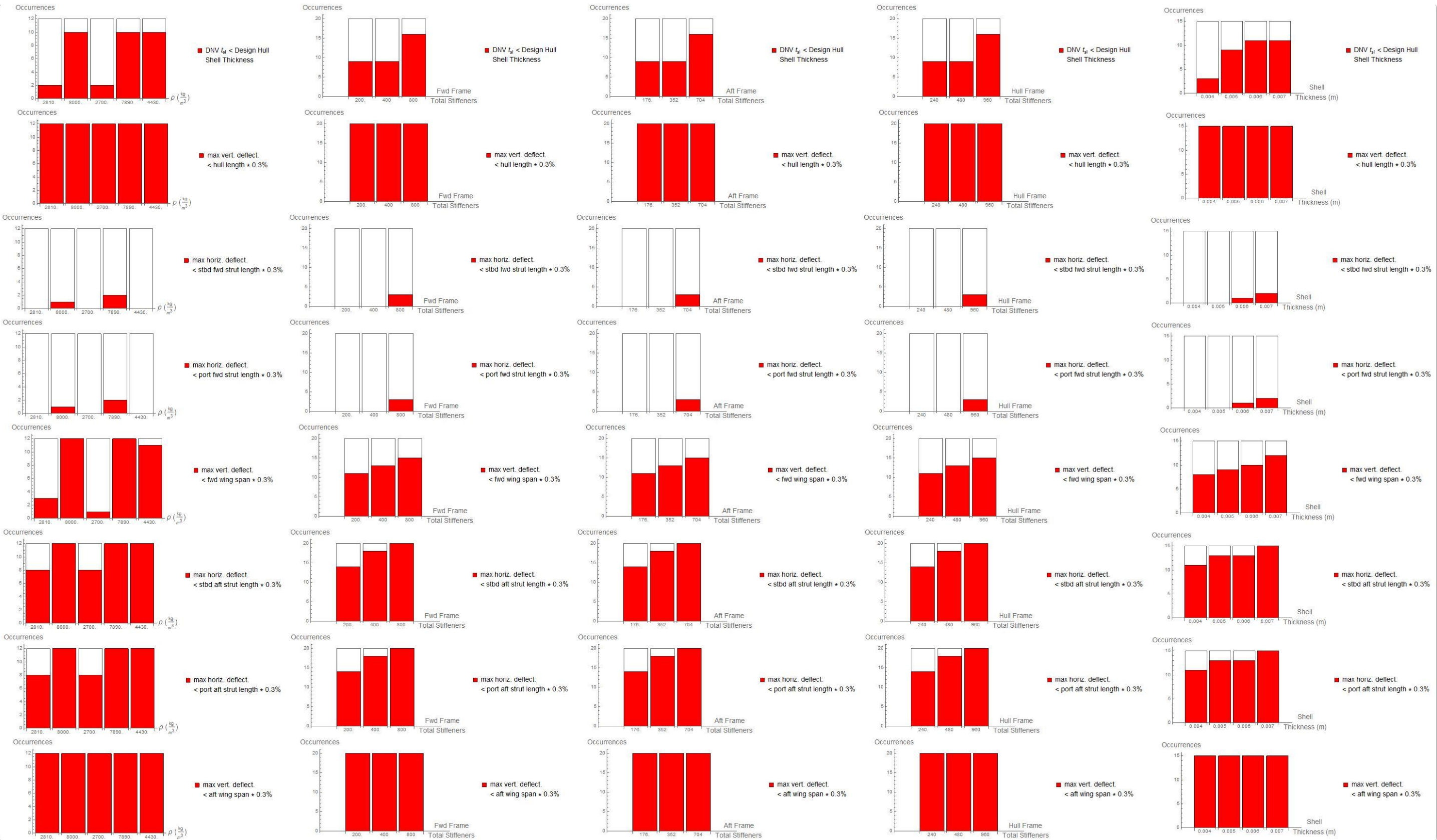


16.APPENDIX I: Hogging Condition Variable Sensitivity Plots

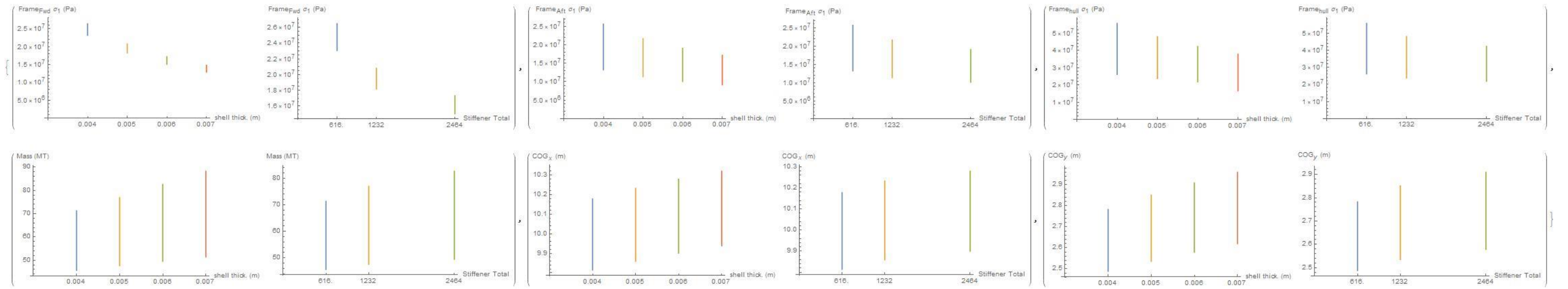


18.APPENDIX K: Sagging Condition Histogram Plots

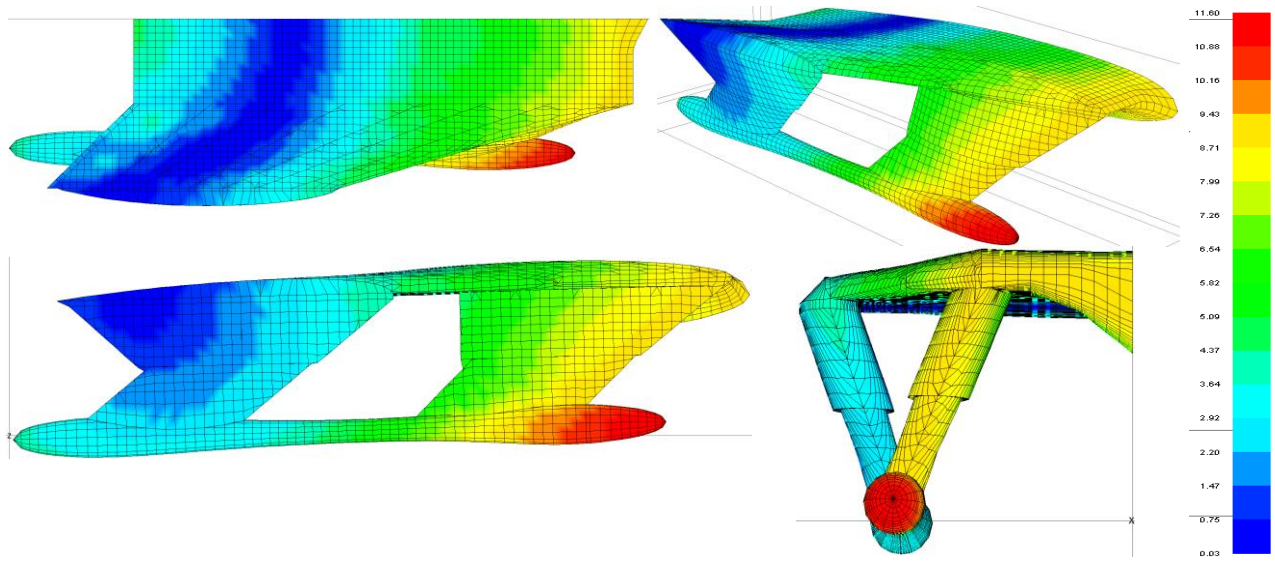




19.APPENDIX L: Sagging Condition Variable Sensitivity Plots

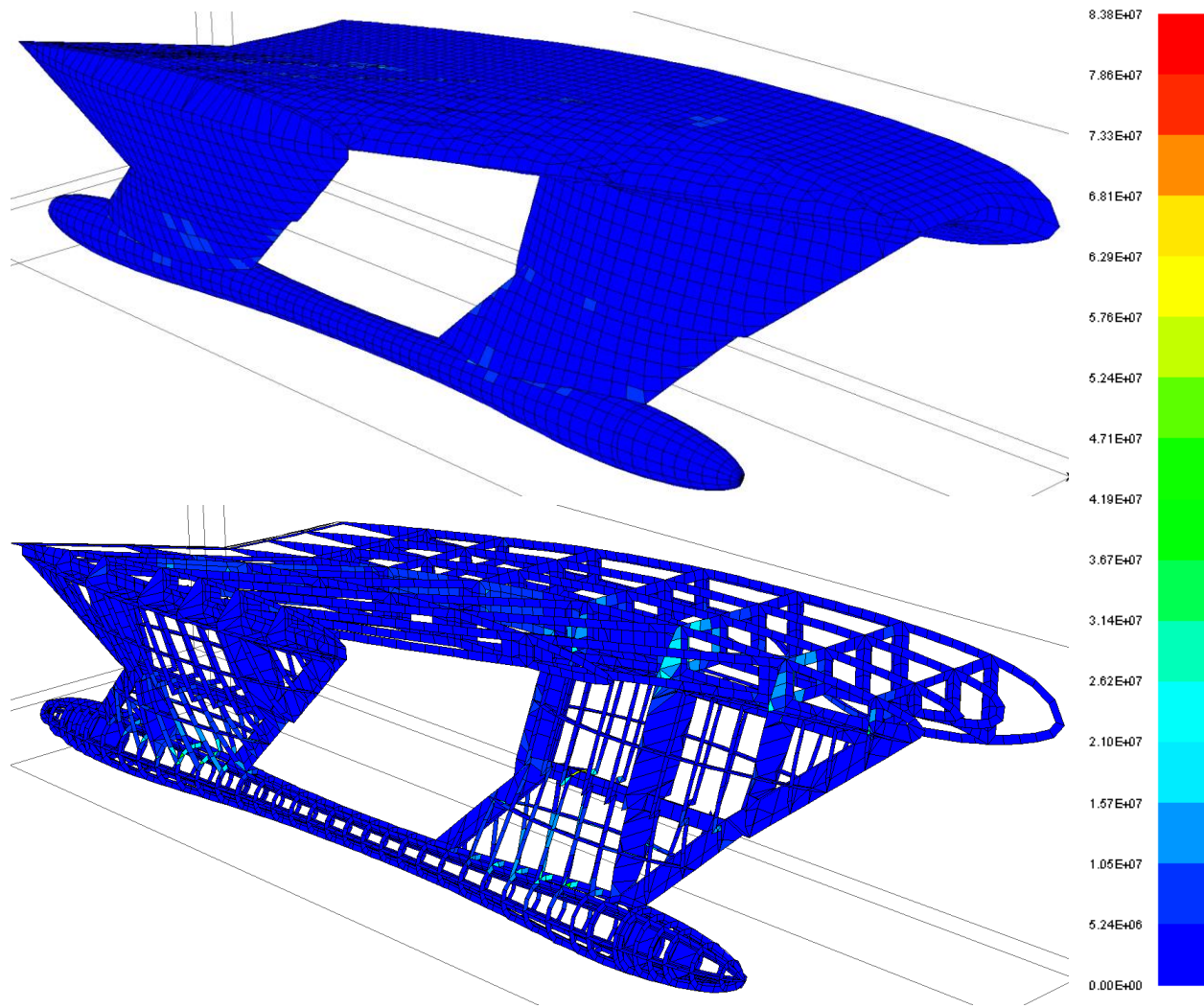


20. Appendix M: HY2-SWATH Structural Improvement Modifications



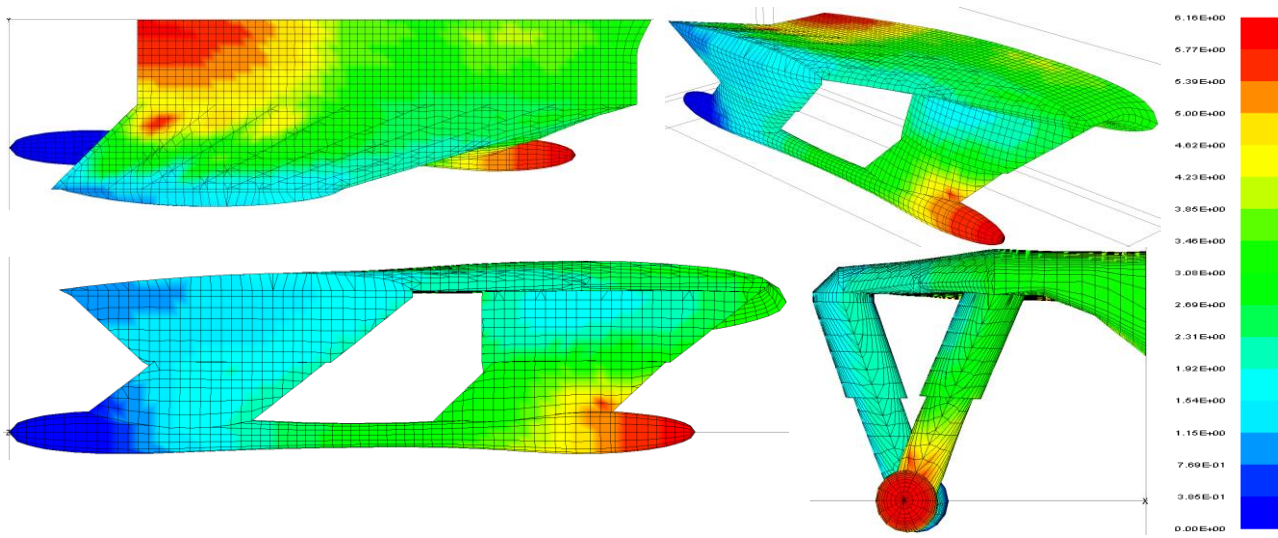
Displacement Magnified by 42x factor – Displacement in mm

Figure 86: Improved MAESTRO Reference Model Displacement Results (Buoyancy Mode)



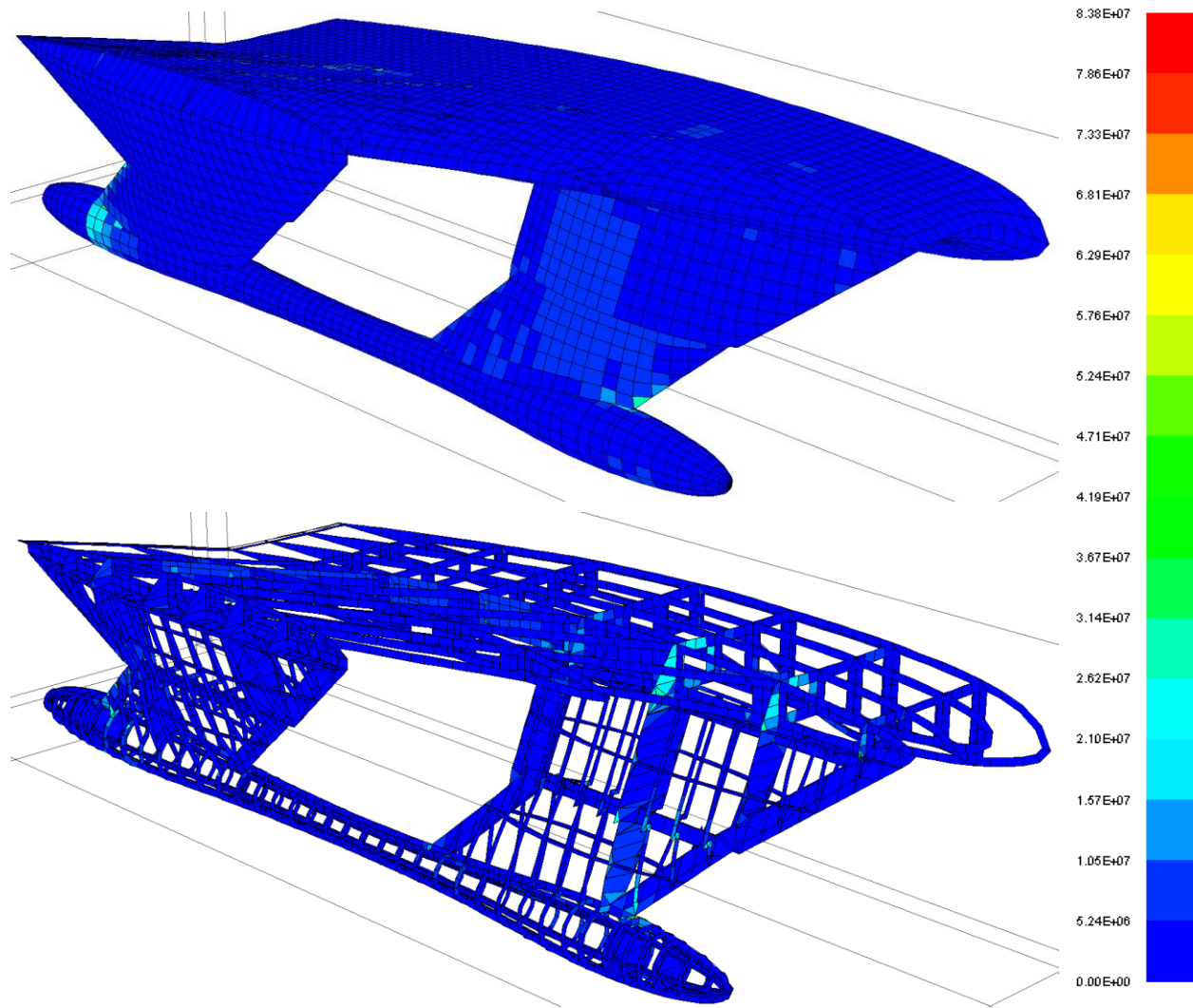
Displacement Magnified by 42x factor - Stress in N/m^2

Figure 87: VM Stress on Improved Shell Plating and Internal Structure (Buoyancy Mode)



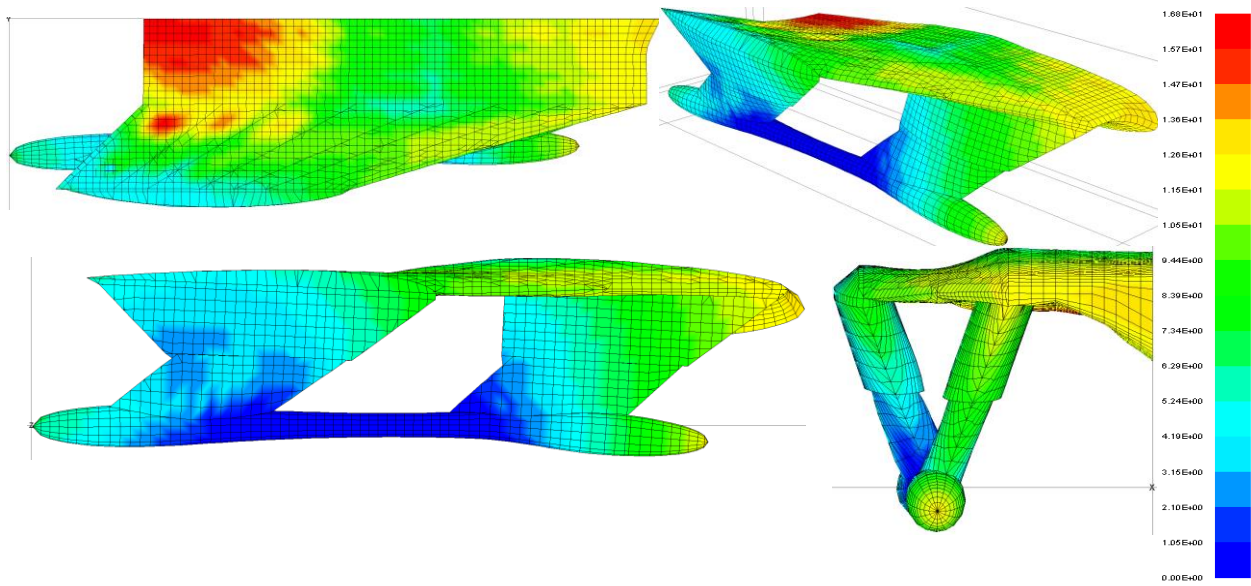
Displacement Magnified by 42x factor – Displacement in mm

Figure 88: Improved MAESTRO Reference Model Displacement Results (Flying Mode)



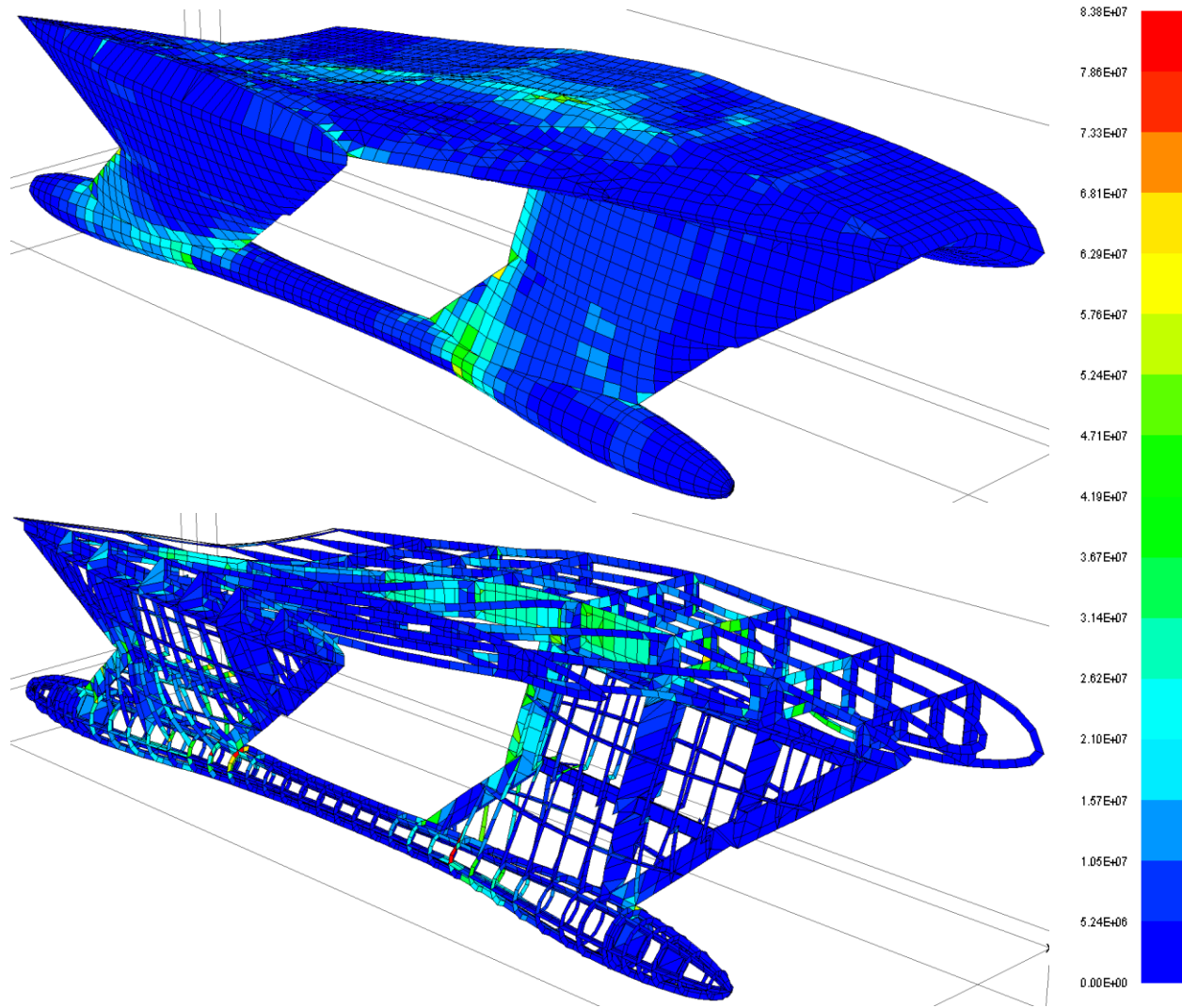
Displacement Magnified by 42x factor - Stress in N/m²

Figure 89: VM Stress on Improved Shell Plating and Internal Structure (Flying Mode)



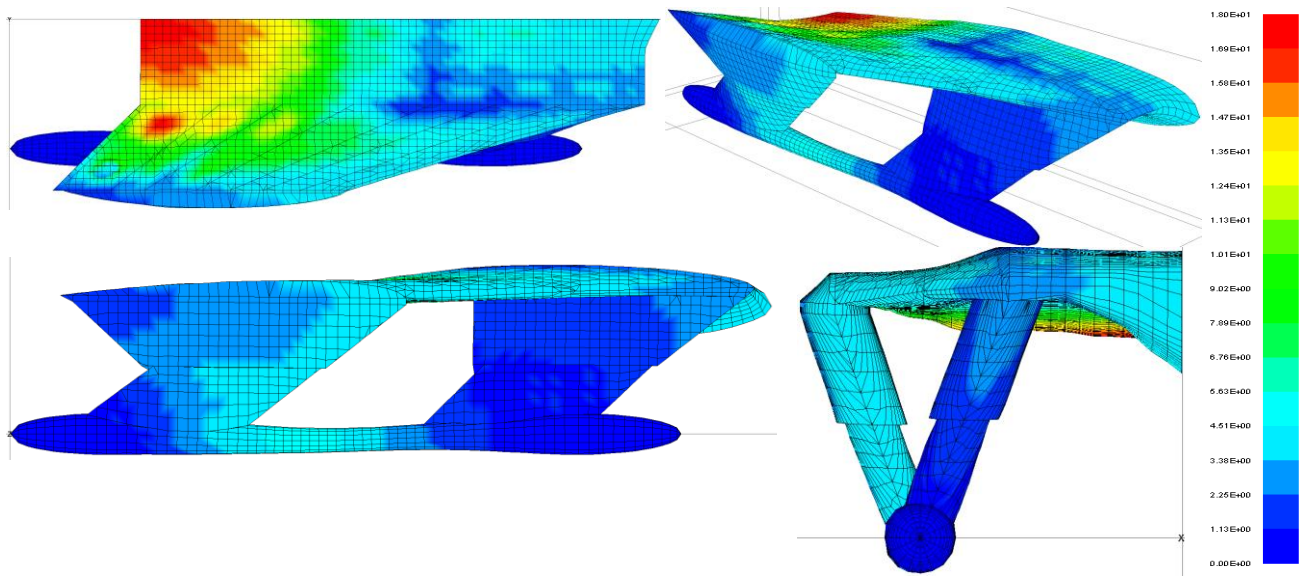
Displacement Magnified by 42x factor – Displacement in mm

Figure 90: Improved MAESTRO Reference Model Disp. Results (Hogging Condition)



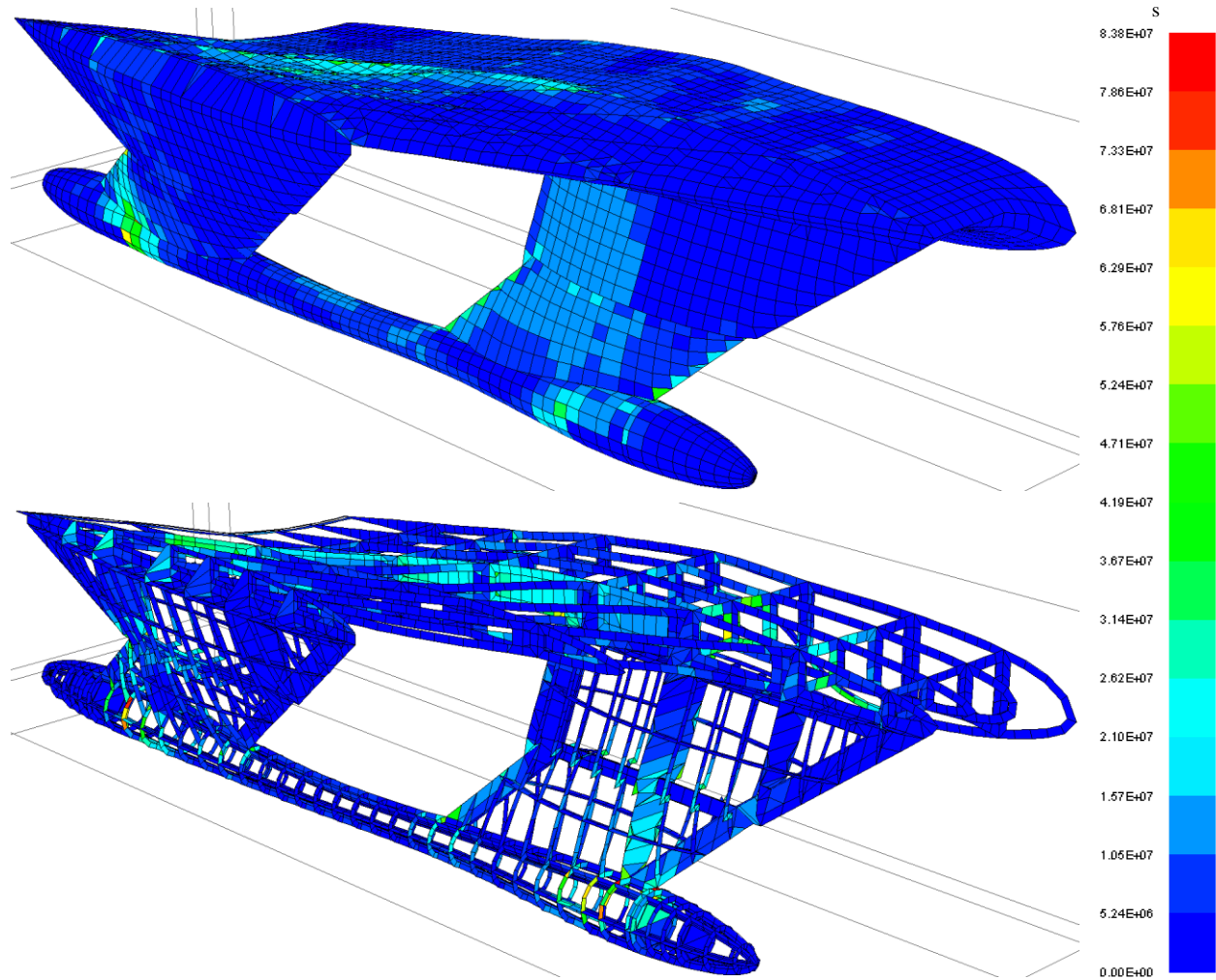
Displacement Magnified by 42x factor - Stress in N/m²

Figure 91: VM Stress on Improved Shell Plating and Internal Structure (Hogging Condition)



Displacement Magnified by 42x factor – Displacement in mm

Figure 92: Improved MAESTRO Reference Model Disp. Results (Sagging Condition)



Displacement Magnified by 42x factor - Stress in N/m²

Figure 93: VM Stress on Improved Shell Plating and Internal Structure (Sagging Condition)